Distribution Agreement

In presenting this thesis or dissertation as a partial fulfillment of the requirements for an advanced degree from Emory University, I hereby grant to Emory University and its agents the non-exclusive license to archive, make accessible, and display my thesis or dissertation in whole or in part in all forms of media, now or hereafter known, including display on the world wide web. I understand that I may select some access restrictions as part of the online submission of this thesis or dissertation. I retain all ownership rights to the copy right of the thesis or dissertation. I also retain the right to use in future works (such as articles or books) all or part of this thesis or dissertation.

Signature:

_____ _____

Crystal E. Fagan Date

Molecular mechanisms involved in maintaining ribosomal fidelity

By

Crystal E. Fagan
Doctor of Philosophy

Graduate Division of Biological and Biomedical Science
Biochemistry, Cell and Developmental Biology

_____
Christine Dunham, Ph.D.
Advisor

_____
Xiaodong Cheng, Ph.D.
Committee Member

_____
Anita Corbett, Ph.D.
Committee Member

_____
Eric Ortlund, Ph.D.
Committee Member

_____
Daniel Reines, Ph.D.
Committee Member

Accepted:

_____
Lisa A. Tedesco, Ph.D.
Dean of the James T. Laney School of Graduate Studies

_____
Date

Molecular mechanisms involved in maintaining ribosomal fidelity

By

Crystal E. Fagan
B.S., Georgia Institute of Technology

Advisor: Christine Dunham, Ph.D.

An abstract of
A dissertation submitted to the Faculty of the
James T. Laney School of Graduate Studies of Emory University
in partial fulfillment of the requirements for the degree of
Doctor of Philosophy
In
Graduate Division of Biological and Biomedical Science
Biochemistry, Cell and Developmental Biology
2014

Abstract

Molecular mechanisms involved in maintaining ribosomal fidelity

By Crystal E. Fagan

The ability to faithfully translate the genetic instructions into functional proteins is critical. The process of translation is carried out by the ribosome using a set of finely tuned tRNA adapter molecules to translate the messenger RNA three nucleotides at a time. In order to accurately decode the mRNA, the ribosome must both select the correct tRNA to decode the mRNA and preserve the three nucleotide mRNA reading frame. If errors do occur, a quality control mechanism is activated to terminate the synthesis of that erroneous protein. The work presented here analyzes the molecular mechanisms responsible for maintaining intrinsic ribosomal fidelity in bacteria. In order to understand how correct tRNA decoding is signaled across the ribosome, I structurally characterized 16S rRNA *r*ibosomal *am*biguity (*ram*) mutations that resulted in a strong miscoding phenotype. Through this work I have identified a global regulator of translational fidelity, the intersubunit bridge B8. This bridge increases the stringency of mRNA decoding by negatively regulating GTPase activation, an essential process in tRNA selection. To understand the role of tRNA structure in maintaining the mRNA reading frame, I characterized a tRNA that contains an expanded anticodon stem-loop. Our results show distortions in the tRNA shape could impede gripping interactions with the ribosome and other translation factors resulting in incorrect mRNA decoding. Finally, I investigated the molecular mechanisms responsible for the identification of errors after they have been incorporated into the nascent peptide chain. This work suggests incorrect tRNA-mRNA interaction could alter the position of the mRNA. These different research projects have helped to provide a more complete understanding of the intrinsic ribosomal mechanisms responsible for maintaining translational fidelity

Molecular mechanisms involved in maintaining ribosomal fidelity

By

Crystal E. Fagan
B.S., Georgia Institute of Technology

Advisor: Christine Dunham, Ph.D.

A dissertation submitted to the Faculty of the
James T. Laney School of Graduate Studies of Emory University
in partial fulfillment of the requirements for the degree of
Doctor of Philosophy
In
Graduate Division of Biological and Biomedical Science
Biochemistry, Cell and Developmental Biology
2014

TABLE OF CONTENTS

LIST OF FIGURES AND TABLES

Chapter 1

Chapter 2

Chapter 3

ABBREVIATIONS

A: adenosine
aa-tRNA: aminoacyl tRNA
ASD: anti-Shine-Dalgarno
ASL: anticodon stem loop
A-site: aminoacyl site
C: cytosine
D: dihydrouridine
D. radiodurans: Deinococcus radiodurans
DNA: deoxy ribonucleic acid
E. coli: Escherichia coli
E-site: exit site
EF-G: elongation factor G
EF-Tu: elongation factor Tu
fMet: formylmethionine
FRET: fluorescence resonance energy transfer
G: guanine
GDP: guanosine diphosphate
GTP: guanosine triphosphate
H. marismortui: Haloarcula marismortui
I: inosine
IC: initiation complex
IF: initiation factor
IVT: *in vitro* transcribe
Lys: lysine
mRNA: messenger ribonucleic acid
NLS: nuclear localization sequence
PDB ID: protein database identification code
PIC: preinitiation complex
Phe: phenylalanine
Post PT QC: post peptidyl-transfer-quality-control
PTC: peptidyl transferase center
P-site: peptidyl site
ram: ribosomal ambiguity
RF: release factor
RNA: ribonucleic acid
RNC: ribosome nascent chain
RRF: ribosomal recycling factor
rRNA: ribosomal ribonucleic acid
r-proteins: ribosomal proteins
SD: Shine-Dalgarno
SmD: streptomycin-dependent
SmR: streptomycin-resistant
SRL: sarcin-ricin loop
str: stringency
Suf: suppressor of frameshift
T: ribothymidine
TC: ternary complex
TEL: telithromyocin
Thr: threonine

tRNA: transfer ribonucleic acid
Tth: Thermus thermophilus
U: uracil

CHAPTER 1. GENERAL INTRODUCTION

The ability to efficiently and accurately translate genomic information into functional proteins is essential for cellular survival. The flow of genetic information from DNA to RNA to proteins is the fundamental pathway of genetic inheritance that is collectively referred to as the central dogma of molecular biology. This unidirectional transfer of information is governed by three distinct polymerization reactions: replication, transcription, and translation. In bacterial cells, nearly two-thirds of the total cellular energy is spent on protein production (1); one could imagine that increased growth rates might be achieved by increasing the catalytic rate of these three polymerization reactions. However, mutations that increase the catalytic rates of these polymerases often display a lower fidelity, or inaccurate replication of the template, and reduced growth rates (2-6). Instead, decreasing the catalytic rate in favor of increased accuracy results in polymerases that are more efficient, saving time and energy associated with correcting errors. As a consequence, maximal growth rates are achieved through the optimal balance between speed and fidelity (7-10).

Each polymerization reaction occurs with a varying degree of accuracy, which is directly correlated with both the product's lifetime and its potential effect on maintaining organismal integrity. The replication of the genome by DNA polymerases occurs with remarkable accuracy, with errors happening at an estimate of less than 1 in 10^9 incorporations (11, 12). If not corrected, errors made during DNA replication will become permanent mutations that will be passed on to future generations. The transcription of DNA into RNA by RNA polymerases also proceeds with a high level of accuracy, with error rates of 1 in 10^5 (13). Any errors made during transcription will be transferred to all proteins expressed using this messenger RNA (mRNA) template. Finally, the translation of RNA into proteins by the ribosome has evolved with the lowest fidelity, with error rates of 1 in 10^3-10^4 (14-16). Presumably, this high error rate is tolerated because mistakes made during translation will only be present in that one specific protein.

Ideally, all three polymerization reactions would proceed in a manner whereby only the correct substrate is able to stably recognize the nucleotide template, ensuring a correctly encoded product. Initial attempts to explain this substrate selectivity relied on the specificity of Watson-Crick base pairing, where only complementary nucleotides form specific hydrogen-bonding interactions (17). However, a number of thermodynamic experiments demonstrate that free energy differences between correct and mismatched base pairs were not enough to account for the high fidelity observed in each polymerization reaction (13, 18, 19). Instead, each polymerase has evolved to recognize the invariant properties associated with the geometry of a Watson-Crick base pair (20).

Even though replication, transcription, and translation are carried out by different polymerases, the accuracy of each polymerization reaction is maintained using some common mechanisms. During the initial selection step, Watson-Crick base pair geometry is directly monitored by the polymerase to identify the correct incoming substrate (11, 20). Upon interrogation of the base pair geometry, the correct substrate induces a conformational change in the active site of the polymerase that accelerates the rate of new bond formation; while mismatched substrates produce a conformational change that slows this rate of new bond formation, allowing for the incorrect substrate to be rejected (13, 21-24). After new bond formation, a proofreading step occurs whereby mismatched nucleotides are identified and induce a conformational change to an inactive state, which triggers a post-incorporation correction mechanism that enhances the fidelity of these polymerization reactions (25-27).

In contrast to replication and transcription, which both use a DNA template to generate a nucleic acid product; translation involves a conversion of nucleic acid vocabulary (mRNA) into twenty different amino acids. This process requires the use of nucleic acid adaptor molecules, known as transfer RNAs (tRNAs), to decode the mRNA template three nucleotides at a time (28). During translation, the three nucleotide mRNA codon is decoded by the formation of three base pairs with the anticodon nucleotides of the tRNA adaptor. Because each tRNA has a unique

sequence and carries with it a specific amino acid, this adaptor is able to convert the mRNA message into an amino acid code.

Accurate decoding of the mRNA is further complicated by the degeneracy present in the genetic code, whereby 61 unique codons are used to encode 20 amino acids; however, prokaryotes contain only 30-40 distinct tRNA genes. This apparent discrepancy between the number of mRNA codons and tRNA molecules used for decoding was reconciled by the Wobble Hypothesis, which correctly posited that the rules for base pairing interactions between the third position of the mRNA codon and the tRNA anticodon are more relaxed (29). In the first and second positions of the codon-anticodon helix, only the A-U and G-C Watson-Crick base pairs were allowed. However, the third position of the codon-anticodon helix could also contain G•U, I•A, I•U, or I•C base pairs (**Fig. 1.1**). The Wobble Hypothesis was later expanded to include modification at position 34 of the anticodon, which permits one tRNA to decode all four nucleotides at the third position of the codon-anticodon helix (or, simply, at the wobble position) (30, 31).

The use of tRNA adapter molecules presents additional challenges to maintaining translational fidelity. First, fully complementary, or cognate tRNA, and those with a single base pair mismatch, or near-cognate tRNA, cannot be accurately distinguished from each other through free energy differences between codon-anticodon pairs (32). Also, because the mRNA is decoded using consecutive, three nucleotide codons, any uncoupled movement between the mRNA codon and tRNA anticodon would result in an mRNA frameshift, which triggers changes to the sequence of the nascent peptide (33, 34). Furthermore, the processes of decoding and peptide bond formation are physically separated by the tRNA, requiring correct decoding to be signaled over a distance of ~80 Å (**Fig. 1.2**). Finally, the nascent peptide chain remains covalently attached to a tRNA throughout the entire translation process, making it impossible to remove the incorrect amino acid once it has been incorporated as there is no way to reverse the formation of a new peptide bond in this synthesis process.

Despite nearly half a century of biochemical and structural studies, our understanding of the molecular mechanisms employed by the ribosome to facilitate accurate translation of the mRNA message remains incomplete. While we understand many aspects of cognate tRNA selection, it is still unclear how this selection is signaled to the peptidyl transferase center. Moreover, we do not understand how the three-nucleotide mRNA reading frame is maintained throughout the process of translation. Recent studies have shown that tRNA selection mechanisms can be disrupted by near-cognate tRNAs that have already been incorporated into the ribosome (27, 35). The work presented in this dissertation enhances our current knowledge of translational fidelity using both biochemical and structural studies of the bacterial ribosome.

The bacterial ribosome

All proteins in a cell are synthesized by the ribosome. In all three domains of life, this large macromolecular machine is comprised of two asymmetric subunits, each with a specific role in protein translation (**Fig. 1.2**). Despite differences thought to arise from divergent evolution, the eukaryotic and bacterial ribosomes share a conserved structural core of proteins and ribosomal RNA (rRNA) that contains the major functional centers of the ribosome (36, 37). These shared core components make the simple bacterial ribosome an ideal model system for exploring the molecular mechanisms involved in maintaining ribosomal fidelity.

In bacteria, ribosomes are composed of the two asymmetric subunits, each named after their size in Svedberg units, or sedimentation rate, the 30S and 50S subunits. The smaller 30S subunit is composed of 16S rRNA and ~20 ribosomal proteins (r-proteins), is responsible for decoding the mRNA through the selection of cognate tRNA; while the larger 50S subunit contains the 23S and the 5S rRNAs and ~30 r-proteins and facilitates new peptide bond formation (38-40). Each subunit forms part of the three tRNA binding sites: the acceptor (A), peptidyl (P), and exit (E) sites.

The 30S subunit forms four structurally distinct domains: the 5', central, 3' major, and 3' minor domains (**Fig. 1.3**) (41). When first characterized using electron microscopy, these domains were described using anthropomorphic terms: body, head, platform, and penultimate stem, respectively (42, 43). The 5' body domain was further divided into three subdomains, with the first third forming the shoulder domain, and the last third containing the spur domain. This multi-domain architecture of the 30S is reflective of the conformational dynamics necessary to decode the mRNA message, allowing the domains to move in relation to each other during the different stages of translation.

The large subunit of the ribosome forms a single compact mass with five protruding mobile elements: the L1 stalk, the A-site finger, the L7/L12 stalk, protein L9, and the central protuberance (**Fig. 1.4**). Each of these mobile elements plays a specific role during translation. The L1 stalk interacts with the tRNA in the E site, regulating tRNA movement and release from the ribosome (44, 45). The A-site finger is comprised of Helix 38 (H38) of the 23S rRNA, which protrudes from the 50S to contact the small 30S subunit near the A site. This flexible helix acts to attenuate the movement of tRNA through the ribosome by controlling the speed of tRNA movement and the rotation state of the two subunits (46, 47). The L7/L12 stalk is part of the GTPase activation center and helps to recruit and stabilize guanosine 5'-triphosphate (GTP) hydrolyzing enzymes, also known as GTPases (48). These GTPases act as molecular switches, regulating initiation, elongation, and termination through interactions with the GTPase activation center and resulting in the hydrolysis of GTP to GDP. The peptidyl transferase center (PTC), or catalytic site for this reaction, is located at the top of the P- and A-tRNA binding sites (49). Finally, the central protuberance, comprised mainly of 5S rRNA and r-proteins L5, L18, and L27, is believed to facilitate communication between the peptidyl transferase center (PTC) and the GTPase center (reviewed in (50)).

In the 70S ribosome, the 30S and 50S subunits are held together by 12 intersubunit contacts, or bridges, formed predominantly by RNA-RNA interactions (**Fig. 1.5**) (49, 51-53). Notably, bridge B1b is the only intersubunit bridge comprised solely of protein contacts, between 30S r-proteins S13 and S19 and L5 from the 50S subunit. Mutations that disrupt this intersubunit bridge are lethal because they compromise cell growth, presumably through the disruption of ribosomal subunit association (54). When the two subunits are joined through the formation of these intersubunit bridges, the three tRNA binding sites are formed.

The tRNA structure

tRNA is the essential adaptor molecule in translation that converts the nucleic acid mRNA sequence into the amino acid sequence of a protein. Each tRNA must accurately decode its specific cognate codon but still interact with translational machinery in a uniform manner. To overcome the intrinsic differences in the strengths of the codon-anticodon helix, tRNAs have evolved idiosyncratic nucleotide sequences while maintaining nearly universal secondary and tertiary structures. In addition to optimization of the canonical RNA nucleotides, tRNAs undergo extensive post-transcriptional modification, containing almost 10-fold more modifications than any other nucleic acid molecule (55). These modifications fine-tune tRNA flexibility and codon recognition, resulting in tRNAs that are highly specific for their unique cognate codon but still interact with translational machinery in a uniform manner.

Nearly all tRNAs adopt a characteristic "cloverleaf" secondary structure that can be divided into the following subdomains: the acceptor stem, the D stem loop, the anticodon stem loop (ASL), the TΨC stem loop, and a variable region (**Fig. 1.6A**) (56, 57). The acceptor stem, formed by the 5' and 3' termini of the RNA, contains the 3' CCA tail of the tRNA, where the amino acyl group is covalently attached. The ASL contains the anticodon used to decode the

mRNA. The D and TΨC stem loops are named after the invariable dihydrouridine (D) and ribothymidine (T) nucleotides found in each loop of the arm domains.

Even though deviations from the nearly universal "cloverleaf" secondary structure are known, the immutable L-shaped tertiary structure ensures each tRNA can interact with the two subunits of the ribosome (**Fig. 1.6**) (58). The L-shaped tertiary structure of all tRNAs is formed by two nearly perpendicular A-form double helices that are roughly 70 Å long and 20 Å wide (59). The two ends of the L, formed by the acceptor stem and the ASL, are separated by a distance of almost 80 Å, allowing these two essential regions of the tRNA to simultaneously interact with the decoding center in the small subunit and the PTC in the large subunit. The upper arm of the L is formed by stacking of the acceptor stem and the TΨC stem to create a continuous eleven-base-pair double helix. While the ASL and the D stem form a similar stacking interaction to create the lower arm of the L, there is a notable kink (~26°) between the two stem axes that creates a flexible hinge domain (60, 61). The L-shaped tertiary structure of the tRNA is stabilized by a long-range base-pair interaction between the D and TΨC loops, termed a kissing loop, forming the outer corner, or elbow region of the tRNA.

Prior to translation, tRNAs are charged with their specific aminoacyl groups by tRNA synthetases. These aminoacyl groups are attached to their specific tRNA at the 3' adenosine (A76) through an ester linkage. This labile aminoacyl bond is protected from hydrolysis by the formation of a ternary complex composed of the aa-tRNA, GTP, and elongation factor Tu (EF-Tu). The strong affinity of EF-Tu•GTP for aa-tRNA and the high concentration of EF-Tu in the cell ensures that almost all aa-tRNA will be bound in the ternary complex with EF-Tu and GTP, both protecting the labile aminoacyl bond and preparing the tRNA for use in translation (62). For clarity, charged tRNAs can be distinguished from deacylated tRNAs through the inclusion of a three-letter amino acid code written before the tRNA identity. For example, Lys-$tRNA^{Lys}$, is a $tRNA^{Lys}$ charged with a lysyl aminoacyl group.

The translation cycle

There are four fundamental steps in translation that are conserved in all domains of life: initiation, elongation, termination, and recycling **(Fig. 1.7**). During translation initiation, mRNA is selected and initiator tRNA is recruited along with IF2 to the start codon in the 30S P site. Translation initiation is completed by the recruitment of the 50S and concomitant dissociation of IF1 and IF3 to form a complete 70S ribosome. During the elongation phase of translation, new aminoacylated-tRNA (aa-tRNA) substrates are presented to the A site of the ribosome in the form of a ternary complex. Correct mRNA decoding results in release of the aa-tRNA from the ternary complex and full accommodation into the 50S A site. The proximity and precise orientation of A-site and P-site tRNA results in spontaneous peptide formation to elongate the nascent peptide chain by one amino acid. Elongation factor G (EF-G) mediates translocation, or movement of the codon-anticodon helix from the A to P and P to E sites on the 30S, freeing the A site of the ribosome for the next round of amino acid incorporation. This process continues until a stop codon in the A site of the ribosome is recognized by a class I release factor (RF1 or RF2), triggering the hydrolysis of the nascent peptide chain. Finally, the ribosome recycling factor (RRF) and EF-G separate the ribosomal subunits so this process can start all over again for the next round of translation.

Translation initiation

In bacteria, the coupling of transcription and translation allows ribosomes to bind to the nascent mRNA even before transcription has finished. This coupling not only allows bacteria to rapidly adapt to environmental changes, but also protects the mRNA from degradation. Initiation of translation is the rate-limiting step, with the complete assembly of a ribosome on the mRNA

occurring on the order of seconds, while peptide bond formation occurs at a rate of ~12-20 amino acids per sec (63-66).

Translation initiation occurs in three discrete steps requiring initiation factors 1 (IF1), IF2, and IF3. First, the mRNA binds to the 30S subunit in a sequence-independent manner. Base pairing between the Shine-Dalgarno (SD) sequence, a polypurine tract upstream of the initiator codon, and the complementary 16S rRNA anti-Shine Dalgarno sequence (ASD) positions the start codon in the P site of the ribosome (67, 68). Then IF2, initiator fMet-tRNA^{fMet}, and GTP bind to the 30S subunit to form the transient preinitiation complex (30S PIC). Correct positioning of the mRNA required for efficient and accurate translation is enhanced by the SD sequence, which in *E. coli* has a six-base consensus sequence of 5'-AGGAGG-3'; the spacing between the SD sequence and the start codon, which is typically 7-10 nucleotides; and the nucleotide sequence of the start codon, which is most often 5'-AUG-3' (all shown in the 5'-3' direction)(69-71). The second step in translation initiation occurs when initiation factor IF2 binds the fMet moiety of the initiator fMet-tRNA^{fMet}, positioning the tRNA anticodon for recognition of the AUG start codon (66, 72, 73). This recognition converts the 30S PIC into the active 30S initiation complex (30S IC). Initiation is completed by the rapid docking of the 50S subunit, accompanied by dissociation of IF1 and IF3 to form the 70S initiation complex (66, 74). This final step in translation initiation results in a complete 70S ribosome containing a single fMet-tRNA^{Met} in the P site of the ribosome that is ready to undergo the first round of tRNA selection.

Translation elongation

The elongation phase of translation is a repetitive cycle in which the mRNA template is decoded by the correct tRNA adaptor molecule and the nascent peptide chain is elongated by one amino acid. This process can be broken down into three discrete steps: decoding, or selection of

the correct tRNA; peptide bond formation; and translocation of the codon-anticodon helix to prepare for the next round of elongation (**Fig. 1.7**).

The selection phase of elongation starts by recruitment of a ternary complex to the GTPase center of the 50S through interactions with the multimeric ribosomal protein L7/L12. This rapid initial binding of the ternary complex is highly dynamic and independent of mRNA interactions (48, 75). The aa-tRNA undergoes a conformational distortion characterized by a ~30° bend, allowing the tRNA to scan the mRNA codon in the 30S decoding center (76-79). This strained conformation was aptly termed the A/T state (79), where the anticodon end of the tRNA interacts with the mRNA codon in the A site decoding center while the 3' end remains bound to EF-Tu as part of the ternary complex in the GTPase center on the 50S subunit (**Fig. 1.8)**. In the decoding center, interactions with the mRNA codon stabilize cognate tRNA, while non-cognate and near-cognate tRNAs are less stable and could dissociate from the ribosome.

The formation of a cognate codon-anticodon interaction causes a conformational change in the decoding center of the 30S subunit that is conveyed over ~80 Å to EF-Tu in the GTPase center of the 50S subunit (**Fig. 1.8**). The mechanism used to signal cognate decoding is still a topic of debate and could be conveyed through a number of different pathways. As a large part of my dissertation research focuses on how this signal is communicated, the current model for communicating cognate decoding will be discussed later in this introduction.

After GTP hydrolysis and release from EF-Tu, the aa-tRNA moves from a distorted A/T state to a fully accommodated A/A state (**Fig. 1.2**) (60, 80). The ASL domains of non- and near-cognate tRNA are not stabilized in the 30S decoding center and have higher K_{off} values that result in dissociation from the ribosome after release from EF-Tu (24, 81).

Accommodation into the A site results in the alignment of the 3' ends of both tRNAs in the A and P sites for spontaneous peptide-bond formation (82-84). The 3' CCA ends of the two tRNAs are held in place through interaction with the N-terminus of r-protein L27 and 23S rRNA residues

A2602, A2451, and U2584. The new peptide bond is formed through the nucleophilic attack of the carbonyl carbon of the peptidyl-tRNA by the α-amino group of the aa-tRNA, resulting in the transfer of the nascent peptide chain to the A-site bound tRNA (83, 85).

After peptide bond formation, the A-site decoding center in the 30S subunit is still occupied by the peptidyl-tRNA. In order for translation to continue, the codon-anticodon helix must be moved to the next tRNA binding site in a process called translocation. Once the new peptide bond is formed, the 3' ends of the deacylated tRNA in the P site and the peptidyl-tRNA in the A site move to the E and P sites, respectively, while the ASL portions of the tRNAs remain bound to the mRNA in the P and A sites resulting in the P/E and A/P hybrid states (86). This movement of the tRNA into the hybrid states is accompanied by a ratchet-like subunit rotation where the 30S subunit rotates ~10° relative to the 50S subunit (87).

The second step of translocation involving the movement of the mRNA-tRNA helix is catalyzed by the elongation factor G (EF-G) and GTP. Binding of EF-G to the ribosome stabilizes this ratchet-like subunit rotation (88, 89). The movement of the codon-anticodon helix is accomplished by a counterclockwise swiveling of the head domain, in the direction of translocation (90, 91). EF-G synchronizes this movement of the codon-anticodon helix and the 30S head domain through the use of two protruding loops (92) . The coupled movement of the tRNA with the mRNA, such that the mRNA only advances by one codon, is mediated by the insertion of loop I from domain IV of EF-G into the minor groove of the codon-anticodon helix. A second loop (loop II) from domain IV of EF-G is inserted into the minor groove of h34 in the head domain of the 30S subunit, linking the swiveling movement of the head domain with the codon-anticodon helix. Once the tRNAs have been moved into the E and P sites, the ribosome reverses the rotation of the head domain and the ratchet-like subunit rotation in order to prepare for the next round of translation elongation.

Translation termination

Translation is terminated when a stop codon is present in the A-site decoding center, signaling the end of the protein coding sequence. This stop codon is recognized by a class I release factor (RF) protein, which terminates protein synthesis through water-mediated hydrolysis and release of the nascent polypeptide chain from the ribosome. In bacteria, there are two class I release factors with overlapping specificities: RF1 recognizes 5'-UAG-3' and 5'-UAA-3' stop codons, while RF2 recognizes 5'-UGA-3' and 5'-UAA-3' stop codons (93). When RFs bind to a stop codon in the A site, the first two bases of the stop codon are extensively probed by a hydrogen bond network to ensure RF termination only occurs at stop codons with premature RF termination of translation occurring at a rate of 1 false stop per 100,000 codons in *E. coli* (94). Crystallographic studies of a RF2 bound to the ribosome, locked in either a pre- or post-release state, confirm that the RF2 induces conformational changes in the PTC that expose the peptidyl ester of the peptidyl-tRNA for water mediated hydrolysis of the nascent peptide chain (95-98).

Ribosome recycling

The final step in translation is the disassembly of the 70S ribosome by RRF and EF-G via a mechanism that is still poorly understood (99). After the release of the nascent peptide by RF-mediated hydrolysis, the mRNAs and tRNAs remain bound to the 70S ribosome. Separation of the two asymmetric subunits during this last step of the translation cycle frees the mRNA and tRNAs, preparing the subunits for the next round of translation (100).

The role of the ribosome in translational fidelity

The first indication that the ribosome might be involved in the selection of tRNA came from the observation that both antibiotics that bind to the ribosome and mutations in ribosomal components could alter the fidelity of translation. Streptomycin was the first antibiotic known to

target the ribosome (101). The addition of streptomycin in *in vitro* translation assays caused tRNA selection errors identified by the misincorporation of amino acids not encoded by the mRNA (102). Streptomycin also increased the frequency of nonsense suppression, or the ability to read-through a stop codon. Using the mutagen N-methyl-N-nitroso-N-nitroguanidine, several auxotropic mutants of *E. coli* were generated, each containing premature stop codons in genes of essential enzymes required for the biosynthesis of different amino acids (103). In the presence of streptomycin, these auxotrophs expressed enough of the essential enzymes sufficient to partially restore growth by nonsense suppression of the premature stop codon (103). Because streptomycin specifically targeted the ribosome and could alter the decoding of the mRNA, it was clear that the ribosome could influence the fidelity of protein synthesis.

Our understanding of the ribosome and its role in translation was enhanced by the identification of spontaneous streptomycin resistant (SmR) and streptomycin-dependent (SmD) strains of *E. coli* that increased the accuracy of translation (103, 104). The SmR and SmD mutations, collectively referred to as restrictive mutations due to their ability to prevent translation errors, were mapped to the ribosomal protein S12 in the 30S subunit (105, 106). These restrictive mutations created hyperaccurate ribosomes, not only decreasing streptomycin-induced ambiguity, but also decreasing the frequency of translation errors induced by kanamycin, neomycin, paromomycin, ethyl alcohol and high concentrations of Mg^{2+} (102, 105-107). Restrictive mutations also displayed a slower rate of translation compared to wild-type ribosomes, suggesting that while the potential for increased translational fidelity was achievable, the ribosome had evolved an optimal balance between speed and accuracy (6, 108).

Early genetic studies identified second-site mutations in ribosomal proteins S4 or S5 that reverse the hyperaccurate phenotype of restrictive mutations (109, 110). These spontaneous ribosomal ambiguity (*ram*) mutations were identified in nonsense suppression screens of similar auxotropic mutants of *E. coli* as described above, however these *E. coli* also contained a SmR or

SmD mutation. These *ram* mutations counterbalanced the yet unknown structural changes resulting from restrictive mutations by reintroducing ambiguity into the decoding of the mRNA (109, 110). Subsequent *in vivo* and *in vitro* characterization of these S4 and S5 *ram* mutations showed an increase in nonsense suppression and tRNA selection errors similar to the ambiguity induced by the addition of streptomycin (109). Intriguingly, the error-prone effects of *ram* mutations and streptomycin were additive, suggesting that they each affected ribosomal accuracy using different pathways (111).

Most of the identified chromosomal mutations that altered ribosomal fidelity in early genetic studies were located in ribosomal proteins that were encoded by a single gene. The isolation of rRNA mutations that affected fidelity was hindered by multiple copies of rRNA genes present in the genome. The discovery that the anti-Shine-Dalgarno sequence at the 3' end 16S rRNA could be mutated to allow for the selection of mRNAs with different SDs allowed for a generation of mutant ribosomes that could be used as a selection tool (112). By changing the anti-Shine-Dalgarno sequence of a plasmid encoded 16S rRNA, a specialized population of ribosomes could be generated that would only translate mRNAs with the corresponding SD sequence (113, 114). Using this specialized ribosome population, the 16S rRNA was screened for missense suppressor and nonsense suppressor mutation (115).

A randomly mutagenized 16S rRNA plasmid library was generated by propagation of the plasmid in XL1-Red, an *E. coli* strain that contained deficiencies in three of the primary DNA repair pathways (115). The resulting plasmid library was screened for mutations that decreased translational fidelity through tRNA selection errors by missense suppression and nonsense suppression screens. The missense suppressor mutations were identified by their ability to suppress a missense substitution of the catalytic glutamate in the *lacZ* gene through selection of a near-cognate $tRNA^{Glu}$ instead of the encoded $tRNA^{Asp}$ (115). Nonsense suppressors were identified by their ability to bypass a premature stop codon in the *lacZ* gene (115). Using these missense and nonsense suppressor screens, several 16S rRNA *ram* mutations were identified.

These 16S rRNA *ram* mutations clustered into three distinct groups: near the decoding center, near the S4/S5 interface and near intersubunit bridge B8, a point of contact between the 16S rRNA h8 and h14 in the 30S subunit and protein L14 and L19 in the 50S subunit (115). The similarities between the missense and nonsense suppression of 16S rRNA *ram* mutations and *ram* mutations identified in ribosomal proteins S4 or S5 suggested all *ram* mutations could share a common mechanism (115).

The analysis of streptomycin and the subsequent identification of ribosomal mutations that could alter translation demonstrated that the ribosome directly affected the accuracy of protein synthesis. Initial model for this ribosomal fidelity during decoding proposed the ribosome used direct interactions with the codon-anticodon interface to distinguish cognate and near-cognate tRNA by recognition of correct base-pairing geometry (102, 116). However, the restrictive and *ram* mutations were located in different regions of the ribosome that were hard to reconcile with this idea of geometric recognition.

The kinetic proofreading model

Biochemical characterization of the ribosome established that selection of the correct tRNA involves a kinetic proofreading mechanism wherein tRNA selection can be divided into two distinct dissociation steps that are separated by irreversible GTP hydrolysis (117-119). GTP hydrolysis on the ribosome is essentially an irreversible process (120). As a consequence, tRNA selection is a unidirectional process in which tRNA must pass through both steps prior to being incorporated into the ribosome.

The ribosome controls selection of the aa-tRNA through the use of four rate constants (81, 117, 118). In addition to stabilizing cognate tRNA at both dissociation steps, the ribosome accelerates the forward rate of GTPase activation (~4000-fold) and accommodation (~60-fold) for cognate tRNA (81). As a result of the differences in these four rate constants, cognate tRNAs are rapidly accommodated into the ribosome, while near-cognate tRNAs are more likely to be

rejected. The considerable increase in the rate of GTPase activation suggests that the ribosome recognizes the structural differences between cognate and near-cognate tRNA, and responds accordingly through an induced-fit mechanism (81).

Structural basis of cognate tRNA recognition

Crystallographic studies of the 30S subunit confirmed that cognate tRNA is identified through steric complementarity and a hydrogen bonding network with the universally conserved 16S rRNA nucleotides A1492, A1493, and G530 (**Fig. 1.9**) (22, 24). When cognate tRNA binds to the A site of the ribosome, nucleotides A1492 and A1493 flip out from the internal loop of helix 44 (h44) to form A-minor interactions with the minor groove of the first and second base pairs of the codon-anticodon helix (**Fig. 1.9B**) (22). Additionally, nucleotide G530 rotates from a *syn* to an *anti* conformation to directly engage the nucleotides in the second position of the tRNA anticodon and the third position of the mRNA codon. The minor groove of the first base pair in the codon-anticodon helix is interrogated through a tight packing type I A-minor interaction between 16S rRNA nucleotide A1493 and both 2' OH groups of codon-anticodon base pairs (**Fig. 1.9C**) (22). Universally conserved G530 creates a purine-purine interaction with A1492 to form an expanded type II A-minor interaction that spans the second base pair of the codon-anticodon helix, again interacting with both 2' OH groups (**Fig. 1.9D**) (22). The close packing of these three 16S rRNA nucleotides allows recognition of Watson-Crick geometry in the first two base pairs of the codon-anticodon helix through steric complementarity, using favorable hydrophobic contacts, base stacking, and van der Waals interactions to create an energetically favorable interaction (22, 121). The third, or wobble, base pair of the codon-anticodon helix is not closely monitored, with the 2' OH group of the third nucleotide in the codon forming a single hydrogen bond with G530 and an indirect metal-mediated interaction with 16S nucleotide C518 and the carbonyl backbone of Pro 48 of S12 (**Fig. 1.9E**) (22). The lack of close contacts and hydrogen

bonding between the ribosome and the third base pair of the codon-anticodon helix explains the degeneracy present in the genetic code, where the first two base pairs must form only canonical Watson-Crick interactions while the third base pair can form a wide variety of interactions. Once recognition of a cognate tRNA-mRNA interaction occurs in the A-site decoding center, an inward rotation of the 30S shoulder domain towards the platform domain and a swiveling of the 30S head domain towards the shoulder and subunit interface occur, resulting in 30S "closure" around the A-site tRNA. (**Fig. 1.10**) (24).

Binding of a near-cognate codon in the decoding center induces structural changes that are distinct from cognate decoding (**Fig. 1.11**). When a G•U mismatched base pair is present in the first or second position of the codon-anticodon helix, the uracil nucleotide of the codon moves away from the minor groove of the helix (24). This disrupts the hydrogen bond network with A1492 and A1493 and causes desolvation of the hydrogen bonds. The near-cognate codon-anticodon interactions do not induce a 30S domain closure, instead swiveling of the head domain occurs in the opposite direction, resulting in an inactive ribosome conformation.

The aminoglycoside paromomycin affects the rate of almost every step during tRNA selection, but most pronounced are the changes in the rates of GTPase activation and accommodation (122). Structural studies of paromomycin bound to the 30S subunit shows paromomycin binds to the major groove of h44, forcing A1492 and A1493 to adopt the same orientation as observed with cognate codon-anticodon interactions (123). By pre-ordering the decoding center through the flipping out of A1492 and A1493, paromomycin stabilizes near-cognate tRNA binding to the decoding center (24). Because paromomycin reduces the energetic costs of domain closure, the suboptimal A-minor interactions with near-cognate tRNA binding are sufficient to drive full domain closure of the 30S subunit (24, 124).

An integrated model for tRNA selection

The drastic increases in GTPase activation by the kinetic proofreading mechanism suggests there is signaling of a cognate decoding interaction in the 30S subunit is conveyed over ~80 Å to EF-Tu in the GTPase center of the 50S subunit (**Fig. 1.8**). The inward movement of the 30S shoulder domain associated with domain closure could be the first step in signaling codon recognition. In addition to the structural analysis of decoding in the 30S A site, crystallographic studies of a ternary complex bound to the 70S ribosome showed that movement of the shoulder domain moves 16S rRNA towards EF-Tu, resulting in interactions between domain 2 of EF-Tu and h5 of 16S rRNA (79). In fact, these regions both in EF-Tu and 16S rRNA are extremely conserved (> 90%) across all domains of life, suggesting this interaction is essential for function(79).

This domain closure model helped explain mutation the restrictive and *ram* mutation phenotypes (24, 119). Several *ram* mutations were localized at the ribosome interface between S4 and S5 proteins. Because the inward movement of the shoulder domain resulted in a disruption of the r-protein interface between S4 and S5 on the solvent side of the 30S subunit, it was hypothesized that these *ram* mutations functioned by destabilizing the open conformation of the ribosome (24). By disrupting the interactions between S4 and S5, these *ram* mutations were believed to reduce the energy barrier for adopting the closed conformation, allowing near-cognate tRNA to also induce domain closure. Conversely, restrictive mutations located in S12 on the interface side of the 30S subunit altered contacts with 16S rRNA h44 and h27 that were formed as a result of domain closure (24). These restrictive mutations were believed to increase the stringency of tRNA selection by destabilizing the closed form of the 30S and increasing the energy barrier for cognate tRNA selection.

Despite the effectiveness of the domain closure model to rationalize the fidelity of tRNA selection, a growing body of evidence suggested additional interactions between the 30S subunit

and EF-Tu were necessary to signal cognate decoding. Disruption of the S4-S5 interface did not correlate with ribosomal accuracy (125). In fact, some mutations that disrupt the S4-S5 interface actually reduce tRNA selection errors. Restrictive mutations in S12 were found to have no effect on the rate of GTPase activation, and instead altered decoding through interactions with L19 of the 50S subunit (126, 127). Finally, the domain closure model could not account for the role of intersubunit bridge B8 in tRNA selection (see **Fig. 2.1** in Chapter 2) (115, 126, 128).

To explore the structural basis of tRNA selection, I analyzed two distinct classes of 16S rRNA *ram* mutations. The 16S rRNA *ram* mutations near the S4/S5 interface were expected to alter decoding through disruption of domain closure. However, the 16S rRNA *ram* mutations near bridge B8 suggested this intersubunit bridge played a role in maintaining translational fidelity by negatively regulating GTPase activation. The structural analysis of two representative 16S rRNA *ram* mutations, G299A, located near the S4/S5 interface, and G347U, located near B8, is presented in Chapter 2. My work shows that despite their different locations, both 16S rRNA *ram* mutations increase the rate of GTPase activation through disruption of the intersubunit bridge B8. This work highlights a previously unappreciated conformational rearrangement required for EF-Tu-mediated GTP hydrolysis and establishes a long-range signaling network linking the small and large subunits. The majority of ribosomal mutations that alter the accuracy of translation cluster around the S4/S5 interface, or near the intersubunit bridge B8. My work suggests that despite their disparate locations, all *ram* mutation alter tRNA selection by destabilization of the intersubunit bridge B8.

Loss of translational fidelity through mRNA frameshifts

During translation, the mRNA is decoded three nucleotides at a time. Changes in the mRNA reading frame, or frameshift errors, most often result in premature termination of translation through an out-of-phase stop codon producing truncated or misfolded proteins that are toxic (34).

The first evidence that the genetic code could be reprogrammed through changes in the mRNA reading frame came from genetic suppressor experiments in *Saccharomyces cerevisiae* and *Salmonella typhimurium* (129-133). These early studies found that despite genetic insertions or deletions in essential proteins, cells were able to survive using mutagen-induced suppressors of frameshifts (suf). These extragenic suppressors were found to compensate for genetic insertions through the decoding of a non-triplet codon.

The majority of frameshift suppressor mutations were found to be extragenic insertions within the ASL domain of tRNA genes that displayed Watson-Crick complementarity to the suppressible four nucleotide codon (129, 131, 134-136). Because of this Watson-Crick complementarity between the inserted nucleotide in the anticodon and the additional nucleotide in the expanded four nucleotide mRNA codon, early models for +1 frameshift suppression suggested these expanded ASLs could form a four-base pair codon-anticodon helix (see **Fig. 3.1A** in Chapter 3) (137-141). After the identification of frameshift suppressor tRNA that did not require Watson-Crick complementarity between the inserted nucleotide and the expanded codon, the yardstick model was proposed, whereby the insertion could alter the architecture of the ASL such that the anticodon was larger than canonical tRNA (139). This model postulates that the enlargement of the anticodon alone is responsible for the +1 frameshift regardless of the ability to form a Watson-Crick base pair in the fourth position of the codon-anticodon interface.

While the simplicity of these two models has made them an attractive explanation for the mechanism of +1 frameshifts , there was evidence that suggested +1 frameshift suppression occurred in the P site of the ribosome (142-144). Overexpression or depletion of the subsequent in-frame tRNA affects the frequency of +1 frameshifting events. This suggests some +1 frameshifting events occurred after the frameshift suppressor tRNA had been translocated to the P site (see **Fig. 3.1C** in Chapter 3). Additional biochemical characterization shows +1 frameshifts occurred through a repairing of the mRNA-tRNA interface in the P site when the peptidyl-tRNA

has a reduced affinity for the mRNA resulting from hypomodification, near-cognate decoding, or insertions outside of the anticodon (142, 145-148). Finally, mutations in the C-terminal tail of ribosomal protein S9, which directly interacts with P-site tRNA, were shown to cause +1 frameshifts (142, 148).

In order to better understand how the mRNA reading frame is maintained, we biochemically and structurally analyzed frameshift suppressor $tRNA^{SufJ}$, which decodes the four nucleotide codons ACC-A, ACC-U, and ACC-C as threonine. This work, presented in Chapter 3, shows that the C31.5 insertion of frameshift suppressor $tRNA^{SufJ}$ causes an 11.5 ° twist of the stem domain, moving the phosphate backbone by 7 Å on the 3' side and 4 Å on the 5' side (**Fig. 3.4**). However, the three nucleotide anticodon is preserved, allowing cognate mRNA-tRNA interaction with the first three nucleotides of the mRNA codon in the zero frame (Fig. 3.4, Fig. 3.S1). Using structural superpositioning, we suggest +1 frameshifts occur through the loss of gripping interactions with either EF-G during translocation, or with 16S rRNA after movement to the P site.

Retrospective editing

During DNA replication and mRNA synthesis, errors in the nascent chain are identified and removed through a retrospective proofreading step (11, 13). These polymerases have the ability to identify misincorporated nucleotides and remove them through cleavage of the nascent bond. After removal of the incorrect nucleotide, these polymerases are able to continue synthesis of the nascent product. In contrast to DNA and RNA polymerases, ribosomes do not have a similar proofreading mechanism. Unlike the synthesis of nascent nucleotides, the nascent peptide chain is covalently attached to a single tRNA, making it impossible to correct errors after they have been incorporated into the nascent peptide chain. As a result, models for ribosomal accuracy relied

primarily on correct selection of the incoming tRNA and maintenance of the mRNA reading frame .

Recent findings indicate an additional proofreading mechanism exists that functions after peptide bond formation and translocation to the P site of the ribosome (27, 35, 149). Analysis of this post-peptidyl-transfer-quality-control (post PT QC) mechanism shows that after incorporation of a near-cognate tRNA, a global loss of translational fidelity occurs. Once in the P site, the near-cognate tRNA compromises the accuracy of tRNA selection and triggers the premature termination of translation by RFs in the absence of a stop codon (27). This post PT QC mechanism invokes an active role for the P site in maintaining ribosomal accuracy.

Despite our knowledge of ribosomal structure, it is unclear how the mRNA-tRNA interface is monitored in the P site. In contrast to the A site of the ribosome, where the codon-anticodon helix is extensively monitored, only the third position, or wobble, base pair of the helix is held in place through stacking interactions formed with 16S rRNA nucleotides C1400 and G966 in the P site (53). Work presented in Chapter 4 provides insight into the molecular perturbations resulting from a near-cognate tRNA in the P site of the ribosome. X-ray crystallographic characterization of near-cognate $tRNA^{Lys}$ in the P site shows that formation of a mismatched U•U base pair in any position of the codon-anticodon helix alters the path of the mRNA. Due to the absence of an A-site tRNA, only the sugar of the first nucleotide of the A-site codon was visible in these ribosome complexes. However, the observed movement of the mRNA could potentially disrupt the boundary between the P-site and A-site codons, resulting in promiscuous interactions with incoming aa-tRNA and RFs.

Summary

The translational machinery has evolved to ensure the faithful replication of the genetic code in functional proteins. This accuracy is controlled by long-range signaling networks between the

subunit and the precise position of the tRNA on the mRNA message. The work presented in this dissertation helps expand our knowledge of the many molecular mechanisms that are essential for proper ribosomal function. While each project analyzes a different part of ribosomal accuracy, they each demonstrate ribosomal fidelity is maintained by the coordinated movement of several elements across the entire ribosome.

FIGURES

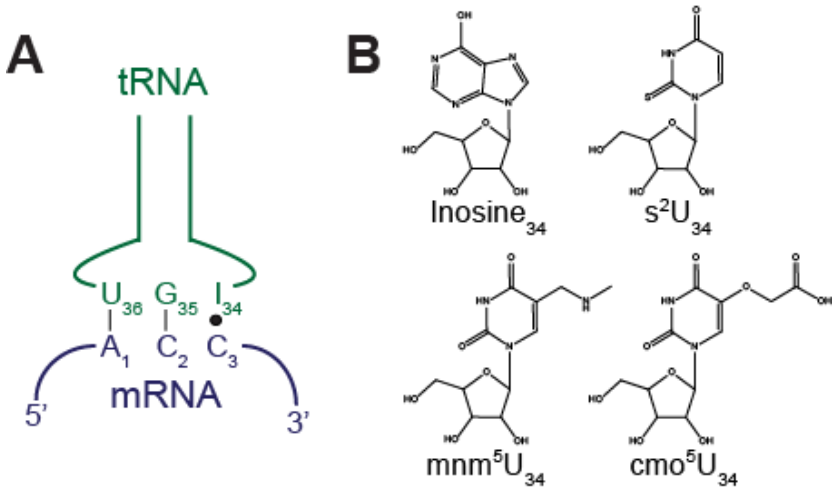

Figure 1.1. mRNA-tRNA decoding interactions. (A) The mRNA (blue) is decoded by the correct tRNA (green) through the formation of three base pair interaction. Cognate decoding requires Watson-Crick base pairing in the first and second positions (indicated by a line); in this case between mRNA A+1 and tRNA U36, and mRNA C+2 and tRNA G35, respectively. In the wobble position, additional types of interactions can form, in this case between mRNA C+3 and tRNA I34 (indicated by a dot). **(B)** Position 34 of the tRNA can be post-transcriptionally modified to allow the formation of nontraditional base pair interactions.

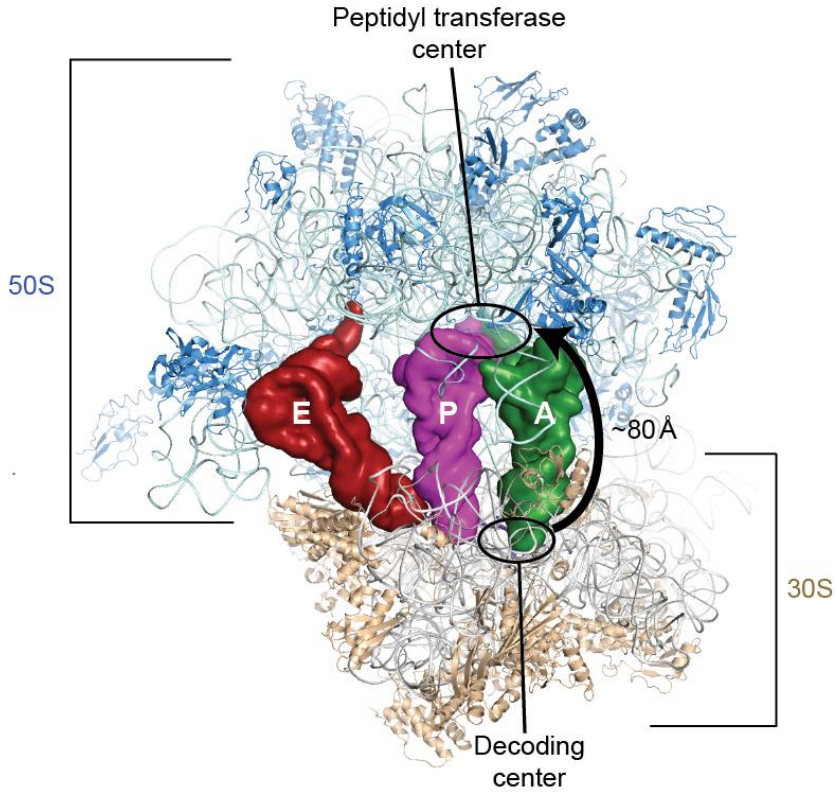

Figure 1.2. Overview of 70S ribosome subunits with A-, P-, and E-site tRNA. New substrate selection occurs in the decoding center of the 30S subunit (PDB ID 2WDG(80)), while peptide bond formation occurs in the peptidyl transferase center of the 50S subunit (PDB ID 2WDI). This view of the interface cavity shows the three tRNA binding sites: A site (green), P site (magenta), and E site (red).

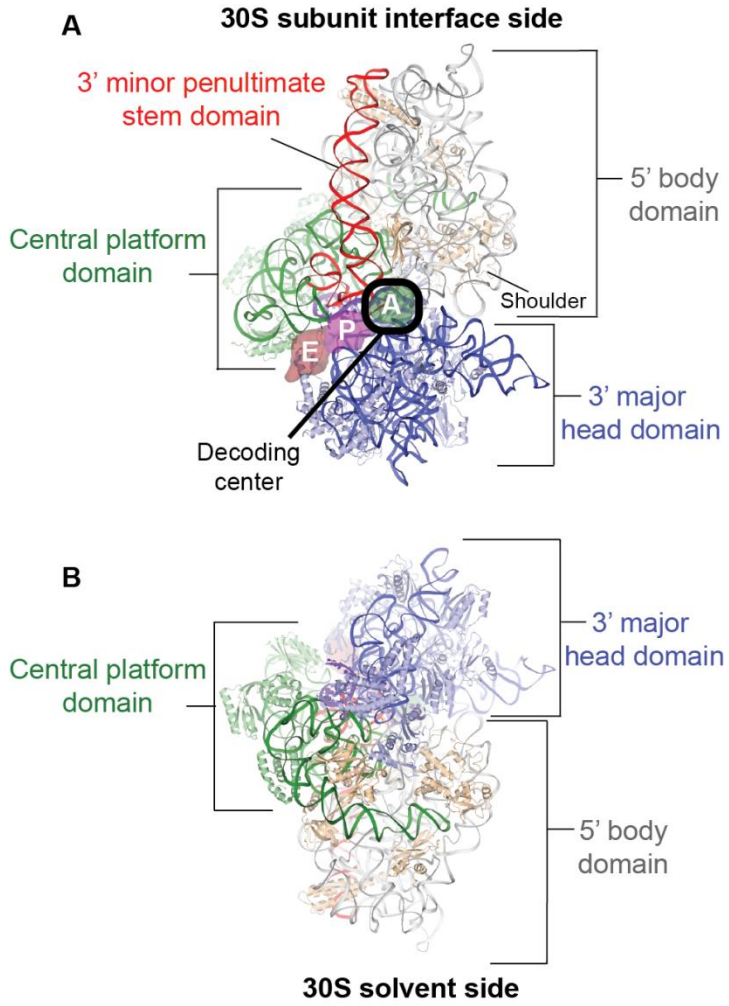

Figure 1.3. Tertiary structure of 30S ribosomal subunit. The subunit interface **(A)** and back solvent **(B)** view of the 30S subunit (PDB ID 1IBM(22)). The 30S is divided into the 5' body (gray), Central platform (green), 3' major head (blue), and 3' minor penultimate stem (red) domains. The three tRNA binding sites are shown in the subunit interface view.

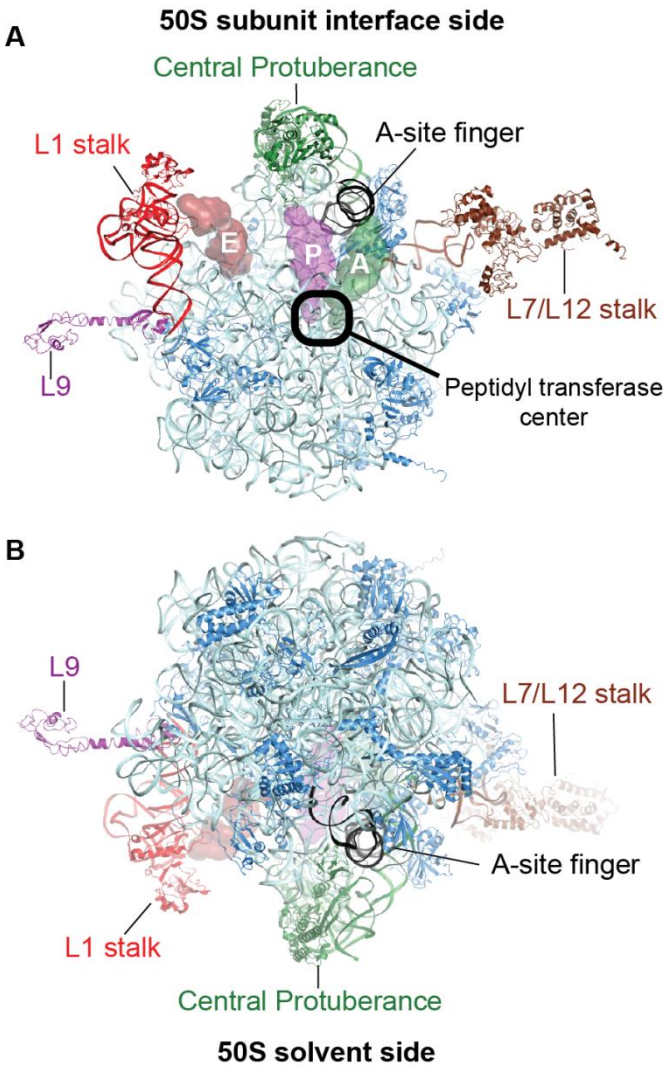

Figure 1.4. Key components of the 50S subunit. The subunit interface **(A)** and solvent **(B)** view of the 50S subunit (PDB ID 4HUB (150)). The mobile elements of the 50S include the L1 stalk (red), the A-site finger (black), the L7/L12 stalk (brown), L9 (purple), and the central protuberance (green). The three tRNA binding sites are shown in the subunit interface view.

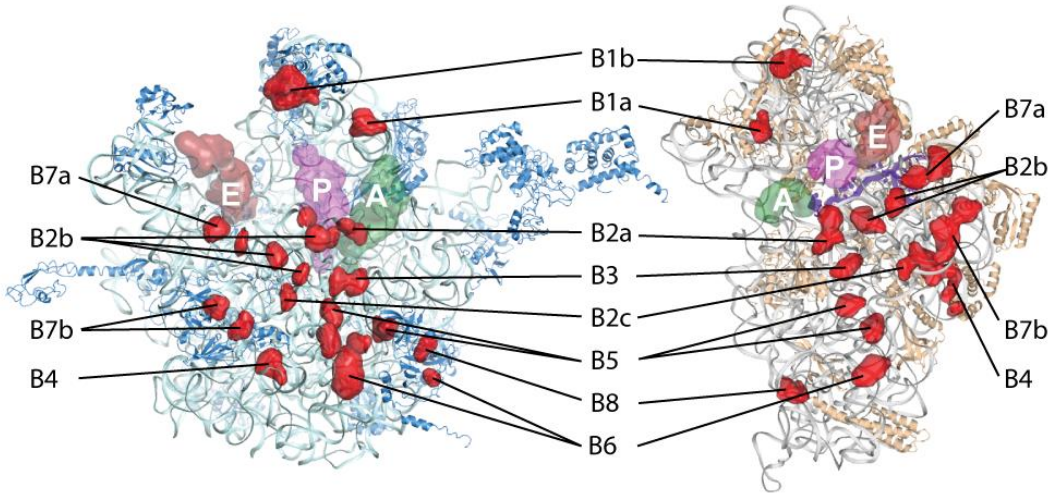

Figure 1.5. Intersubunit bridges between the 50S and 30S. The points of contact between the 50S (PDB ID 2J01) on the right and the 30S (PDB ID 2J00) on the left are shown in red in the space filling model. The A-, P-, and E-site tRNA are shown. Figure adapted from (49, 53).

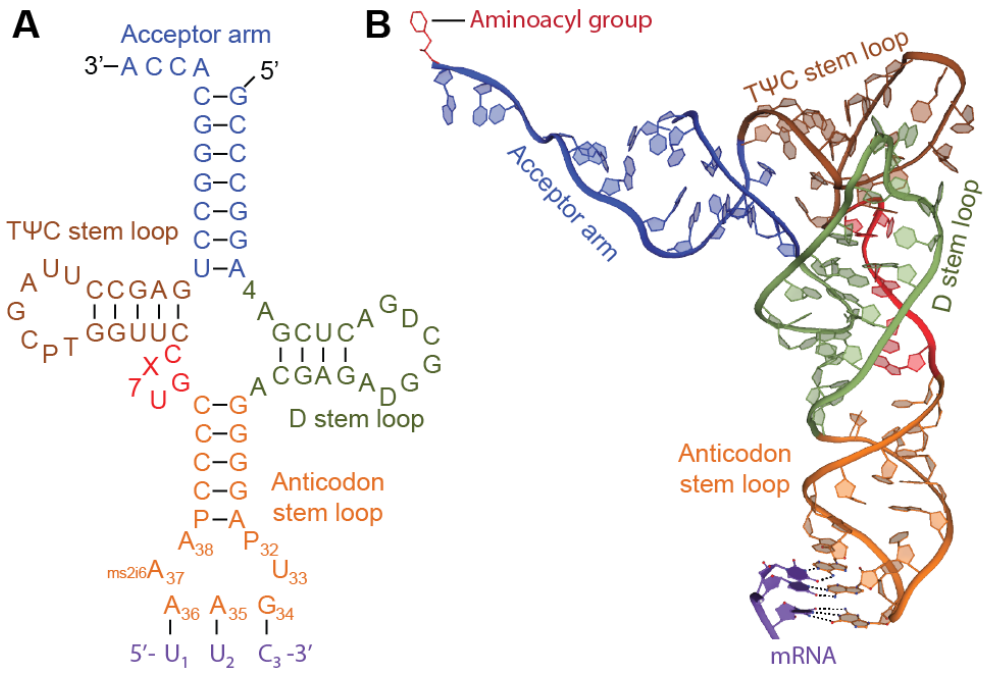

Figure 1.6. Structural domains of tRNAPhe bound to a cognate mRNA codon. (A) The characteristic "cloverleaf" secondary structure of $tRNA^{Phe}$ is composed of the acceptor stem (blue), the D stem loop (green), the anticodon stem loop (ASL, orange), the TΨC stem loop (brown), and the variable loop (red). **(B)** The tertiary structure of Phe-$tRNA^{Phe}$ with the attached phenylalanine amino acid is shown in red (PDB ID 2WDG) (80).

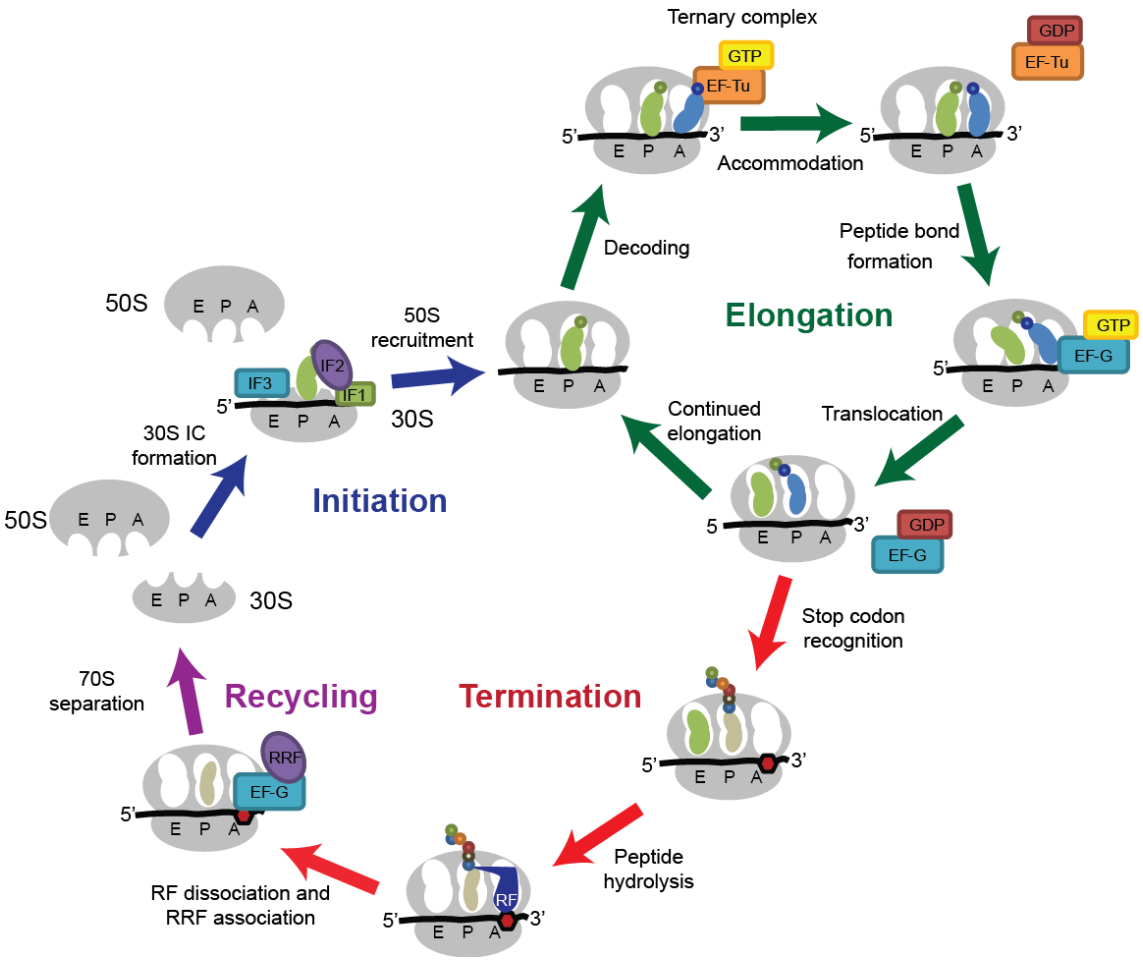

Figure 1.7. Schematic overview of the bacterial translation cycle. Translation occurs in four fundamental steps: initiation, elongation, termination, and recycling. For simplification purposes, only major steps are shown. Figure adapted from (151).

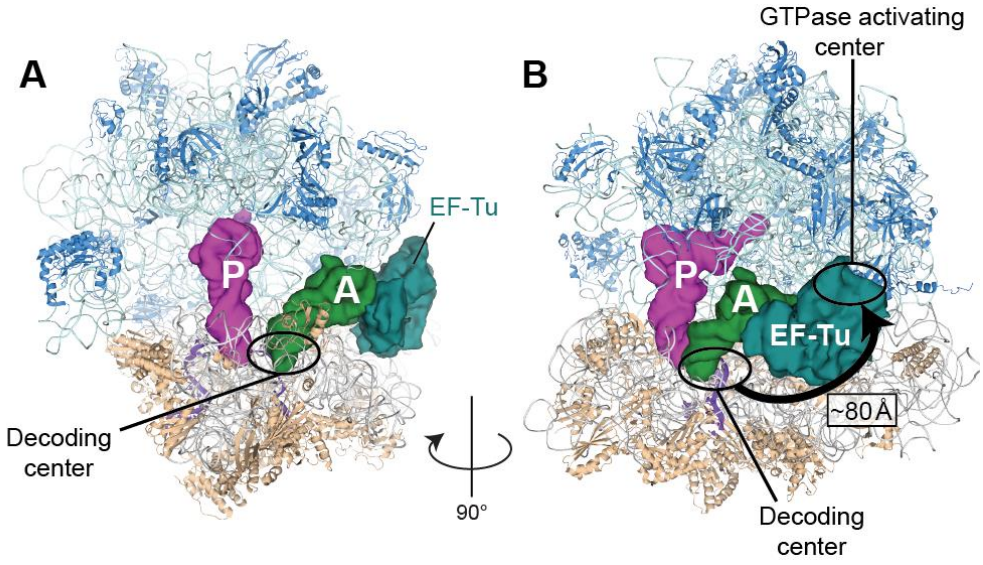

Figure 1.8. Ternary complex binding to the 70S ribosome. The aa-tRNA is brought to the ribosome in the form of a ternary complex with EF-Tu and GTP (PDB IDs 2WDG and 2WDI) (152). **(A)** From this orientation, the A/T state tRNA (green) can be seen in the bent conformation with the ASL domain decoding the mRNA in the A site, while the 3' end of the tRNA remains bound to EF-Tu (blue) as part of the ternary complex. **(B)** Cognate decoding must be signaled from the decoding center in the 30S subunit up to the GTPase center in the 50S, over ~80 Å away.

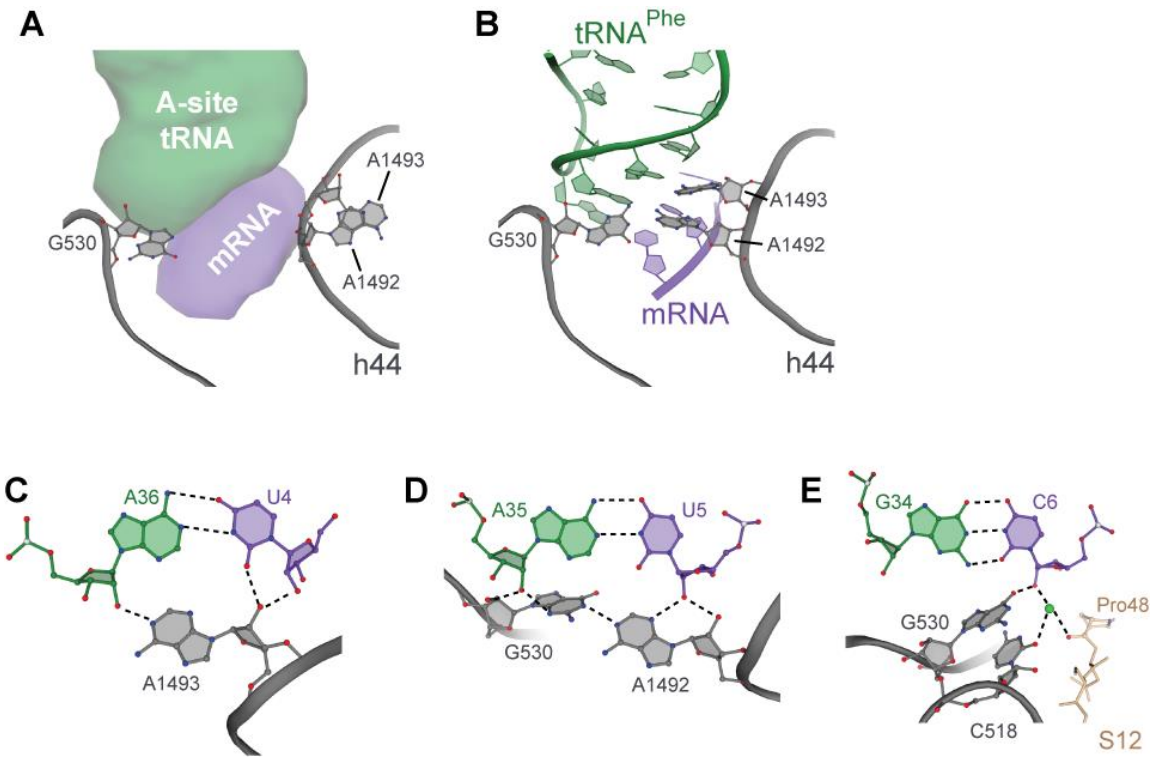

Figure 1.9. Identification of cognate decoding interactions by A-site decoding center. (A) In the absence of a tRNA, 16S rRNA nucleotides A1492 and A1493 occupy an internal loop of 16S rRNA helix 44 (h44), and G530 is in the *syn* conformation. The normal positions of the A-site tRNA (green) and mRNA (purple) are indicated. (PDB ID 1J5E) (153). **(B)** In the presence of a cognate decoding, 16S rRNA nucleotides A1492 and A1493 flip out of h44, and G530 rotates to the *anti* conformation to form A-minor type interactions with the codon-anticodon helix (PDB ID 1IBM) (22). **(C)** The Watson-Crick base pairing specificity of the first base pair in the codon-anticodon helix is monitored by the 16S rRNA nucleotide A1493 (gray) through formation of a type I A-minor interaction. **(D)** The second base pair of the codon-anticodon helix is monitored through the formation of an expanded type II A-minor interaction by 16S rRNA A1492 and G530. **(E)** The mRNA nucleotide in the wobble position forms a hydrogen bond with 16S rRNA G530 and a Mg^{2+} interaction with 16S rRNA C518 and the backbone of Pro48 in S12.

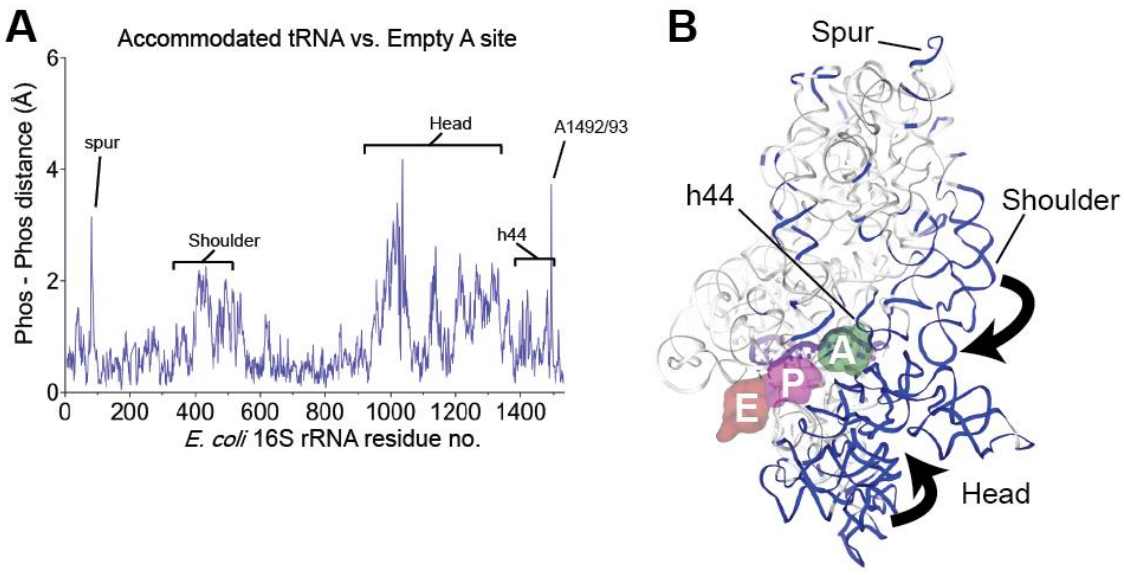

Figure 1.10. 30S domain closure. (A) Comparison of the 16S rRNA phosphate backbone displacement shows movement in the head and shoulder domains upon cognate tRNA decoding. 16S rRNA in the absence (PDB ID 1J5E,) or presence (PDB ID 1IBM, (22)) of a cognate tRNA were aligned by superpositioning of the platform domain (nucleotides 560-912). **(B)** Regions that displayed movements >1 Å were mapped onto the 16S rRNA and the general direction of movement is indicated by arrows. This figure was adapted from (24).

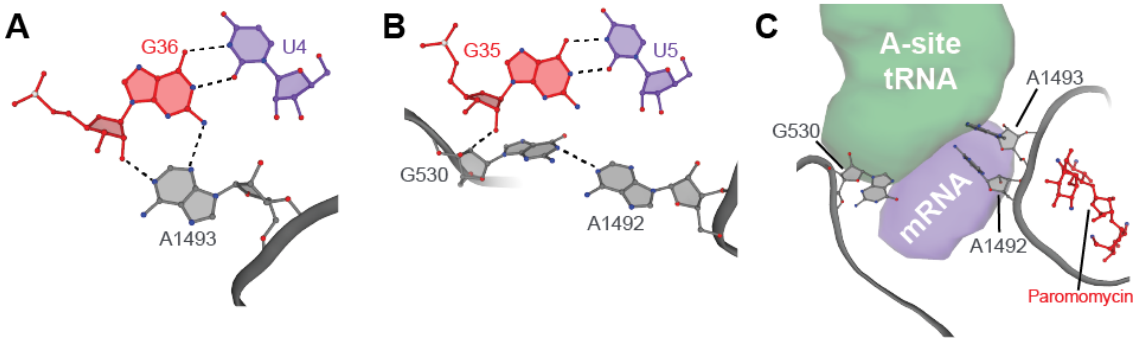

Figure 1.11. Mechanisms of near-cognate tRNA decoding. (A) The formation of a G•U base pair in the first position of the decoding center disrupts the type I A-minor interaction with 16S rRNA nucleotide A1493 by displacement of mRNA nucleotide U4 (PDB ID 1N32) (24). **(B)** The formation of a G•U interaction results in a similar disruption of the A-minor interaction with 16S rRNA nucleotides through the displacement of the mRNA. **(C)** The antibiotic paromomycin (red) binds to the major groove of h44, displacing 16S rRNA A1492 and A1493. The normal positions of A-site tRNA (green) and mRNA (purple) are indicated.

REFERENCES

1. Russell JB & Cook GM (1995) Energetics of bacterial growth: balance of anabolic and catabolic reactions. *Microbiological reviews* 59(1):48-62.
2. Furio V, Moya A, & Sanjuan R (2007) The cost of replication fidelity in human immunodeficiency virus type 1. *Proc Biol Sci* 274(1607):225-230.
3. Piepersberg W, Noseda V, & Bock A (1979) Bacterial ribosomes with two ambiguity mutations: effects of translational fidelity, on the response to aminoglycosides and on the rate of protein synthesis. *Mol Gen Genet* 171(1):23-34.
4. Zengel JM, Young R, Dennis PP, & Nomura M (1977) Role of ribosomal protein S12 in peptide chain elongation: analysis of pleiotropic, streptomycin-resistant mutants of Escherichia coli. *J Bacteriol* 129(3):1320-1329.
5. Galas DJ & Branscomb EW (1978) Enzymatic determinants of DNA polymerase accuracy. Theory of coliphage T4 polymerase mechanisms. *Journal of molecular biology* 124(4):653-687.
6. Galas DJ & Branscomb EW (1976) Ribosome slowed by mutation to streptomycin resistance. *Nature* 262(5569):617-619.
7. Ehrenberg M & Kurland CG (1984) Costs of accuracy determined by a maximal growth rate constraint. *Q Rev Biophys* 17(1):45-82.
8. Kurland CG & Ehrenberg M (1984) Optimization of translation accuracy. *Prog Nucleic Acid Res Mol Biol* 31:191-219.
9. Andersson DI, van Verseveld HW, Stouthamer AH, & Kurland CG (1986) Suboptimal growth with hyper-accurate ribosomes. *Archives of microbiology* 144(1):96-101.
10. Kirkwood TBL, Rosenberger RF, & Galas DJ (1986) *Accuracy in molecular processes : its control and relevance to living systems* (Chapman and Hall, London ; New York) pp xiv, 398 p.
11. Kunkel TA & Bebenek K (2000) DNA replication fidelity. *Annu Rev Biochem* 69:497-529.
12. McCulloch SD & Kunkel TA (2008) The fidelity of DNA synthesis by eukaryotic replicative and translesion synthesis polymerases. *Cell Res* 18(1):148-161.
13. Sydow JF & Cramer P (2009) RNA polymerase fidelity and transcriptional proofreading. *Curr Opin Struct Biol* 19(6):732-739.
14. Bouadloun F, Donner D, & Kurland CG (1983) Codon-specific missense errors in vivo. *EMBO J* 2:1351-1356.
15. Edelmann P & Gallant J (1977) Mistranslation in E. coli. *Cell* 10(1):131-137.
16. Kramer EB & Farabaugh PJ (2007) The frequency of translational misreading errors in E. coli is largely determined by tRNA competition. *Rna* 13(1):87-96.
17. Watson JD & Crick FH (1953) Genetical implications of the structure of deoxyribonucleic acid. *Nature* 171(4361):964-967.
18. Loeb LA & Kunkel TA (1982) Fidelity of DNA synthesis. *Annu Rev Biochem* 51:429-457.
19. Ogle JM, Carter AP, & Ramakrishnan V (2003) Insights into the decoding mechanism from recent ribosome structures. *Trends Biochem Sci* 28(5):259-266.
20. Westhof E, Yusupov M, & Yusupova G (2014) Recognition of Watson-Crick base pairs: constraints and limits due to geometric selection and tautomerism. *F1000prime reports* 6:19.
21. Johnson KA (1993) Conformational coupling in DNA polymerase fidelity. *Annu Rev Biochem* 62:685-713.
22. Ogle JM, *et al.* (2001) Recognition of cognate transfer RNA by the 30S ribosomal subunit. *Science* 292:897-902.

23. Goodman MF (1997) Hydrogen bonding revisited: geometric selection as a principal determinant of DNA replication fidelity. *Proceedings of the National Academy of Sciences of the United States of America* 94(20):10493-10495.
24. Ogle JM, Murphy FV, Tarry MJ, & Ramakrishnan V (2002) Selection of tRNA by the ribosome requires a transition from an open to a closed form. *Cell* 111:721-732.
25. Johnson SJ & Beese LS (2004) Structures of mismatch replication errors observed in a DNA polymerase. *Cell* 116(6):803-816.
26. Sydow JF, *et al.* (2009) Structural basis of transcription: mismatch-specific fidelity mechanisms and paused RNA polymerase II with frayed RNA. *Mol Cell* 34(6):710-721.
27. Zaher HS & Green R (2009) Quality control by the ribosome following peptide bond formation. *Nature* 457:161-166.
28. Crick FH, Griffith JS, & Orgel LE (1957) Codes without Commas. *Proceedings of the National Academy of Sciences of the United States of America* 43(5):416-421.
29. Crick FH (1966) Codon--anticodon pairing: the wobble hypothesis. *Journal of molecular biology* 19(2):548-555.
30. Agris PF (1991) Wobble position modified nucleosides evolved to select transfer RNA codon recognition: a modified-wobble hypothesis. *Biochimie* 73(11):1345-1349.
31. Agris PF, Vendeix FA, & Graham WD (2007) tRNA's wobble decoding of the genome: 40 years of modification. *Journal of molecular biology* 366(1):1-13.
32. Rodnina MV & Wintermeyer W (2001) Fidelity of aminoacyl-tRNA selection on the ribosome: kinetic and structural mechanisms. *Annu Rev Biochem* 70:415-435.
33. Manley JL (1978) Synthesis and degradation of termination and premature-termination fragments of beta-galactosidase in vitro and in vivo. *Journal of molecular biology* 125:407-432.
34. Kurland CG (1992) Translational accuracy and the fitness of bacteria. *Annu Rev Genet* 26:29-50.
35. Zaher HS & Green R (2011) A primary role for release factor 3 in quality control during translation elongation in Escherichia coli. *Cell* 147(2):396-408.
36. Smith TF, Lee JC, Gutell RR, & Hartman H (2008) The origin and evolution of the ribosome. *Biology direct* 3:16.
37. Spahn CM, *et al.* (2001) Structure of the 80S ribosome from Saccharomyces cerevisiae--tRNA-ribosome and subunit-subunit interactions. *Cell* 107(3):373-386.
38. Nomura M, Traub P, Guthrie C, & Nashimoto H (1969) The assembly of ribosomes. *Journal of cellular physiology* 74(2):Suppl 1:241+.
39. Garrett RA & Wittmann HG (1973) Structure and function of the ribosome. *Endeavour* 32(115):8-14.
40. Wittmann HG (1976) Structure, function and evolution of ribosomes. *Eur J Biochem* 61(1):1-13.
41. Noller HF & Woese CR (1981) Secondary structure of 16S ribosomal RNA. *Science* 212(4493):403-411.
42. Lata KR, *et al.* (1996) Three-dimensional reconstruction of the Escherichia coli 30 S ribosomal subunit in ice. *Journal of molecular biology* 262(1):43-52.
43. McCutcheon JP, *et al.* (1999) Location of translational initiation factor IF3 on the small ribosomal subunit. *Proceedings of the National Academy of Sciences of the United States of America* 96(8):4301-4306.
44. Fei J, Kosuri P, MacDougall DD, & Gonzalez RL, Jr. (2008) Coupling of ribosomal L1 stalk and tRNA dynamics during translation elongation. *Mol Cell* 30(3):348-359.
45. Cornish PV, *et al.* (2009) Following movement of the L1 stalk between three functional states in single ribosomes. *Proceedings of the National Academy of Sciences of the United States of America* 106:2571-2576.

46. Komoda T, *et al.* (2006) The A-site finger in 23 S rRNA acts as a functional attenuator for translocation. *The Journal of biological chemistry* 281(43):32303-32309.
47. Reblova K, *et al.* (2010) Dynamics of the base of ribosomal A-site finger revealed by molecular dynamics simulations and Cryo-EM. *Nucleic acids research* 38(4):1325-1340.
48. Diaconu M, *et al.* (2005) Structural basis for the function of the ribosomal L7/12 stalk in factor binding and GTPase activation. *Cell* 121(7):991-1004.
49. Yusupov MM, *et al.* (2001) Crystal structure of the ribosome at 5.5 A resolution. *Science* 292:883-896.
50. Gongadze GM (2011) 5S rRNA and ribosome. *Biochemistry (Mosc)* 76(13):1450-1464.
51. Horan LH & Noller HF (2007) Intersubunit movement is required for ribosomal translocation. *Proceedings of the National Academy of Sciences of the United States of America* 104(12):4881-4885.
52. Hennelly SP, *et al.* (2005) A time-resolved investigation of ribosomal subunit association. *Journal of molecular biology* 346(5):1243-1258.
53. Selmer M, *et al.* (2006) Structure of the 70S ribosome complexed with mRNA and tRNA. *Science* 313(5795):1935-1942.
54. Liiv A & O'Connor M (2006) Mutations in the intersubunit bridge regions of 23 S rRNA. *The Journal of biological chemistry* 281(40):29850-29862.
55. Jackman JE & Alfonzo JD (2013) Transfer RNA modifications: nature's combinatorial chemistry playground. *Wiley interdisciplinary reviews. RNA* 4(1):35-48.
56. Holley RW, *et al.* (1965) Structure of a Ribonucleic Acid. *Science* 147(3664):1462-1465.
57. Saenger W (1984) *Principles of nucleic acid structure* (Springer-Verlag, New York) pp xx, 556 p.
58. Watanabe Y, Suematsu T, & Ohtsuki T (2014) Losing the stem-loop structure from metazoan mitochondrial tRNAs and co-evolution of interacting factors. *Frontiers in genetics* 5:109.
59. Kim SH, *et al.* (1973) X-ray crystallographic studies of polymorphic forms of yeast phenylalanine transfer RNA. *Journal of molecular biology* 75(2):421-428.
60. Valle M, *et al.* (2003) Incorporation of aminoacyl-tRNA into the ribosome as seen by cryo-electron microscopy. *Nat Struct Biol* 10(11):899-906.
61. Caulfield TR, Devkota B, & Rollins GC (2011) Examinations of tRNA Range of Motion Using Simulations of Cryo-EM Microscopy and X-Ray Data. *Journal of biophysics* 2011:219515.
62. Bremer H & Dennis PP (Modulation of chemical composition and other parameters of the cell by growth rate.
63. Wintermeyer W, *et al.* (2004) Mechanisms of elongation on the ribosome: dynamics of a macromolecular machine. *Biochem Soc Trans* 32(Pt 5):733-737.
64. Lovmar M & Ehrenberg M (2006) Rate, accuracy and cost of ribosomes in bacterial cells. *Biochimie* 88(8):951-961.
65. Rodnina MV, Beringer M, & Wintermeyer W (2007) How ribosomes make peptide bonds. *Trends Biochem Sci* 32(1):20-26.
66. Simonetti A, *et al.* (2009) A structural view of translation initiation in bacteria. *Cell Mol Life Sci* 66(3):423-436.
67. Shine J & Dalgarno L (1974) The 3'-terminal sequence of Escherichia coli 16S ribosomal RNA: complementarity to nonsense triplets and ribosome binding sites. *Proceedings of the National Academy of Sciences of the United States of America* 71(4):1342-1346.
68. Gold L (1988) Posttranscriptional regulatory mechanisms in Escherichia coli. *Annu Rev Biochem* 57:199-233.
69. Studer SM & Joseph S (2006) Unfolding of mRNA secondary structure by the bacterial translation initiation complex. *Mol Cell* 22(1):105-115.

70. Clark BF, Dube SK, & Marcker KA (1968) Specific codon-anticodon interaction of an initiator-tRNA fragment. *Nature* 219(5153):484-485.
71. Ringquist S, MacDonald M, Gibson T, & Gold L (1993) Nature of the ribosomal mRNA track: analysis of ribosome-binding sites containing different sequences and secondary structures. *Biochemistry* 32(38):10254-10262.
72. Allen GS, Zavialov A, Gursky R, Ehrenberg M, & Frank J (2005) The cryo-EM structure of a translation initiation complex from Escherichia coli. *Cell* 121(5):703-712.
73. Julian P, *et al.* (2011) The Cryo-EM structure of a complete 30S translation initiation complex from Escherichia coli. *PLoS Biol* 9(7):e1001095.
74. Milon P, Konevega AL, Gualerzi CO, & Rodnina MV (2008) Kinetic checkpoint at a late step in translation initiation. *Mol Cell* 30(6):712-720.
75. Kothe U, Wieden HJ, Mohr D, & Rodnina MV (2004) Interaction of helix D of elongation factor Tu with helices 4 and 5 of protein L7/12 on the ribosome. *Journal of molecular biology* 336(5):1011-1021.
76. Blanchard SC, Gonzalez RL, Kim HD, Chu S, & Puglisi JD (2004) tRNA selection and kinetic proofreading in translation. *Nat Struct Mol Biol* 11(10):1008-1014.
77. Geggier P, *et al.* (2010) Conformational sampling of aminoacyl-tRNA during selection on the bacterial ribosome. *Journal of molecular biology* 399(4):576-595.
78. Valle M, *et al.* (2002) Cryo-EM reveals an active role for aminoacyl-tRNA in the accommodation process. *Embo J* 21(13):3557-3567.
79. Schmeing TM, *et al.* (2009) The crystal structure of the ribosome bound to EF-Tu and aminoacyl-tRNA. *Science* 326:688-694.
80. Voorhees RM, Weixlbaumer A, Loakes D, Kelley AC, & Ramakrishnan V (2009) Insights into substrate stabilization from snapshots of the peptidyl transferase center of the intact 70S ribosome. *Nat Struct Mol Biol* 16(5):528-533.
81. Gromadski KB, Daviter T, & Rodnina MV (2006) A uniform response to mismatches in codon-anticodon complexes ensures ribosomal fidelity. *Mol Cell* 21(3):369-377.
82. Hansen JL, Schmeing TM, Moore PB, & Steitz TA (2002) Structural insights into peptide bond formation. *Proceedings of the National Academy of Sciences of the United States of America* 99(18):11670-11675.
83. Schmeing TM, Huang KS, Kitchen DE, Strobel SA, & Steitz TA (2005) Structural insights into the roles of water and the 2' hydroxyl of the P site tRNA in the peptidyl transferase reaction. *Mol Cell* 20:437-448.
84. Schmeing TM, Huang KS, Strobel SA, & Steitz TA (2005) An induced-fit mechanism to promote peptide bond formation and exclude hydrolysis of peptidyl-tRNA. *Nature* 438(7067):520-524.
85. Hiller DA, Singh V, Zhong M, & Strobel SA (2011) A two-step chemical mechanism for ribosome-catalysed peptide bond formation. *Nature* 476(7359):236-239.
86. Moazed D & Noller HF (1989) Intermediate states in the movement of transfer RNA in the ribosome. *Nature* 342:142-148.
87. Frank J & Agrawal RK (2000) A ratchet-like inter-subunit reorganization of the ribosome during translocation. *Nature* 406:319-322.
88. Blanchard SC, Kim HD, Gonzalez RL, Jr., Puglisi JD, & Chu S (2004) tRNA dynamics on the ribosome during translation. *Proceedings of the National Academy of Sciences of the United States of America* 101(35):12893-12898.
89. Valle M, *et al.* (2003) Locking and unlocking of ribosomal motions. *Cell* 114(1):123-134.
90. Schuwirth BS, *et al.* (2005) Structures of the bacterial ribosome at 3.5 A resolution. *Science* 310(5749):827-834.
91. Zhou J, Lancaster L, Donohue JP, & Noller HF (2013) Crystal structures of EF-G-ribosome complexes trapped in intermediate states of translocation. *Science* 340(6140):1236086.

92. Ramrath DJ, *et al.* (2013) Visualization of two transfer RNAs trapped in transit during elongation factor G-mediated translocation. *Proceedings of the National Academy of Sciences of the United States of America* 110(52):20964-20969.
93. Youngman EM, McDonald ME, & Green R (2008) Peptide release on the ribosome: mechanism and implications for translational control. *Annu Rev Microbiol* 62:353-373.
94. Jorgensen F, Adamski FM, Tate WP, & Kurland CG (1993) Release factor-dependent false stops are infrequent in Escherichia coli. *Journal of molecular biology* 230:41-50.
95. Weixlbaumer A, *et al.* (2008) Insights into translational termination from the structure of RF2 bound to the ribosome. *Science* 322(5903):953-956.
96. Korostelev A, *et al.* (2008) Crystal structure of a translation termination complex formed with release factor RF2. *Proceedings of the National Academy of Sciences of the United States of America* 105(50):19684-19689.
97. Jin H, Kelley AC, Loakes D, & Ramakrishnan V (2010) Structure of the 70S ribosome bound to release factor 2 and a substrate analog provides insights into catalysis of peptide release. *Proceedings of the National Academy of Sciences of the United States of America* 107(19):8593-8598.
98. Korostelev A, Zhu J, Asahara H, & Noller HF (2010) Recognition of the amber UAG stop codon by release factor RF1. *EMBO J* 29(15):2577-2585.
99. Hirashima A & Kaji A (1973) Role of elongation factor G and a protein factor on the release of ribosomes from messenger ribonucleic acid. *The Journal of biological chemistry* 248(21):7580-7587.
100. Kiel MC, Kaji H, & Kaji A (2007) Ribosome recycling: An essential process of protein synthesis. *Biochemistry and molecular biology education : a bimonthly publication of the International Union of Biochemistry and Molecular Biology* 35(1):40-44.
101. Spotts CR & Stanier RY (1961) Mechanism of streptomycin action on bacteria: a unitary hypothesis. *Nature* 192:633-637.
102. Davies J, Gilbert W, & Gorini L (1964) Streptomycin, Suppression, and the Code. *Proceedings of the National Academy of Sciences of the United States of America* 51:883-890.
103. Gorini L & Kataja E (1964) Phenotypic Repair by Streptomycin of Defective Genotypes in E. Coli. *Proceedings of the National Academy of Sciences of the United States of America* 51:487-493.
104. Demerec M (1951) Studies of the Streptomycin-Resistance System of Mutations in E. Coli. *Genetics* 36(6):585-597.
105. Birge EA & Kurland CG (1969) Altered ribosomal protein in streptomycin-dependent Escherichia coli. *Science* 166(3910):1282-1284.
106. Ozaki M, Mizushima S, & Nomura M (1969) Identification and functional characterization of the protein controlled by the streptomycin-resistant locus in E. coli. *Nature* 222(5191):333-339.
107. Chakrabarti S & Gorini L (1975) Growth of bacteriophages MS2 and T7 on streptomycin-resistant mutants of Escherichia coli. *J Bacteriol* 121(2):670-674.
108. Chumpolkulwong N, *et al.* (2004) Effects of Escherichia coli ribosomal protein S12 mutations on cell-free protein synthesis. *Eur J Biochem* 271(6):1127-1134.
109. Rosset R & Gorini L (1969) A ribosomal ambiguity mutation. *Journal of molecular biology* 39(1):95-112.
110. Brownstein BL & Lewandowski LJ (1967) A mutation suppressing streptomycin dependence. I. An effect on ribosome function. *Journal of molecular biology* 25(1):99-109.
111. Biswas DK & Gorini L (1972) Restriction, de-restriction and mistranslation in missense suppression. Ribosomal discrimination of transfer RNA's. *Journal of molecular biology* 64(1):119-134.

112. Hui A & de Boer HA (1987) Specialized ribosome system: preferential translation of a single mRNA species by a subpopulation of mutated ribosomes in Escherichia coli. *Proceedings of the National Academy of Sciences of the United States of America* 84(14):4762-4766.
113. Lee K, Holland-Staley CA, & Cunningham PR (1996) Genetic analysis of the Shine-Dalgarno interaction: selection of alternative functional mRNA-rRNA combinations. *Rna* 2(12):1270-1285.
114. Abdi NM & Fredrick K (2005) Contribution of 16S rRNA nucleotides forming the 30S subunit A and P sites to translation in Escherichia coli. *Rna* 11(11):1624-1632.
115. McClory SP, Leisring JM, Qin D, & Fredrick K (2010) Missense suppressor mutations in 16S rRNA reveal the importance of helices h8 and h14 in aminoacyl-tRNA selection. *Rna* 16(10):1925-1934.
116. Potapov AP, Triana-Alonso FJ, & Nierhaus KH (1995) Ribosomal decoding processes at codons in the A or P sites depend differently on 2'-OH groups. *The Journal of biological chemistry* 270(30):17680-17684.
117. Pape T, Wintermeyer W, & Rodnina M (1999) Induced fit in initial selection and proofreading of aminoacyl-tRNA on the ribosome. *EMBO J* 18(13):3800-3807.
118. Gromadski KB & Rodnina MV (2004) Kinetic determinants of high-fidelity tRNA discrimination on the ribosome. *Molecular cell* 13:191-200.
119. Ogle JM & Ramakrishnan V (2005) Structural insights into translational fidelity. *Annual review of biochemistry* 74:129-177.
120. Blomberg C, Ehrenberg M, & Kurland CG (1980) Free-energy dissipation constraints on the accuracy of enzymatic selections. *Q Rev Biophys* 13(2):231-254.
121. Khade PK, Shi X, & Joseph S (2013) Steric complementarity in the decoding center is important for tRNA selection by the ribosome. *Journal of molecular biology* 425(20):3778-3789.
122. Pape T, Wintermeyer W, & Rodnina MV (2000) Conformational switch in the decoding region of 16S rRNA during aminoacyl-tRNA selection on the ribosome. *Nat Struct Biol* 7(2):104-107.
123. Carter AP, *et al.* (2000) Functional insights from the structure of the 30S ribosomal subunit and its interactions with antibiotics. *Nature* 407:340-348.
124. Zeng X, Chugh J, Casiano-Negroni A, Al-Hashimi HM, & Brooks CL, 3rd (2014) Flipping of the Ribosomal A-Site Adenines Provides a Basis for tRNA Selection. *Journal of molecular biology*.
125. Vallabhaneni H & Farabaugh PJ (2009) Accuracy modulating mutations of the ribosomal protein S4-S5 interface do not necessarily destabilize the rps4-rps5 protein-protein interaction. *Rna* 15(6):1100-1109.
126. Maisnier-Patin S, Paulander W, Pennhag A, & Andersson DI (2007) Compensatory evolution reveals functional interactions between ribosomal proteins S12, L14 and L19. *Journal of molecular biology* 366:207-215.
127. Zaher HS & Green R (2010) Hyperaccurate and error-prone ribosomes exploit distinct mechanisms during tRNA selection. *Molecular Cell* 39:110-120.
128. Sun Q, Vila-Sanjurjo A, & O'Connor M (2011) Mutations in the intersubunit bridge regions of 16S rRNA affect decoding and subunit-subunit interactions on the 70S ribosome. *Nucleic acids research* 39:3321-3330.
129. Riyasaty S & Atkins JF (1968) External suppression of a frameshift mutant in salmonella. *Journal of molecular biology* 34(3):541-557.
130. Yourno J & Tanemura S (1970) Restoration of in-phase translation by an unlinked suppressor of a frameshift mutation in Salmonella typhimurium. *Nature* 225(5231):422-426.

131. Yourno J (1972) Externally suppressible +1 "glycine" frameshift: possible quadruplet isomers for glycine and proline. *Nat New Biol* 239(94):219-221.
132. Riddle DL & Roth JR (1970) Suppressors of frameshift mutations in Salmonella typhimurium. *Journal of molecular biology* 54(1):131-144.
133. Sherman F, Stewart JW, Jackson M, Gilmore RA, & Parker JH (1974) Mutants of yeast defective in iso-1-cytochrome c. *Genetics* 77(2):255-284.
134. Riddle DL & Roth JR (1972) Frameshift suppressors. II. Genetic mapping and dominance studies. *Journal of molecular biology* 66(3):483-493.
135. Prather NE, Murgola EJ, & Mims BH (1981) Nucleotide insertion in the anticodon loop of a glycine transfer RNA causes missense suppression. *Proceedings of the National Academy of Sciences of the United States of America* 78(12):7408-7411.
136. Cummins CM, Donahue TF, & Culbertson MR (1982) Nucleotide sequence of the SUF2 frameshift suppressor gene of Saccharomyces cerevisiae. *Proceedings of the National Academy of Sciences of the United States of America* 79(11):3565-3569.
137. Yarus M (1982) Translational efficiency of transfer RNA's: uses of an extended anticodon. *Science* 218(4573):646-652.
138. Gaber RF & Culbertson MR (1984) Codon recognition during frameshift suppression in Saccharomyces cerevisiae. *Mol Cell Biol* 4(10):2052-2061.
139. Curran JF & Yarus M (1987) Reading frame selection and transfer RNA anticodon loop stacking. *Science* 238(4833):1545-1550.
140. Moore B, Persson BC, Nelson CC, Gesteland RF, & Atkins JF (2000) Quadruplet codons: implications for code expansion and the specification of translation step size. *Journal of molecular biology* 298(2):195-209.
141. Anderson JC, Magliery TJ, & Schultz PG (2002) Exploring the limits of codon and anticodon size. *Chem Biol* 9(2):237-244.
142. Nasvall SJ, Nilsson K, & Bjork GR (2009) The ribosomal grip of the peptidyl-tRNA is critical for reading frame maintenance. *Journal of molecular biology* 385(2):350-367.
143. Atkins JF & Bjork GR (2009) A Gripping Tale of Ribosomal Frameshifting: Extragenic Suppressors of Frameshift Mutations Spotlight P-Site Realignment. *Microbiology and Molecular Biology Reviews* 73:178-210.
144. Farabaugh PJ (2000) Translational frameshifting: implications for the mechanism of translational frame maintenance. *Prog Nucleic Acid Res Mol Biol* 64:131-170.
145. Peter K, Lindsley D, Peng L, & Gallant JA (1992) Context rules of rightward overlapping reading. *New Biol* 4(5):520-526.
146. O'Connor M (1998) tRNA imbalance promotes -1 frameshifting via near-cognate decoding. *Journal of molecular biology* 279(4):727-736.
147. Urbonavicius J, Qian Q, Durand JM, Hagervall TG, & Bjork GR (2001) Improvement of reading frame maintenance is a common function for several tRNA modifications. *Embo J* 20(17):4863-4873.
148. Jager G, Nilsson K, & Bjork GR (2013) The phenotype of many independently isolated +1 frameshift suppressor mutants supports a pivotal role of the P-site in reading frame maintenance. *PloS one* 8(4):e60246.
149. Zaher HS & Green R (2010) Kinetic basis for global loss of fidelity arising from mismatches in the P-site codon:anticodon helix. *Rna* 16:1980-1989.
150. Ban N, Nissen P, Hansen J, Moore PB, & Steitz TA (2000) The complete atomic structure of the large ribosomal subunit at 2.4 A resolution. *Science* 289:905-920.
151. Rodnina MV (2012) Quality control of mRNA decoding on the bacterial ribosome. *Advances in protein chemistry and structural biology* 86:95-128.
152. Voorhees RM, Schmeing TM, Kelley AC, & Ramakrishnan V (2010) The mechanism for activation of GTP hydrolysis on the ribosome. *Science (New York, N.Y.)* 330:835-838.
153. Wimberly BT, *et al.* (2000) Structure of the 30S ribosomal subunit. *Nature* 407:327-339.

CHAPTER 2: REORGANIZATION OF AN INTERSUBUNIT BRIDGE INDUCED BY DISPARATE 16S RIBOSOMAL *AMBIGUITY* MUTATIONS MIMICS AN EF-TU-BOUND STATE

Crystal E. Fagan, Jack A. Dunkle, Tatsuya Maehigashi, Mai N. Dang, Aishwarya Devaraj, Stacey J. Miles, Daoming Qin, Kurt Fredrick and Christine M. Dunham

Fagan CE, *et al.* (2013) Reorganization of an intersubunit bridge induced by disparate 16S ribosomal ambiguity mutations mimics an EF-Tu-bound state. *Proceedings of the National Academy of Sciences of the United States of America* 110(24):9716-9721

To ensure the accurate translation of the genetic code into a functioning protein, the ribosome must select the correct tRNA according to the sequence of the mRNA. To understand how this selectivity is maintained, I solved two X-ray crystal structures of 70S ribosomes containing 16S rRNA *r*ibosomal *am*biguity (*ram*) mutations G299A or G347U that result in a strong i*n vivo* miscoding phenotype. Despite their disparate locations on the ribosome more than 77 Å apart, both mutations disrupt the intersubunit bridge B8 similar to when ternary complex binds. These structures highlight a previously unappreciated role for bridge B8 in maintaining the accuracy of translation. This work was previously published in the *Proceedings of the National Academy of Sciences of the United States of America*.

Author contributions: C.M.D and K.F. designed research; M.N.D. and D.Q. made the *Tth* mutants; S.M. purified the ribosomes; A.D. performed the GTPase assays; C.E.F. prepared and crystallized the ribosomal complexes; C.E.F., T.M. and C.M.D. collected and processed X-ray crystallography data and refined the structures; C.E.F., J. D. and C.M.D. analyzed the structures; and C.E.F., J.D., K.F and C.M.D wrote the paper

ABSTRACT

After four decades of research aimed at understanding tRNA selection on the ribosome, the mechanism by which ribosomal ambiguity (*ram*) mutations promote miscoding remains unclear. Here, we present two X-ray crystal structures of the *Thermus thermophilus* 70S ribosome containing 16S rRNA *ram* mutations, G347U and G299A. Each of these mutations cause miscoding *in vivo* and stimulate EF-Tu-dependent GTP hydrolysis *in vitro*. Mutation G299A is located near the interface of ribosomal proteins S4 and S5 on the solvent side of the subunit, whereas G347U is located 77 Å distant, at intersubunit bridge B8, close to where EF-Tu engages the ribosome. Despite these disparate locations, both mutations induce almost identical structural rearrangements that disrupt the B8 bridge, namely the interaction of h8/h14 with L14 and L19. This conformation most closely resembles that seen upon EF-Tu•GTP•aminoacyl-tRNA binding to the 70S ribosome. These data provide evidence that disruption and/or distortion of B8 is an important aspect of GTPase activation. We propose that, by destabilizing B8, G299A and G347U reduce the energetic cost of attaining the GTPase-activated state and thereby decrease the stringency of decoding. This previously unappreciated role for B8 in controlling the decoding process may hold relevance for many other ribosomal mutations known to influence translational fidelity.

INTRODUCTION

The molecular mechanisms controlling the fidelity of DNA replication, transcription, and translation have been areas of intense interest since the discovery of the genetic code. Thermodynamic differences between standard Watson-Crick and alternative (*e.g.*, wobble) base pairs in solution are insufficient to explain the high fidelity for any of the three polymerase reactions of the central dogma (1), indicating an active role for the enzymes in substrate selectivity (1-3). Mechanistic studies of polymerases have revealed some common themes, such as the specific recognition of Watson-Crick base pair geometry, larger forward rate constants for correct substrates (induced fit), separate opportunities for incorrect substrate rejection (kinetic proofreading), and post-incorporation correction mechanisms (1-5).

During translation, the ribosome must select aminoacyl-tRNA (aa-tRNA) substrates based on the mRNA sequence. Extensive biochemical studies have shed light on the kinetics of this decoding process (reviewed in (6)). Aa-tRNA is delivered to the ribosome as part of a ternary complex (TC) with EF-Tu and GTP. Initial binding of TC, mediated primarily by L7/L12 of the 50S subunit, is followed by the sampling of codon-anticodon interactions in the 30S A site. Codon-anticodon pairing leads to GTPase activation and GTP hydrolysis, which allows release of the acceptor end of aa-tRNA from EF-Tu. The aa-tRNA then either moves completely into the ribosomal A site (a step termed *accommodation*), where it can participate in peptide bond formation, or is rejected and released into solution (7, 8).

For each decoding event, the ribosome selects cognate aa-tRNA from a large pool of non- and near-cognate aa-tRNAs with high speed ($> 20\ s^{-1}$) and fidelity (error rate $\approx 10^{-4}$) (1). High fidelity can be explained in part by a kinetic proofreading mechanism, in which differences in substrate binding affinity are exploited twice to increase the overall level of discrimination (7-9). Basically, the functionally irreversible GTP hydrolysis step of the pathway provides a second independent opportunity for rejection of near-cognate aa-tRNA. It is clear, however, that kinetic proofreading is not maximally exploited for fidelity (6, 10). Instead, the ribosome additionally

employs an induced-fit mechanism to achieve both high speed and fidelity in decoding. Indicative of this mechanism is that cognate codon recognition increases the forward rate constants for GTPase activation / GTP hydrolysis and accommodation (11-14). This allows rapid incorporation of cognate aa-tRNA specifically, effectively obviating the need for substrate binding equilibria to be approached.

An important question is how cognate codon recognition stimulates GTPase activation by EF-Tu. Cognate codon-anticodon pairing results in docking of A-site rRNA nucleotides A1492, A1493, and G530 into the minor groove of the first two base pairs of the codon-anticodon helix (13). Presumably these changes in the decoding center are transmitted via conformational signaling ~80 Å to the GTPase domain of EF-Tu, although the molecular basis of such signaling remains unclear. One potential conduit for signaling is the tRNA itself, which is known to adopt a distorted or bent conformation in the GTPase-activated state (15, 16). Another possibility is that conformational signaling occurs through the 30S subunit. Crystallographic studies of the 30S subunit suggest that cognate A-site codon recognition is accompanied by a global conformational change in the subunit termed *domain closure* (13). Domain closure involves an inward rotation of the 30S shoulder domain, which may facilitate productive engagement of TC and GTPase activation (5).

Most chromosomal mutations affecting the fidelity of decoding have mapped to ribosomal protein genes rather than rRNA genes, presumably because the latter typically exist in multiple copies. Recently, a specialized ribosome system was used to isolate a number of 16S rRNA mutations that increase miscoding (referred to as ribosome ambiguity or *ram* mutations) (17). Many of these *ram* mutations clustered along interfaces between the 30S shoulder domain and other portions of the ribosome, generally consistent with a role for shoulder movement in aa-tRNA selection. Nearly half the mutations mapped to helices 8 (h8) and 14 (h14), which interact with each other and with the 50S subunit proteins L14 and L19, forming intersubunit bridge B8. Ribosomes with truncation of either h8 or h14 retain activity but are error-prone and exhibit

elevated rates of EF-Tu-dependent GTP hydrolysis (17). These data indicate that B8 acts in some way to negatively regulate GTP hydrolysis by EF-Tu.

Another cluster of 16S *ram* mutations mapped to h12 (17), close to the interface of ribosomal proteins S4 and S5. In earlier studies, numerous mutations affecting decoding fidelity were mapped to the S4/S5 interface (18-20). These mutations were isolated based on their ability to suppress certain S12 mutations, which confer streptomycin-dependence and hyper-accurate decoding. Unlike S5, S4 is part of the shoulder domain, and hence domain closure results in slight separation of these two proteins. It has been proposed that the S4/S5 mutations destabilize the open state of the 30S subunit and thereby influence decoding fidelity (5). However, several of these S4 suppressor mutations have been found to confer a restrictive (hyper-accurate) phenotype rather than the expected *ram* phenotype (21). Moreover, analysis of S4/S5 mutations in a yeast two-hybrid system showed no correlation between S4-S5 interaction and decoding fidelity (22). These observations cannot be easily reconciled with the domain closure model and hint that another mechanism may be at play.

Here, we present two X-ray crystal structures of the *Thermus thermophilus* 70S ribosome, containing *ram* mutations at either G299A or G347U. These mutations lie 77 Å apart, in h12 and h14, respectively (**Fig. 2.1**). Despite this, both structures show similar rearrangements of the B8 bridge that mimic rearrangements resulting from TC binding (23, 24). These data provide evidence that GTPase activation involves B8 disruption and reveal, for the first time, long-distance conformational signaling across the 30S.

RESULTS

Mutations G299A and G347U promote activation of EF-Tu. It was shown previously that mutations predicted to disrupt the interaction between h8 and h14 cause defects in the initial selection phase of decoding (17). These mutations (*e.g.*, G347U and truncations of either h8 or h14) stimulate EF-Tu-dependent GTP hydrolysis, particularly in the near-cognate case. To test

whether G299A similarly affects initial selection, control and G299A ribosomes were purified and used to assemble 70S initiation complexes programmed with either a cognate 5'-UUU-3' or a near-cognate 5'-CUU-3' codon in the A site (see Materials and Methods). Each complex (at various concentrations ≥ 0.5 μM) was rapidly mixed with EF-Tu•[γ-^{32}P]•GTP•Phe-tRNA^{Phe} (< 0.3 μM) and the rate of GTP hydrolysis was measured. Apparent rates were plotted as a function of ribosome concentration, and the data were fit to a hyperbolic function to obtain the maximal rate (k_{GTPmax}) and the concentration at which half-maximal rate is observed ($K_{1/2}$) (**Table 2.1, Fig. 2.2)**. In the cognate case, the G299A mutation increased k_{GTPmax} and $K_{1/2}$ by ~2-fold, while in the near-cognate case, G299A increased k_{GTPmax} by 9-fold with little or no effect on $K_{1/2}$. These effects of G299A are similar to those seen for G347U, h8Δ3, and h14Δ2 (17). Previous studies of EF-Tu-dependent GTP hydrolysis by Rodnina and coworkers have demonstrated that a conformational change attributed to GTPase activation is rate-limiting in the near-cognate case and partially rate-limiting in the cognate case (11, 12, 25). Hence, each of these 16S *ram* mutations acts, at least in part, by accelerating the GTPase activation step (17). Indeed, in the framework of the Rodnina model, an increase of the forward rate constant for GTPase activation of the same magnitude in both the cognate and near-cognate cases would be be sufficient to reduce the selectivity of the reaction, as we observe.

Crystallization and structural analysis of T. thermophilus G299A and G347U ribosomes. To understand the structural basis of the effects of *ram* mutations G299A and G347U, *T. thermophilus* strains containing homogeneous populations of mutant ribosomes were genetically engineered. *T. thermophilus* ribosomes were used because of their ability to produce crystals that are amenable for X-ray structure determination (26). One of the two 16S rRNA genes (*rrsB*) was first replaced with the mutant allele, and then the other (*rrsA*) was replaced with the null allele Δ*rrsA::htk1* (27). In both *E. coli* (strain Δ7 prrn) and *T. thermophilus*, G299A conferred a larger growth defect than G347U. Mutation G299A slowed the growth of *E. coli* by 40% and *T.*

thermophilus by 37%, while G347U slowed the growth of *E. coli* by 6% and *T. thermophilus* by 7% (**Table 2.2**).

From these *T. thermophilus* strains, 70S ribosomes carrying either the G299A or G347U mutation were purified, pretranslocation complexes were formed with P-site $tRNA^{fMet}$ and A-site $tRNA^{Phe}$, and these complexes were crystallized using established conditions (26). The structures were solved using molecular replacement with the most complete, available model of the 70S ribosome (28). The 70S G299A and G347U structures were refined at 3.5 and 3.9 Å resolution, respectively (see **Materials and Methods**; **Table 2.3**).

In both structures, P-site $tRNA^{fMet}$, A-site $tRNA^{Phe}$ and mRNA were clearly visible in the original, unbiased difference F_o-F_c density. Regions that had noticeably shifted compared to the start model and required rebuilding included h8 and h14 (**Fig. 2.3)** and h12 for the G299A structure only (**Fig. 2.4**). The codon-anticodon interactions in the A and P sites, the placement of the tRNAs in the E, P and A sites, and the mRNA path, all look identical to those of the wild-type 70S structure (28).

G347U directly alters h14, thereby disrupting bridge B8. The 16S rRNA nucleotide G347 is located in h14, which together with h8, contacts L14 and L19 of the large subunit to form intersubunit bridge B8 (**Fig. 2.1 and 2.5**) (29). The G347U mutation is 87 Å from where tRNA initially engages the ribosome at the 30S A site and is one of several *ram* mutations that cluster to the B8 region (17, 30). G347 is normally involved in a base triple interaction with C342 of h14 and A160 of h8 (**Fig. 2.6A**), forming a Watson-Crick and Hoogsteen interaction, respectively (31). Our structure reveals that the G347U mutation disrupts this base triple resulting in a widening of the entire h14 (**Fig. 2.6B**). This widening also causes movement away from the large ribosomal subunit, thereby preventing interactions that form B8 (**Fig. 2.6B**). From original, unbiased F_o-F_c difference density, the entire phosphate backbone of h14 moves away from the large subunit between 2 - 6 Å (**Figs. 2.3A & 2.6B**). In wild-type 70S structures, interactions are

observed between the E36 side chain of L19 and the phosphate oxygens of 16S rRNA h14 nucleotides 345 and 346 via a Mg^{2+} ion; the K35 side chain of L19 and the phosphate oxygen of 16S rRNA nucleotide 346; and the main chain of residues V116/A118 of L14 and the phosphate oxygen of nucleotide 347 via a Mg^{2+} ion (**Fig. 2.6B**). The movement of the 16S rRNA h14 backbone away from the 50S subunit results in distances that are too large to maintain this hydrogen bonding network with L14 and L19. Not all the side chains of L14 and L19 were interpretable and therefore these residues were kept modeled as in the wild-type 70S structure. Only one specific B8 interaction remains between the R97 side chain of L14 and the 16S rRNA backbone phosphate oxygen of C339.

G299A indirectly alters h14, also disrupting bridge B8. The 16S rRNA G299A mutation is located in h12, near previously identified *ram* mutations at the interface of ribosomal proteins S4 and S5 (18, 19) (**Figs. 2.1 & 2.4A**). G299 normally interacts with the conserved 16S rRNA 560 loop, which contains several sharp backbone turns and links the 5' and central domains of 16S rRNA (**Fig. 2.4B**). The Watson-Crick face of G299A makes hydrogen bonds with the Hoogsteen face of G566 and coordinates a Mg^{2+} ion with G558, appearing to stabilize the 560 loop (**Fig. 2.4B**) (26). The G299A mutation results in a loss of coordination to the Mg^{2+} ion presumably due to the predicted electrostatic repulsion between the N6 of adenosine and the metal (17). In addition to the loss of the Mg^{2+} ion, the mutation to adenosine precludes interaction with G566 (**Fig. 2.4B).** The loss of these two interactions however does not disrupt the compressed fold of the 560 loop.

Despite the modest nature of the local changes around the G299A mutation, significant structural changes occur ~80 Å away, at B8 (**Fig. 2.3B)**. As in the G347U structure, contacts between h14 and L14 are abrogated as h8 and h14 shift away from the 50S subunit (**Fig. 2.5**). This indicates an important role for RNA tertiary interactions between h12 and the 560 loop, which have long range implications for h14 positioning. These data provide direct evidence that

16S rRNA helices are capable of transmitting conformational signals across the ribosome subunits. Moreover, the similar structural effects of G299A and G347U imply that they influence decoding via a common mechanism.

Comparison of G347U and G299A structures with previous 70S structures. We compared our two 70S *ram* structures with other ribosome structures using the program Theseus (32, 33). This program uses maximum-likelihood superpositioning of the phosphate backbone and is a powerful method to look at conformational changes between two similar structures. Consistent with the original difference maps (**Fig. 2.3**), the most striking backbone differences between our two 70S *ram* structures with that of an analogous wild-type 70S structure (28) occurs in the 16S rRNA at h8 and h14 (**Figs. 2.7B and 2.8B**). These helices, along with h5, move upon binding of TC binding to the 70S (stabilized with a non-hydrolyzable GTP analog or the antibiotic kirromycin) (23, 24). When we compare the two 70S *ram* structures to either TC-bound structures, we see little to no backbone changes at h8/h14 for the G299A structure **(Fig. 2.7C)** and reduced changes for the G347U structure **(Figs. 2.8C)** (The G347U mutation causes additional distortions in h14 not observed in either the G299A or TC-bound 70S structures **(Fig. 2.8C)** presumably because the mutation is located nearby). These data indicate that G347U and G299A mutations partially recapitulate the conformational changes that occur upon TC binding, in the absence of this factor (**Fig. 2.9**). Overall, there were minimal differences between the 5S and 23S rRNA except for previously seen L1 stalk movements that depend upon which tRNA is bound at the E site (nucleotides 2116-2165) (34) and 5S rRNA changes (nucleotides 83-94) that appear to arise from either different crystal packing interactions (23, 24) or the lack of A-site ligands (35).

The mutant ribosomes were crystallized in the presence of the miscoding antibiotic paromomycin, which might raise concern that the observed conformational changes are due to the antibiotic. However, all of the structures compared above derive from complexes containing paromomycin, and thus the changes seen in h8/h14 can be specifically attributed to the 16S rRNA

mutations. Moreover, there is no evidence for paromomycin-dependent conformational changes in h8/h14 from earlier structural studies (26, 28).

DISCUSSION

In this study, we report X-ray crystal structures of 70S ribosomes carrying mutation G299A or G347U in 16S rRNA. Each of these mutations confers a strong miscoding phenotype *in vivo* and accelerates the GTPase activation / GTP hydrolysis step of aa-tRNA selection *in vitro* (17). The most prominent structural effects of these mutations are remarkably similar—each widens h14, resulting in a loss of the base triple involving nucleotides 342, 347, and 160 and disruption of many of the specific contacts contributing to B8. Comparison of the mutant ribosome structures with other previously determined ribosome structures shows that the altered conformation of h8/h14 is most similar to that seen in the TC-bound structures (16, 23), which are believed to closely resemble the GTPase-activated state of decoding. Together, these observations provide compelling evidence that disruption of B8 is an important aspect of GTPase activation. Consistent with this interpretation, *ram* mutations are found in B8 on both subunits, in h8/h14 on the 30S and in L14 and L19 on the 50S (17, 30). Moreover, truncations of either h8 or h14, which undoubtedly disrupt B8, cause miscoding and accelerate GTPase activation / GTP hydrolysis by EF-Tu (17). We propose that all of these *ram* mutations, which compromise (or effectively "pre-disrupt") B8, reduce the energetic cost of attaining the GTPase-activated state and thereby increase miscoding.

The combination of biochemical and structural results reported herein indicate that B8 puts a "brake" on, or negatively regulates GTPase activation of TC. How does this occur since B8 components h8 and h14 do not physically interact with TC (23)? Helix 5 of 16S rRNA, which is physically adjacent to h14 (**Fig. 2.9A**), interacts with domain 2 of EF-Tu and the acceptor end of aa-tRNA in the TC-bound ribosome structures. Data from EF-Tu mutants confirms this interaction is crucial for GTPase activation (36). Comparison of structures of wild-type 70S with

and without bound TC suggests that movement of h8/h14 away from the 50S subunit is accompanied by a movement of h5. Despite h8/h14 clearly moving in TC-bound ribosome structures (23, 24), its significance was not noted. Our structures reported here show that *ram* mutants can disrupt B8 in the absence of TC, positioning both h5 and h14 so that they mimic the GTPase activated conformation (**Fig. 2.9B**). The basis for the coupling of h5 and h14 movement is likely the base triple formed by U56•A356•C352 (**Fig. 2.9B**). As h5 and h14 adopt their GTPase productive conformation, this tertiary interaction between them is maintained rather than broken, causing the helices to move as a unit. This observation establishes a link between B8 disruption and GTPase activation.

Since the general features of aa-tRNA delivery to the ribosome are conserved in all organisms, one would expect the details of GTPase activation of TC to also be conserved. In fact, most h5 and h14 nucleotides are greater than 90% conserved in cytoplasmic ribosomes across all three domains of life, making these helices a "hotspot" for rRNA sequence conservation similar to other known functional regions such as the decoding center (37). Structurally, the U56•A356•C352 base triple is present in all the X-ray crystallographic models of prokaryotic ribosomes as well as the eukaryotic ribosome structure from *S. cerevisiae* (26, 38, 39). This conservation provides additional support for the functional importance of the role for h5 and h14 in GTPase activation.

An unexpected and remarkable finding of our study is that h12 mutation G299A causes the largest structural changes ~80 Å away, in h8/h14 at B8. How such long-range signaling is mediated remains unclear, although we imagine that G299A acts in a manner analogous to well-studied allosteric mutations in protein enzymes (40, 41). In this view, enzymes are inherently dynamic, interconverting between multiple distinct (but similar) conformational states at timescales relevant for catalysis. Intermediates along the reaction coordinate are similarly well described as dynamic ensembles of related conformational states, and hence the reaction proceeds through a combinatorial multitude of interrelated parallel pathways. These dynamics, which

largely govern catalysis, entail coordinated motions of elements across the whole enzyme. By perturbing the overall conformational equilibria of the enzyme, an allosteric mutation impacts the active site from a distance. In the case of G299A, its long-range effect on h8/h14 presumably shifts the conformational equilibria of the ribosome forward along the reaction coordinate of decoding, enabling the GTPase-activated state to be more readily attained.

Mutation G299A lies near the interface of ribosomal proteins S4 and S5, where a number of mutations affecting decoding fidelity have been mapped (18-20). It was hypothesized that these mutations act by destabilizing the S4-S5 interface to promote domain closure (5, 17). However, our current findings suggest that G299A acts by disrupting B8 and raises the possibility that nearby S4/S5 mutations also act by influencing B8. Intriguingly, the majority of ribosomal mutations that affect decoding fidelity cluster to either B8 or the h12/S4/S5 region (**Fig. 2.1**) (17, 19, 30). It is tempting to speculate that nearly all *ram* mutations either directly or indirectly destabilize B8, similarly altering the conformational equilibria of the ribosome. Further experiments will be necessary to investigate this possibility.

In summary, our results provide evidence for a long-range interaction network across the 30S subunit to communicate with the GTPase center of EF-Tu. It is unknown whether this network is normally employed for signaling by wild-type ribosomes, but such a scenario seems plausible. For example, cognate codon recognition in the 30S A site might promote conformational signaling to h8/h14 via the same interaction network, facilitating disruption of B8 and productive interaction of EF-Tu within the intersubunit space. Undoubtedly, GTPase activation is controlled by several other events, such as distortion (bending) of the tRNA and conformational changes resulting from interaction between h5 of the 30S shoulder and domain 2 of EF-Tu. Further biochemical analyses are necessary to elucidate the relative contribution of each of these events to GTPase activation and other aspects of the decoding process.

MATERIALS AND METHODS

Bacterial strains. *E. coli* Δ7 prrn strains harboring derivatives of plasmid p278MS2 (42) were made as described previously (43). *T. thermophilus* strains expressing homogeneous populations of mutant ribosomes were constructed as follows. A ~1500 base pair DNA fragment that includes the 5' two-thirds of *rrsB* and adjacent DNA upstream was amplified from the *T. thermophilus* genome and cloned into pUC18-htk1, a vector encoding a thermostable kanamycin adenyltransferase (27, 44). The resulting plasmid pMD3 was subjected to site-directed mutagenesis to produce the derivatives pMD5 and pMD6, with mutations corresponding to 16S rRNA substitutions G347U and G299A, respectively. These plasmids were each transformed into *T. thermophilus* HB8 (45), selecting for kanamycin resistance (Kan^R). Transformants were screened by PCR to identify those in which the plasmid integrated into the *rrsB* locus, as opposed to *rrsA*. Such isolates were cultured for several days in the absence of kanamycin and then plated for single colonies. These colonies were screened for kanamycin sensitivity (Kan^S), due to loss of the integrated plasmid through a second recombination event, and such Kan^S isolates were further screened by PCR and sequencing to identify those in which *rrsB* was replaced with the mutant allele. Finally, these mutant strains were transformed with chromosomal DNA from HG286 (*ΔrrsA::htk1*) to delete the rrsA gene (27), producing strains KLF1211 and KLF1212.

Kinetic assays. Single-turnover GTP hydrolysis experiments were performed with ribosomes purified from *E. coli* Δ7 prrn strains as described previously (17).

***T. thermophilus* 70S purification and crystallization.** *T. thermophilus* ribosomes containing either the G299A or G347U mutations were purified as described previously (26). *E. coli* $tRNA^{fMet}$ and $tRNA^{Phe}$ were purchased from Chemical Block. The mRNA oligonucleotide was chemically synthesized (Dharmacon) with a sequence of 5′ GGCAAGGAGGUAAAAAUGUUCAAAA 3′, where AUG and UUC represent the P- and A-site

codons, respectively. Ribosome complexes were formed, crystals were grown and cryoprotected using previously established procedures (26). The crystals were soaked in a final cryo solution containing 200 μM paromomycin for 4 hours prior to being harvested and flash frozen in liquid nitrogen for data collection.

Data Collection and Refinement. X-ray diffraction data was collected on three crystals for each structure at the Southeast Regional Collaborative Access Team (SER-CAT) and Northeastern Collaborative Access Team (NE-CAT) beamlines at the Advanced Photon Source (APS) in Argonne, Illinois. Data were integrated and scaled using the XDS software package (46). The structures were solved by molecular replacement using the PHENIX software suite using 2WDG, 2WDH, 2WDI and 2WDJ as a search model with all ligands removed (47). Coordinate refinement was performed with each ribosomal subunit defined as a rigid group followed by additional rigid and TLS refinement with groups defined by the head, body, platform and 3' minor domain of the 30S subunit, along with mobile elements of the 50S subunit: 5S rRNA, L1 arm, protein L9, A-site finger and the central protuberance. Modeling of conformational changes in rRNA and ribosomal proteins along with the placement of mRNA, tRNA and Mg^{2+} ions was performed using Coot guided by Molprobity identification of all-atom contacts (48, 49). Iterative rounds of model building were followed by positional and ADP refinement in PHENIX yielding a final model with the statistics reported in Table S2. Figures were generated using PyMOL (50).

Global phosphate backbone changes. The 23S, 5S or 16S platform domains (residues 560-912) were superpositioned using the program Theseus to generate maximum likelihood covariance weighting for the wild-type, TC-bound, or 70S *ram* mutant structures (33). Individual rRNA were pairwise aligned against the wild-type tRNA 70S structure as a reference (28). Nucleotide movement was analyzed for each pairwise alignment by determining the phosphate to phosphate distance (Å) between the two structures.

ACKNOWLEDGEMENTS

We thank Graeme L. Conn for helpful discussions throughout the project and critical reading of the manuscript; S. Gregory for plasmid pUC18-htk, strain HG286, and helpful suggestions; and Frank Murphy and staff members at the NE-CAT beamline for assistance during data collection. This work is based on research conducted at the Advanced Photon Source on the NE-CAT beamlines, which is supported by National Center for Research Resources (National Institutes of Health) Award RR-15301, and at the SER-CAT beamline. Use of the Advanced Photon Source, an Office of Science User Facility operated for the US Department of Energy (DOE) Office of Science by Argonne National Laboratory, was supported by the US DOE under Contract DE-AC02-06CH11357. C.E.F was supported by the Department of Defense through the National Defense Science & Engineering Graduate Fellowship Program and NIH Training Grant T32 GM8367. Research reported in this publication was supported by the National Institute of General Medical Sciences of the National Institutes of Health under award numbers R01GM093279 (to C.M.D.) and R01GM072528 (to K.F.). C.M.D. is a Pew Scholar in the Biomedical Sciences.

FIGURES

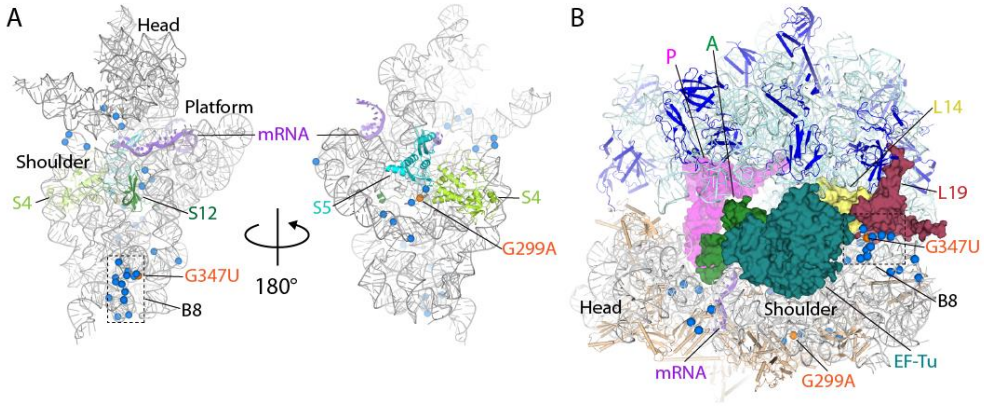

Figure 2.1. Location of ram mutations in 16S rRNA. (A) Positions of 16S rRNA mutations that increase miscoding (blue), mapped onto the 30S ribosomal subunit (PDB 2WDG), viewed from the subunit interface (left) and the solvent side (right). 16S rRNA, mRNA and r-proteins are shown as cartoon. The positions of the mutations G299A and G347U (orange), and the head, shoulder and platform domains and intersubunit bridge B8 of the subunit are indicated. 30S r-proteins are removed for clarity. (B) Most of the 16S rRNA *ram* mutations isolated cluster to regions distant from the tRNA binding sites, nearly half of which map to h8/14, which contacts L14 (yellow) and L19 (maroon) to form B8 (boxed). Although mutation G347U is proximal to B8, G299A resides ~80 Å away

Table 2.1. Kinetic parameters for EF-Tu-dependent GTP hydrolysis on control and mutant ribosomes

	Cognate		Near-cognate			
Ribosomes	k_{GTPmax} (sec^{-1})	$K_{1/2}$ (μM)	k_{GTPmax} (sec^{-1})	$K_{1/2}$ (μM)	Selectivity*	Reference
Control	51 ± 3	1.1 ± 0.2	1.8 ± 0.1	1.5 ± 0.2	39	This work and McClory et al. 2010
G299A	110 ± 9	2.3 ± 0.4	17 ± 1	1.0 ± 0.2	2.7	This work
G347U	130 ± 10	2.8 ± 0.5	15 ± 1	2.5 ± 0.4	7.7	McClory et al. 2010

*(Cognate $k_{GTPmax}/K_{1/2}$)/(Near-cognate $k_{GTPmax}/K_{1/2}$).

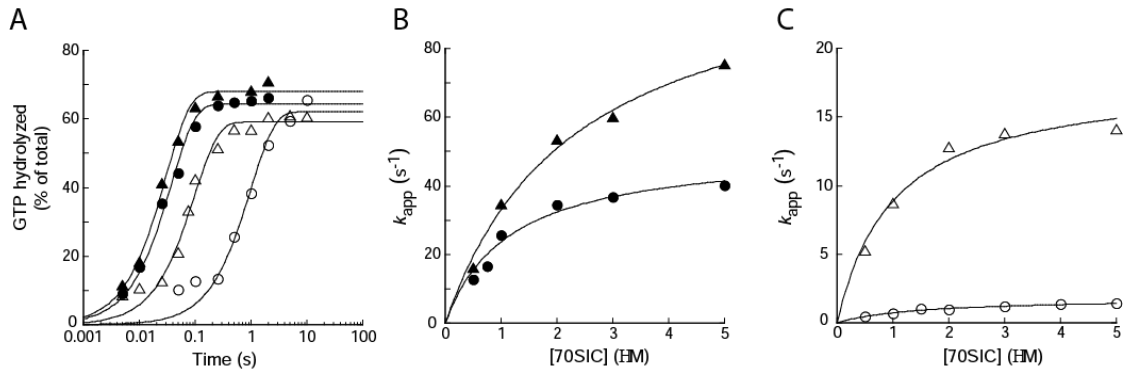

Figure 2.2. Effects of 16S rRNA mutation G299A on initial selection. The 70S initiation complexes (70SIC) programmed with either cognate UUU (closed symbols) or near-cognate CUU (open symbols) in the A site were rapidly mixed with elongation factor thermo unstable EF-Tu•[γ-^{32}P]GTP•Phe-tRNA^{Phe}, and rates of GTP hydrolysis were determined. Wild type, ●/○; G299A, ▲/△. (*A*) Examples of time courses at 1 □M 70SIC. Data were fit to a single exponential function to obtain the apparent rates of GTP hydrolysis (k_{app}). Apparent rates for cognate (*B*) and near-cognate (*C*) reactions plotted vs. [70SIC]. Data were fit to the equation $k_{app} = k_{GTPmax}$•[70SIC]/($K_{1/2}$ + [70SIC]), yielding the parameters shown in Table 2.1.

Table 2.2. Growth rates of bacterial strains containing control or mutant ribosomes

Strain	Description	Growth rate*
Escherichia coli		
KLF2674	Δ7 prrn (wild-type)	1.38 ± 0.06
KLF4004	Δ7 prrn (G299A)	0.84 ± 0.07
KLF4006	Δ7 prrn (G347U)	1.30 ± 0.08
Thermus thermophilus		
HB8	Wild-type	1.14 ± 0.08
KLF1212	rrsB (G299A) ΔrrsA::htk1	0.72 ± 0.08
KLF1211	rrsB (G347U) ΔrrsA::htk1	1.06 ± 0.02

*In units of doublings per hour. Data represent the mean SEM from ≥ 3 independent experiments.

Table 2.3. Summary of crystallographic data and refinement

	G299A	**G347U**
Data collection		
Space group	$P2_12_12_1$	$P2_12_12_1$
Cell dimensions		
a, b, c (Å)	209.95 445.55 620.21	210.29 445.45 622.11
α, β, γ (°)	90.00, 90.00, 90.00	90.00, 90.00, 90.00
Resolution (Å)*	50.0-3.5 (3.7-3.5)	50-3.9 (4.1-3.9)
R_{merge} (%)*	43.8 (130.3)	35.4 (140.9)
R_{pim} (%)*	13.8 (43.8)	13.4 (53.8)
I/σI*	6.3 (1.8)	5.7 (1.8)
Completeness(%)*	99.9 (99.9)	95.0 (90.9)
Redundancy*	11.5 (9.6)	6.6 (6.3)
Refinement		
Resolution (Å)	50.0 - 3.5	50.0 - 3.9
No. reflection	719,893	496,744
R_{work}/R_{free}	21.0/24.9	25.5/27.0
No. atoms	294,835	292,549
r.m.s. deviations		
Bond lengths (Å)	0.009	0.008
Bond angles (°)	1.05	1.20

* Values in parenthesis are for highest-resolution shell.

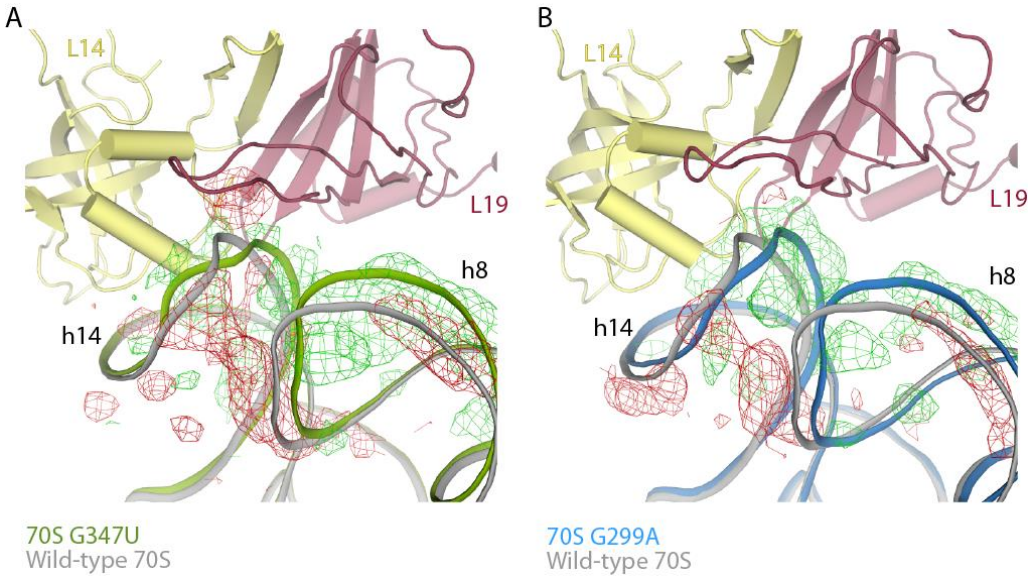

Figure 2.3. Conformational changes of helices 8 (h8) and 14 (h14). **(A)** Original, unbiased difference F_o-F_c density of the 70S G347U structure shows positive density (green) and negative density (red; 2 σ) after crystallographic refinement using the wild-type 70S structure as the starting model [Protein Data Bank (PDB) ID code 2WDG]. The original rRNA is shown as a gray backbone, and the rebuilt h8 and h14 backbone of the 70S G347U structure is shown in green. **(B)** Original, unbiased difference F_o-F_c density of the 70S G299A structure using the wild-type 70S structure as the starting model with the same color scheme as in A. The rebuilt h8 and h14 backbone of the 70S G299A structure is shown in blue.

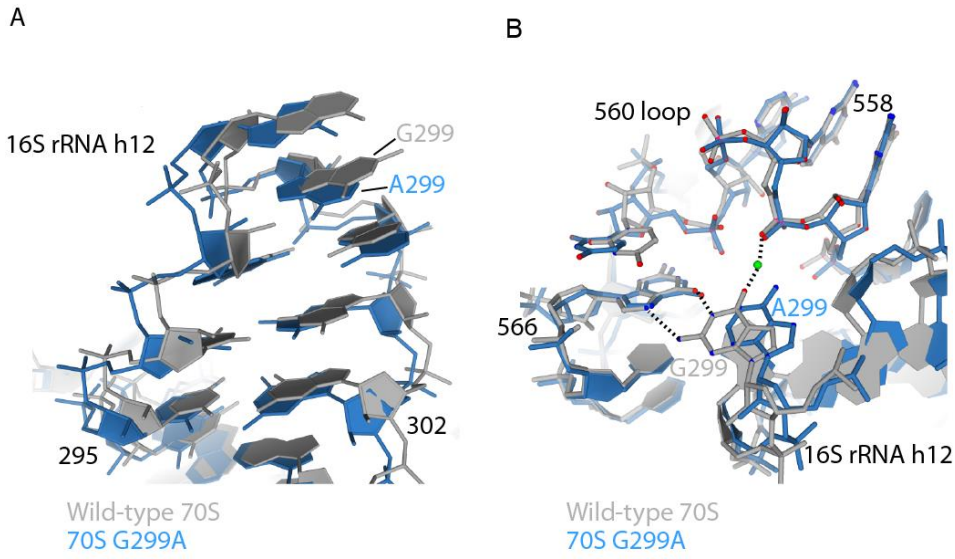

Figure 2.4. Rearrangements in h12 due to the G299A mutation. (A) Displacement of h12 resulting from G299A (blue) compared with the wild-type 70S structure (PDB ID code 2WDG; gray). **(B)** The G299A mutation results in loss of the coordinated Mg^{2+} ion (green sphere) and the 566-299 purine-purine interaction but does not cause an overall loss of tertiary structure.

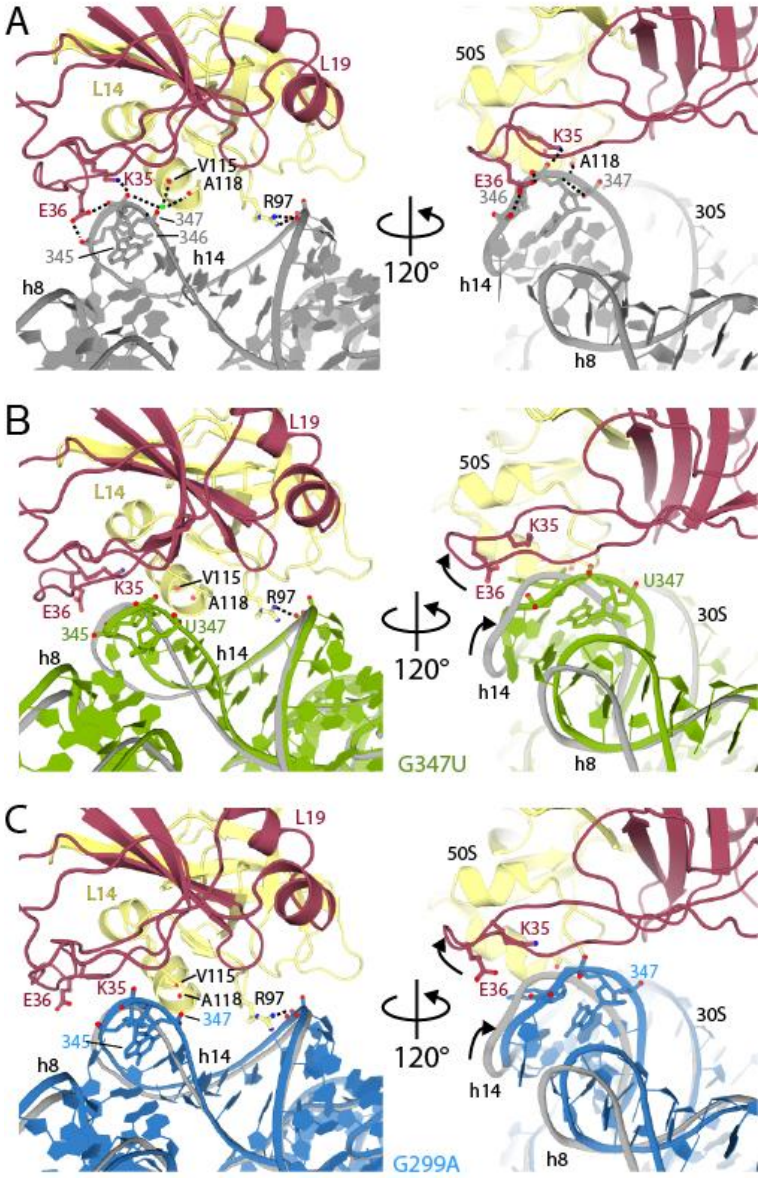

Figure 2.5. 16S rRNA mutations G299A and G347U cause similar conformational rearrangements that disrupt intersubunit bridge B8. (A) B8 is formed by contacts between h14 of the 30S subunit and L14 / L19 of the 50S subunit (PDB 2WDG), many of which are lost in the mutant structures. Color scheme is the same as in Figure 1B. **(B)** 70S G347U (green) and **(C)** G299A (blue) mutations cause h14 displacement away from L14 and L19, disrupting the hydrogen bonding network between the subunits. The rRNA backbone of the wild-type 70S structure is shown for comparison (gray).

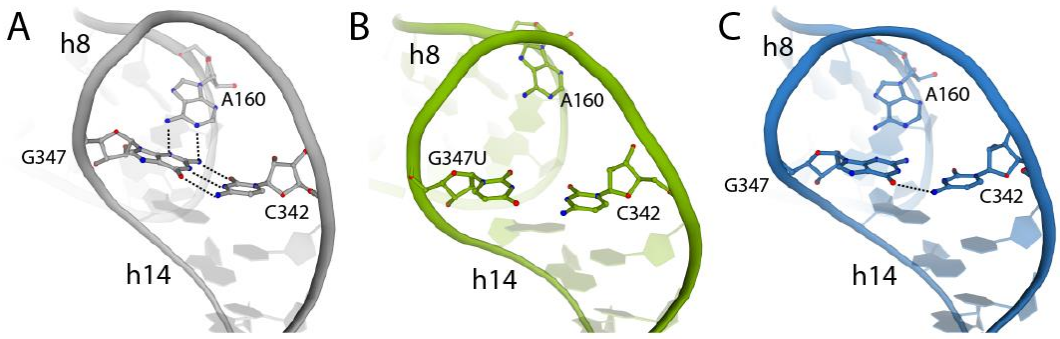

Figure 2.6. Mutations G347U and G299A similarly alter the conformation of h14 and its interaction with h8. (A) The structural integrity of h14 is normally maintained by the base triple G347•A160•C342 as shown in the wild-type 70S structure (gray) (PDB 2WDG). In the presence of either G347U (**B**, green) or G299A mutations (**C**, blue), h14 widens, resulting in disruption of this base triple and the interaction network of B8.

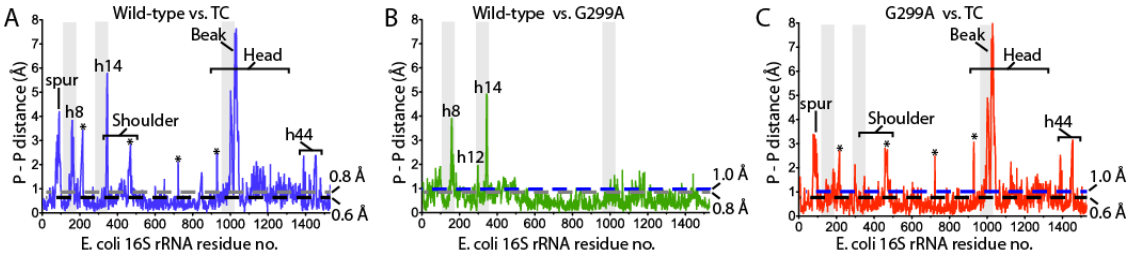

Figure 2.7. Comparison of the 70S G299A structure with other 70S structures. (A) Comparison of the 16S rRNA phosphate-phosphate backbone differences between wild-type 70S (PDB ID code 2WDG) and 70S TC (PDB ID code 2XQD). The coordinate error for the wild-type 70S (0.8 Å) and the 70S TC structures (0.6 Å) are shown as gray and black dashed lines, respectively. The asterisks denotes rRNA adjacent to the mobile spur regions that moves presumably because of different crystal forms used in the 2WDG and 2XQD structures (as not seen in B). **(B)** Same comparison as in *A* of wild-type 70S and 70S G299A. Major differences are almost exclusively in the h8 and h14 regions. The coordinate error for the wild-type 70S (0.8 Å) and 70S G299A structures (1.0 Å) are shown as gray and blue dashed lines, respectively. **(C)** Same comparison as in *A* of 70S TC and 70S G299A. Differences in h8 and h14 as seen in *B* are absent. The coordinate errors for the 70S G299A (1.0 Å) and 70S TC structures (0.6 Å) are shown as blue and black dashed lines, respectively.

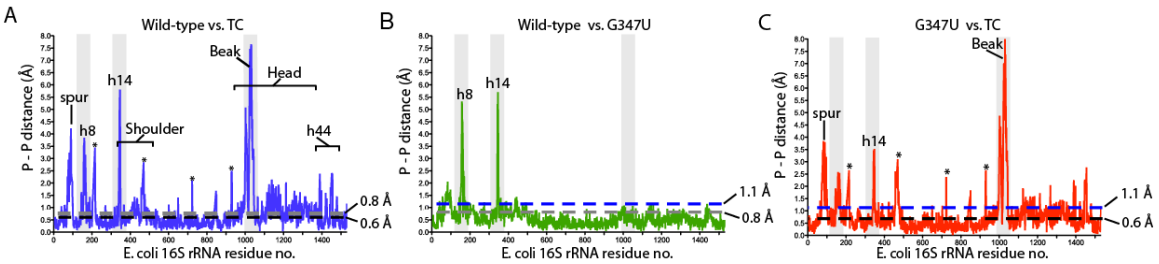

Figure 2.8. Comparison of the 70S G347U structure with other 70S structures. **(A)** Comparison of the 16S rRNA phosphate-phosphate backbone differences between wild-type 70S (PDB ID code 2WDG) and 70S ternary complex (TC; PDB ID code 2XQD). The coordinate error for the wild-type 70S (0.8 Å) and 70S TC structures (0.6 Å) are shown as gray and black dashed lines, respectively. The asterisk denotes rRNA adjacent to the mobile spur regions that moves presumable because of different crystal forms used in the 2WDG and 2XQD structures (as not seen in *B*). **(B)** Same comparison as in *A* of wild-type 70S and 70S G347U. Differences are almost exclusively in the h8 and h14 regions. The coordinate error for wild-type 70S (0.8 Å) and 70S G347U structures (1.1 Å) are shown as gray and blue dashed lines, respectively. **(C)** Same comparison as in *A* of 70S TC and 70S G347U. Smaller differences in h8 and h14 seen in *B* are absent. The coordinate error for the 70S G347U structure (1.1 Å) and the 70S TC structure (0.6 Å) are shown as blue and black dashed lines, respectively. Additional differences (~8 Å) between the G299A and G347U mutant structures and the TC-bound 70S structures are seen at the beak (part of the small subunit head domain), a region known to move upon TC binding (16, 23, 27)

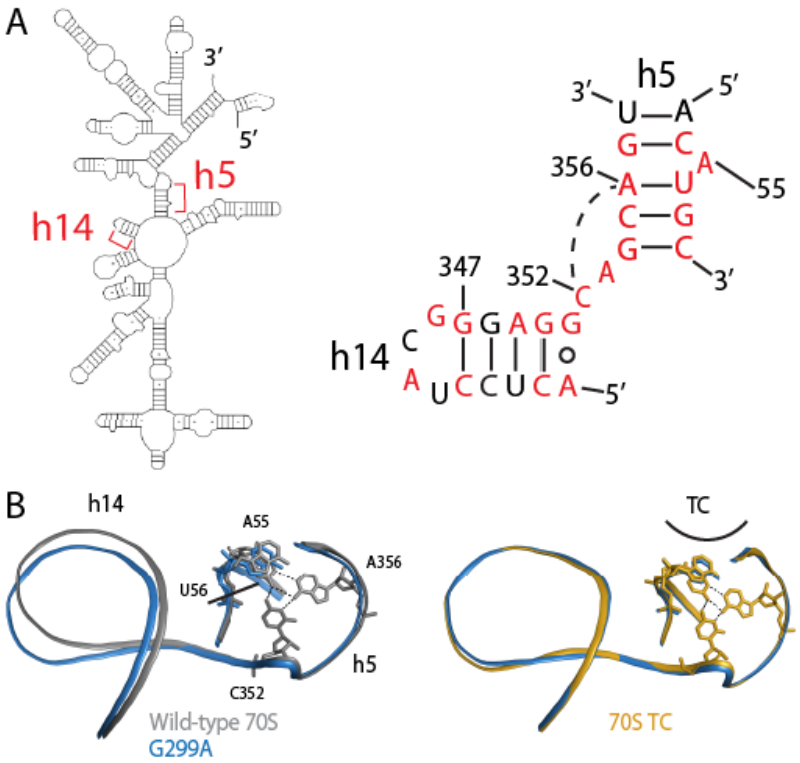

Figure 2.9. Conformational changes in h14 are propagated to h5. **(A)** An overview of the 5' domain of 16S rRNA (*Left*) with the secondary structure diagram of the junction between h5 and h14 of 16S rRNA (*E. coli* numbering) (*Right*). Nucleotides conserved at >90% in all cytoplasmic ribosomes are colored red (36). The base triple between C352 and the U56•A356 base pair is illustrated with a broken line. **(B)** A comparison of 70S G299A and either wild-type 70S (*Left*) or 70S TC (*Right*), reveals how the mutant ribosomes are poised for productive interaction of h5 with EF-Tu, whereas wild-type 70S are less organized for interactions with EF-Tu.

REFERENCES

1. Zaher HS & Green R (2009) Fidelity at the molecular level: lessons from protein synthesis. *Cell* 136(4):746-762.
2. Kunkel TA & Bebenek K (2000) DNA replication fidelity. *Annu Rev Biochem* 69:497-529.
3. Sydow JF & Cramer P (2009) RNA polymerase fidelity and transcriptional proofreading. *Curr Opin Struct Biol* 19(6):732-739.
4. Francklyn CS (2008) DNA polymerases and aminoacyl-tRNA synthetases: shared mechanisms for ensuring the fidelity of gene expression. *Biochemistry* 47(45):11695-11703.
5. Ogle JM & Ramakrishnan V (2005) Structural insights into translational fidelity. *Annu Rev Biochem* 74:129-177.
6. Wohlgemuth I, Pohl C, Mittelstaet J, Konevega AL, & Rodnina MV (2011) Evolutionary optimization of speed and accuracy of decoding on the ribosome. *Philosophical transactions of the Royal Society of London. Series B, Biological sciences* 366(1580):2979-2986.
7. Hopfield JJ (1974) Kinetic proofreading: a new mechanism for reducing errors in biosynthetic processes requiring high specificity. *Proc Natl Acad Sci U S A* 71(10):4135-4139.
8. Ninio J (1975) Kinetic amplification of enzyme discrimination. *Biochimie* 57(5):587-595.
9. Ruusala T, Ehrenberg M, & Kurland CG (1982) Is there proofreading during polypeptide synthesis? *The EMBO journal* 1(6):741-745.
10. Johansson M, Zhang J, & Ehrenberg M (2012) Genetic code translation displays a linear trade-off between efficiency and accuracy of tRNA selection. *Proceedings of the National Academy of Sciences of the United States of America* 109(1):131-136.
11. Gromadski KB, Daviter T, & Rodnina MV (2006) A uniform response to mismatches in codon-anticodon complexes ensures ribosomal fidelity. *Mol Cell* 21(3):369-377.
12. Gromadski KB & Rodnina MV (2004) Kinetic determinants of high-fidelity tRNA discrimination on the ribosome. *Molecular cell* 13(2):191-200.
13. Ogle JM, Murphy FV, Tarry MJ, & Ramakrishnan V (2002) Selection of tRNA by the ribosome requires a transition from an open to a closed form. *Cell* 111(5):721-732.
14. Pape T, Wintermeyer W, & Rodnina M (1999) Induced fit in initial selection and proofreading of aminoacyl-tRNA on the ribosome. *Embo J* 18(13):3800-3807.
15. Valle M, *et al.* (2002) Cryo-EM reveals an active role for aminoacyl-tRNA in the accommodation process. *The EMBO journal* 21(13):3557-3567.
16. Voorhees RM, Schmeing TM, Kelley AC, & Ramakrishnan V (2010) The mechanism for activation of GTP hydrolysis on the ribosome. *Science* 330(6005):835-838.
17. McClory SP, Leisring JM, Qin D, & Fredrick K (2010) Missense suppressor mutations in 16S rRNA reveal the importance of helices h8 and h14 in aminoacyl-tRNA selection. *RNA* 16(10):1925-1934.
18. Dahlgren A & Ryden-Aulin M (2000) A novel mutation in ribosomal protein S4 that affects the function of a mutated RF1. *Biochimie* 82(8):683-691.
19. Maisnier-Patin S, Berg OG, Liljas L, & Andersson DI (2002) Compensatory adaptation to the deleterious effect of antibiotic resistance in Salmonella typhimurium. *Mol Microbiol* 46(2):355-366.
20. Olsson MO & Isaksson LA (1979) Analysis of rpsD mutations in Escherichia coli. I. Comparison of mutants with various alterations in ribosomal protein S4. *Mol Gen Genet* 169(3):251-257.

21. Bjorkman J, Samuelsson P, Andersson DI, & Hughes D (1999) Novel ribosomal mutations affecting translational accuracy, antibiotic resistance and virulence of Salmonella typhimurium. *Molecular microbiology* 31(1):53-58.
22. Vallabhaneni H & Farabaugh PJ (2009) Accuracy modulating mutations of the ribosomal protein S4-S5 interface do not necessarily destabilize the rps4-rps5 protein-protein interaction. *RNA* 15(6):1100-1109.
23. Schmeing TM, *et al.* (2009) The crystal structure of the ribosome bound to EF-Tu and aminoacyl-tRNA. *Science* 326(5953):688-694.
24. Voorhees RM, Schmeing TM, Kelley AC, & Ramakrishnan V (The mechanism for activation of GTP hydrolysis on the ribosome. *Science* 330(6005):835-838.
25. Rodnina MV & Wintermeyer W (1995) GTP consumption of elongation factor Tu during translation of heteropolymeric mRNAs. *Proc Natl Acad Sci U S A* 92(6):1945-1949.
26. Selmer M, *et al.* (2006) Structure of the 70S ribosome complexed with mRNA and tRNA. *Science* 313(5795):1935-1942.
27. Gregory ST & Dahlberg AE (2009) Genetic and structural analysis of base substitutions in the central pseudoknot of Thermus thermophilus 16S ribosomal RNA. *Rna* 15(2):215-223.
28. Voorhees RM, Weixlbaumer A, Loakes D, Kelley AC, & Ramakrishnan V (2009) Insights into substrate stabilization from snapshots of the peptidyl transferase center of the intact 70S ribosome. *Nat Struct Mol Biol* 16(5):528-533.
29. Yusupov MM, *et al.* (2001) Crystal structure of the ribosome at 5.5 A resolution. *Science* 292(5518):883-896.
30. Maisnier-Patin S, Paulander W, Pennhag A, & Andersson DI (2007) Compensatory evolution reveals functional interactions between ribosomal proteins S12, L14 and L19. *Journal of molecular biology* 366(1):207-215.
31. Firdaus-Raih M, Harrison AM, Willett P, & Artymiuk PJ (Novel base triples in RNA structures revealed by graph theoretical searching methods. *BMC Bioinformatics* 12 Suppl 13:S2.
32. Theobald DL & Steindel PA (Optimal simultaneous superpositioning of multiple structures with missing data. *Bioinformatics* 28(15):1972-1979.
33. Theobald DL & Wuttke DS (2008) Accurate structural correlations from maximum likelihood superpositions. *PLoS Comput Biol* 4(2):e43.
34. Fei J, Richard AC, Bronson JE, & Gonzalez RL, Jr. (2011) Transfer RNA-mediated regulation of ribosome dynamics during protein synthesis. *Nat Struct Mol Biol* 18(9):1043-1051.
35. Jenner LB, Demeshkina N, Yusupova G, & Yusupov M (2010) Structural aspects of messenger RNA reading frame maintenance by the ribosome. *Nat Struct Mol Biol* 17(5):555-560.
36. Vorstenbosch E, Pape T, Rodnina MV, Kraal B, & Wintermeyer W (1996) The G222D mutation in elongation factor Tu inhibits the codon-induced conformational changes leading to GTPase activation on the ribosome. *Embo J* 15(23):6766-6774.
37. Cannone JJ, *et al.* (2002) The comparative RNA web (CRW) site: an online database of comparative sequence and structure information for ribosomal, intron, and other RNAs. *BMC Bioinformatics* 3:2.
38. Ben-Shem A, Jenner L, Yusupova G, & Yusupov M (2010) Crystal structure of the eukaryotic ribosome. *Science* 330(6008):1203-1209.
39. Schuwirth BS, *et al.* (2005) Structures of the bacterial ribosome at 3.5 A resolution. *Science* 310(5749):827-834.
40. Goodey NM & Benkovic SJ (2008) Allosteric regulation and catalysis emerge via a common route. *Nature chemical biology* 4(8):474-482.

41. Benkovic SJ, Hammes GG, & Hammes-Schiffer S (2008) Free-energy landscape of enzyme catalysis. *Biochemistry* 47(11):3317-3321.
42. Youngman EM & Green R (2005) Affinity purification of in vivo-assembled ribosomes for in vitro biochemical analysis. *Methods* 36(3):305-312.
43. Qin D, Abdi NM, & Fredrick K (2007) Characterization of 16S rRNA mutations that decrease the fidelity of translation initiation. *Rna* 13(12):2348-2355.
44. Hashimoto Y, Yano T, Kuramitsu S, & Kagamiyama H (2001) Disruption of Thermus thermophilus genes by homologous recombination using a thermostable kanamycin-resistant marker. *FEBS letters* 506(3):231-234.
45. Koyama Y, Hoshino T, Tomizuka N, & Furukawa K (1986) Genetic transformation of the extreme thermophile Thermus thermophilus and of other Thermus spp. *J Bacteriol* 166(1):338-340.
46. Kabsch W (2010) Xds. *Acta crystallographica* 66(Pt 2):125-132.
47. Adams PD, *et al.* (2010) PHENIX: a comprehensive Python-based system for macromolecular structure solution. *Acta crystallographica* 66(Pt 2):213-221.
48. Chen VB, *et al.* (2010) MolProbity: all-atom structure validation for macromolecular crystallography. *Acta crystallographica* 66(Pt 1):12-21.
49. Emsley P, Lohkamp B, Scott WG, & Cowtan K (2010) Features and development of Coot. *Acta crystallographica* 66(Pt 4):486-501.
50. The PyMOL Molecular Graphics System, 1.2r3pre, Schrödinger, LLC.

CHAPTER 3: STRUCTURAL INSIGHTS INTO TRANSLATIONAL RECODING BY FRAMESHIFT SUPPRESSOR tRNA ^{SufJ}

Crystal E. Fagan, Tatsuya Maehigashi, Jack A. Dunkle, Stacey J. Miles, and Christine M. Dunham

The genetic code is converted into proteins using a three nucleotide genetic code. Here, I structurally and biochemically analyzed a tRNA containing an expanded anticodon stem-loop that renders it capable of decoding four nucleotides as a single residue. This work shows the insertion deforms the shape of the tRNA, without changing the structure of the tRNA-mRNA interactions in the ribosome. These data suggest the conformational distortion in a full length tRNA^{SufJ} would impede of interactions with translational machinery. This work has been accepted for publication at *RNA*.

Author contributions: C.M.D and C.E.F. designed research; S.M. purified the ribosomes; C.E.F. performed the ASL and tRNA binding affinity experiments; C.E.F. prepared and crystallized the ribosomal complexes; C.E.F. and T.M. collected and processed X-ray crystallography data; C.E.F. and J.D. refined and analyzed the structures; and C.E.F. and C.M.D wrote the paper

ABSTRACT

The three-nucleotide mRNA reading frame is tightly regulated during translation to ensure accurate protein expression. Translation errors that lead to aberrant protein production can result from the uncoupled movement of the tRNA in either the 5' or 3' direction on mRNA. Here, we report the biochemical and structural characterization of +1 frameshift suppressor $tRNA^{SufJ}$, a tRNA known to decode four, instead of three, nucleotides. Frameshift suppressor $tRNA^{SufJ}$ contains an insertion 5' to its anticodon, expanding the anticodon loop from seven to eight nucleotides. Our results indicate that the expansion of the anticodon loop of either ASL^{SufJ} or $tRNA^{SufJ}$ does not affect its affinity for the A site of the ribosome. Structural analyses of both ASL^{SufJ} and ASL^{Thr} bound to the *Thermus thermophilus* 70S ribosome demonstrate both ASLs decode in the zero frame. Although the anticodon loop residues 34-37 are superimposable with canonical seven nucleotide ASLs, the single C31.5 insertion between nucleotides 31 and 32 in ASL^{SufJ} imposes a conformational change of the anticodon stem, that repositions and tilts the ASL towards the back of the A site. Further modeling analyses reveal that this tilting would cause a distortion in full length A-site $tRNA^{SufJ}$ during tRNA selection and possibly impede gripping of the anticodon stem by 16S rRNA nucleotides in the P site. Together, these data implicate tRNA distortion as a major driver of noncanonical translation events such as frameshifting.

INTRODUCTION

The accurate translation of the genetic code into properly folded and active proteins is crucial to cellular survival. Errors in protein synthesis can result in misfolded or truncated proteins that trigger protein degradation pathways and even cellular apoptosis (1-3). Translation of a triplet nucleic acid sequence on mRNA into twenty different amino acids is carried out by the ribosome with high fidelity (10^{-4} -10^{-3}) where missense errors, or tRNA misincorporation, account for the majority of this error rate (1 in 3000 residues)(4-6). While processivity errors, such as changes in the mRNA reading frame, occur much less frequently (1 in ~30,000 amino acid incorporated), they are considered to be more detrimental than missense errors because they often prevent the production of a full length, functional protein (7). In organisms with a nearly equal genomic GC and AT nucleotide frequency, like *Escherichia coli*, out-of-frame stop codons occur roughly every twenty codons resulting in the rapid termination of translation following a frameshift error (7, 8). While much is known about the prevention of missense errors by ribosomal proofreading mechanisms (9, 10), how the ribosome maintains the mRNA reading frame is still poorly understood.

Genetic suppressor experiments in *Saccharomyces cerevisiae* and *Salmonella typhimurium* first demonstrated the three nucleotide genetic code could be altered (11-15). Extragenic mutations in tRNAs were found to compensate for insertions or deletions in the genetic code by noncanonical decoding of a non-three-nucleotide codon (reviewed in (16)). The first sequenced external **su**ppressor of a genetically encoded **f**rameshift (*sufD*) was a cytosine insertion immediately 5' of the $tRNA^{Gly}$ anticodon (5'-CCC-3'; all codons and anticodons are shown 5'-3') between position 33 and 34 (17). Because this particular frameshift suppressor expanded the glycine codon to GGG-G (first three nucleotides denote a glycine codon with the additional nucleotide preceded by a hyphen and underlined), the Watson-Crick complementarity between the cytosine insertion in the anticodon loop and the extra guanine in the codon suggested a four-base interaction between the tRNA-mRNA pair could form (18). Many frameshift suppressor

tRNAs were subsequently found to contain similar complementarity between insertions in anticodon stem-loops (ASLs) and suppressible four nucleotide codons, providing strong evidence for a quadruplet or four-base decoding model (11, 13, 19-21) (**Fig. 3.1A**). In addition, optimal frameshift suppression and thus increasing frameshift efficiencies were found to increase when a four nucleotide Watson-Crick base pair interaction was present (22-26).

The first exception to this quadruplet decoding model came with the identification of frameshift suppressor $tRNA^{SufJ}$, a modified $tRNA_3^{Thr}$ (GGU) containing a cytosine insertion in the anticodon loop between nucleotides C31 and U32, rather than adjacent to the anticodon (**Fig. 3.2**) (27). The C31.5 insertion allows $tRNA^{SufJ}$ to decode four nucleotide codons (ACC-A, ACC-C and ACC-U) as a single threonine, to restore the correct reading frame in a number of histidine biosynthesis gene derivatives such as *hisA*, *hisC*, *hisF and hisG* (18). While the variability in the additional nucleotide of the codon that frameshift suppressor $tRNA^{SufJ}$ decodes strongly suggests that a direct interaction between the additional nucleotide of the tRNA is not necessary for +1 suppression, it is unclear how an insertion within the anticodon loop, but distant from the anticodon, could expand the size of the codon. Because of the unique location of the insertion and apparent lack of Watson-Crick complementarity, it was proposed that $tRNA^{SufJ}$ mediated +1 frameshifting through a distinct mechanism (27).

More recent work has resulted in two additional models for +1 frameshifts. The first model was derived from X-ray crystal structures of 30S bound to ASLs containing eight nucleotide loops. These ASLs were not identified by suppressor studies but rather, were optimized for unnatural amino acid incorporation exploiting +1 frameshift decoding (28). These structures revealed a noncanonical ASL conformation where widening of the anticodon loop allows for three nucleotides of the ASL to extend over four nucleotides of the codon in the A site (29) (**Fig. 3.1B**). An additional model was proposed after the identification of $tRNA^{SufJ}$ and other subsequent suppressors such as $tRNA^{SufA6}$ and *suf16* tRNA mutations, where the shift into the new mRNA frame was not dependent upon forming Watson-Crick interactions in the A site (23,

30) (**Fig. 3.1C**). Instead, these studies indicated that frameshift efficiencies were heavily influenced by the next incoming tRNA, implying the frameshift in these particular cases, occurs in the P site (31-33). Given these distinct models, it has remained unclear whether a single, unified model could explain all types of +1 frameshifting facilitated by suppressor tRNAs.

Here, we present biochemical and structural studies of frameshift suppressor $tRNA^{SufJ}$ to elucidate how this suppressor decodes a four nucleotide codon in the A site. We performed affinity experiments to determine the effect of the C31.5 insertion on the ability of either ASL^{SufJ} or $tRNA^{SufJ}$ to recognize an A-site codon. We next solved five X-ray crystal structures of the ASLs of $tRNA^{SufJ}$ and $tRNA^{Thr}$ bound to the A site of the *Thermus thermophilus* (*Tth*) 70S ribosome. Our molecular insights reveal that frameshift suppressor tRNA distortion likely promotes +1 frameshifting.

RESULTS

The nucleotide insertion 5' of the anticodon minimally alters affinity for the A site. Expanded ASLs containing insertions 5' of the anticodon show lower affinities than wild-type tRNAs for the ribosomal A site (34). Therefore, as a first step in understanding the behavior of $tRNA^{SufJ}$ on the ribosome, we asked whether the expanded ASL of $tRNA^{SufJ}$ affects its ability to form stable, high affinity codon-anticodon interactions in the A site, typical of a canonical tRNA interacting with a cognate codon. We performed affinity binding experiments with ASL^{SufJ} and ASL^{Thr} using *E. coli* 70S ribosomes programmed with a P-site $tRNA^{fMet}$ containing either an ACC-A, ACC-U or ACC-C codon in the A site (**Fig. 3.3**). ^{32}P-ASL^{SufJ} was incubated with increasing amounts of 70S ribosomes and applied to nitrocellulose filters to determine the amount of ASL^{SufJ} bound. While ASL^{SufJ} bound to the A site of the ribosome with an apparent dissociation constant (K_D) of 85 and 76 nM for the ACC-A and ACC-U codons, respectively, ASL^{SufJ} had a slight decrease in affinity for the ACC-C codon (130 nM) (**Fig. 3.3A-C**; **Table 3.1**). These K_D values are all within the previously reported range for tRNA or ASL binding to

the A site (K_Ds between 33-500 nM) (34-36). The antibiotic paromomycin preferentially enhances the affinity of cognate ASLs (~15 fold) while only modestly enhancing the affinity of near-cognate ASLs (~2 fold) (37). Our results indicate that paromomycin increases the K_D ~6-8 fold for all three +1 suppressible codons, consistent with a cognate interaction between the anticodon of ASL^{SufJ} and the +1 codons. If the interaction in the A site was in the +1 mRNA frame, then the addition of paromomycin should not affect the K_D for the ACC-A codon given that the interaction would be near cognate (G34-A7; **Fig. 3.2**). These data provide initial support for a model where the interaction between ASL^{SufJ} and all three +1 suppressible codons is cognate suggesting ASL^{SufJ} is bound in the zero or normal frame.

To assess whether the 31.5 insertion in ASL^{SufJ} affects A-site binding, we next measured the binding of ASL^{Thr} to all three +1 suppressible codons in the presence or absence of paromomycin (**Table 3.1**). Similar K_D trends were observed, with ASL^{Thr} having a lower affinity for ACC-C (310 nM) compared to the ACC-A and ACC-U codons (150 and 160 nM, respectively) (**Fig. 3.3D-F**). These data indicate the C31.5 insertion in ASL^{SufJ} does not lower affinity as might have been expected of the ASL for the three codons, but instead, slightly increases the affinity.

The binding of tRNA to the A site of the ribosome occurs with slightly higher affinities than ASLs due to other tRNA features that interact with the 50S subunit such as the TΨC loop, the D loop and the CCA tail (38, 39). To test whether $tRNA^{SufJ}$ exhibits the same trends in A-site binding as ASL^{SufJ}, namely an affinity indicative of a cognate codon-anticodon interaction slightly higher than $tRNA^{Thr}$, we again performed binding assays. Consistent with the observed ASL binding trends, $tRNA^{SufJ}$ binds to each of the ACC-A, ACC-C and ACC-U codons with ~2-fold tighter K_D (15-32 nM) than $tRNA^{Thr}$ (27-58 nM; **Table 3.1**). Also consistent with our ASL binding studies, both tRNAs had similar dissociation constants for ACC-A and ACC-U codons ($tRNA^{SufJ}$ 15 and 19 nM, respectively; $tRNA^{Thr}$ 27 and 35 nM, respectively), and a slightly weaker affinity for the ACC-C codon ($tRNA^{SufJ}$ 32 nM; $tRNA^{Thr}$ 58 nM). These results indicate that both suppressor ASL^{SufJ} and $tRNA^{SufJ}$ follow general trends previously seen for other

canonical tRNAs and provide further evidence that the expansion of the anticodon loop to eight nucleotides by the C31.5 insertion does not impede binding to cognate codons in the ribosomal A site.

Structural determination of ASLSufJ bound to +1 suppressible codons in the 70S A site. To determine how $tRNA^{SufJ}$ decodes a four nucleotide codon and understand how an expanded ASL is accommodated in the A site, we solved three X-ray crystal structures of *Tth* 70S programed with a P-site $tRNA^{fMet}$ and ASL^{SufJ} bound to each of the following +1 suppressible codons: ACC-A, ACC-C and ACC-U (**Fig. 3.4A & Fig.3.5; Table 3.2**). The resolutions of the three structures ranged from 3.5 Å to 3.6 Å and, in all three structures, unbiased F_o-F_c difference electron density maps showed a clear signal for mRNA, P-site $tRNA^{fMet}$ and A-site ASL^{SufJ} nucleotides 29-42 (**Fig. 3.6**).

In the 70S structure of ASL^{SufJ} decoding an ACC-A codon in the absence of paromomycin, the three nucleotide anticodon of ASL^{SufJ} (34, 35 and 36) forms Watson-Crick base pairs with the first three nucleotides of the ACC codon in the zero frame (**Fig. 3.4A**). The structures of ASL^{SufJ} bound to the ACC-C and ACC-U codons in the presence of paromomycin reveal the same three Watson-Crick base pair interaction between the codon and anticodon, indicating the antibiotic does not alter the conformations (paromomycin was used to enhance the diffraction of these crystals) (**Fig. 3.5)**. In all three structures, there are no interactions with the fourth nucleotide of the A-site codon (position 7 of the mRNA (Figs.1, 4A and S1)). This lack of interaction is despite the potential to form a Watson-Crick base pair between the codon nucleotide A7 in the ACC-A codon and ASL nucleotide U33 (**Fig. 3.2**). Additionally, the presence of either an A, C or U 3' to the codon (fourth position of the A-site codon or denoted as A7, C7 or U7) does not alter the mRNA path (**Fig. 3.7**). ASL^{SufJ} models in all three structures superimpose well, with a root mean square deviation of 0.25 Å, providing additional evidence that the ASL does not adopt different conformations depending upon the identity of the fourth nucleotide of the A-site codon. In

summary, these structures confirm that the +1 frameshift mediated by $tRNA^{SufJ}$ does not occur during decoding in the A site and therefore, excludes the quadruplet decoding model (**Fig. 3.1A**).

During decoding, 16S rRNA nucleotides A1492, A1493, and G530 monitor the minor groove of the codon-anticodon helix to probe for Watson-Crick base pair geometry (40, 41). These 16S rRNA residues form hydrogen bonds with the first and second nucleotide pairs of the codon-anticodon helix during cognate tRNA decoding (40). In addition to canonical interactions with 16S rRNA, 23S rRNA residue A1913 also forms a hydrogen bond with the 2'-OH of ASL^{SufJ} nucleotide 37. All of these interactions are seen upon ASL^{SufJ} decoding the ACC-A codon (in the absence of paromomycin), indicating the ribosome recognizes this interaction as cognate (**Fig. 3.4A**). The 70S structures of ASL^{SufJ} bound to the ACC-C and ACC-U codons additionally contain paromomycin, which was added to enhance the diffraction properties of these complexes (**Fig. 3.5**). As expected, the structures containing paromomycin also display the same characteristic cognate interactions as the 70S-ACC-C structure lacking paromomycin. However since all three structures contain the same A-site interactions between the ACC codon and the anticodon, this provides strong evidence that all three +1 suppressible codons are recognized as cognate by the ribosome.

To accurately compare ASL^{SufJ} to other ASLs that contain seven nucleotide anticodon loops, we solved two additional 70S complexes containing ASL^{Thr} bound to either ACC-A or ACC-C codons in the A site of the 70S *Tth* ribosome to 3.6 Å resolution **(Fig. 3.8 & Table 3.2)**. Both structures also contained paromomycin. These two codons were selected because of the ~2-fold higher affinity of both ASL^{SufJ} and ASL^{Thr} for the ACC-A codon as compared to the ACC-C codon (**Fig. 3.3 and Table 3.1**). Unbiased F_o-F_c difference electron density maps showed a clear signal for mRNA, P-site $tRNA^{fMet}$ and A-site ASL^{Thr} nucleotides 28-43. Structural analyses revealed that ASL^{Thr} recognizes both ACC-A and ACC-C codons in the zero frame as cognate, with A1492, A1492 and G530 interacting with the first two base pairs of codon-anticodon helix.

The C31.5 insertion in ASL^{SufJ} results in conformational rearrangements in the stem of the ASL. The C31.5 insertion in tRNA^{SufJ} was previously predicted to form a new stacking interaction with U32 allowing a widening of the unpaired loop of the ASL, while preserving the anticodon structure (27). Our results indicate that the anticodon loop nucleotides 33-37 are superimposable with other ASLs containing seven nucleotides, including ASL^{Thr} (**Fig. 3.4B**). The C31.5 insertion neither forces a bulge in the stem to allow for stacking with U32 nor causes a widening of the loop; in fact, the loop of ASL^{SufJ} is narrower than normal ASLs (**Fig. 3.4B & 3.9A**). In contrast, large, concerted movements of both the 5' and 3' phosphate backbone of the anticodon stem facilitate accommodation of the C31.5 insertion (**Fig. 3.4B**). The 5' stem, in which C31.5 is located, displaces the phosphate backbone by ~4 Å towards the 3' ASL stem (**Fig. 3.4B**). Likewise, the 3' stem undergoes an even larger displacement of ~7 Å in the same direction away from the 5' stem. These combined repositionings result in tilting of the anticodon stem ~11.5° away from the P-site tRNA^{fMet}, towards the back of the 30S A site (**Fig. 3.4B**).

The concerted movement of the anticodon stems of ASL^{SufJ} narrows the major groove from 18.4 to 17.4 Å (phosphate-phosphate distances) and the minor groove from 14.2 Å to 9 Å (C2'-C2' distances) **(Fig. 3.9A**). Collectively, these changes cause a reduction in the average base pair incline (or the angle between the base pair) and the helical axis from 14° in ASL^{Thr} to 11.5° in ASL^{SufJ} with a concomitant increase in the overall helical twist (29° in ASL^{Thr} versus 33° in ASL^{SufJ}). An additional noted consequence of the ASL stem rotation towards the back of the A site, is that this movement prevents a conserved interaction between Lys121 of ribosomal protein S13 and the 2'-OH of G40. While the electron density of the Lys121 side chain is not interpretable, the conformational rearrangement of nucleotide G40 of ASL^{SufJ} would prevent any possibility of forming a hydrogen bonding interaction with this residue given the larger distance.

Anticodon stem register is maintained in ASL^{SufJ} despite alteration of the conserved 32-38 base pair. The C31.5 nucleotide occupies the physical position of C31 in the 70S-ASL^{Thr}

structures, thereby shifting the 5' side of the ASL^{SufJ} stem by one nucleotide (**Fig. 3.9A**). However, the base pair register is maintained with the opposite side of the stem via a rotation of the G39 base (25°) about its N-glycosidic bond (**Fig. 3.9B**). While this change in torsion angle preserves the C31-G39 interaction of the stem, it disrupts the conserved U32•A38 base pair (**Fig. 3.9C)**. Although the position of U32 is largely consistent between the 70S-ASL^{Thr} and 70S-ASL^{SufJ} structures, A38 rotates 8° to form a new bifurcated hydrogen bond between its N6 position and both the N3 and O2 atoms of the inserted C31.5 (**Fig. 3.9C)**. The C31.5 insertion in ASL^{SufJ} structurally replaces the U32 in the U32•A38 interaction as seen in ASL^{Thr}, therefore forming a new C31.5•A38 pair (**Fig. 3.9C**).

Projection of tRNASufJ in the A and P sites indicates potential rearrangements due to steric clashes. Previously determined 70S and 30S structures containing A-site tRNAs or ASLs, all contain anticodon stem loops that adopt a conformation that closely approximates an accommodated or pre-peptidyl transferase state (42). However, in special cases such as an insertion in the anticodon or modifications at nucleotide 34, the A-site ASL can adopt an alternate conformation but only at the anticodon or the unpaired anticodon loop (43-45). The conformational changes of the anticodon stem that we observe in ASL^{SufJ} have never been seen previously in any 70S structure. To understand how the 11.5° tilt would affect the position of ASL^{SufJ} in the context of a full-length tRNA, we aligned the anticodons of ASL^{SufJ} and $tRNA^{Phe}$ (PDB code 2WDH) and then projected a full-length $tRNA^{SufJ}$ using fully accommodated Phe-$tRNA^{Phe}$ as a guide (42) (**Fig. 3.10A**). This alignment revealed the tilted stem domain of ASL^{SufJ} repositions the acceptor arm >20 Å distant from the position of a canonical accommodated state tRNA. Moreover, $tRNA^{SufJ}$ would clash with components of the 50S (**Fig. 3.10A**). Clearly $tRNA^{SufJ}$ does not bind in this manner to the 70S and must instead, undergo structural remodeling in order to for tRNA selection. In summary, the 11.5° tilt of the anticodon stem of ASL^{SufJ}

suggests that the C31.5 insertion changes the energetic landscape that governs the transition of tRNA between its various functional conformations.

In the 30S A site, the ribosome exclusively interacts with the anticodon of the tRNA to ensure high fidelity tRNA selection. Upon translocation to the P site by EF-G, the anticodon is no longer closely monitored. Instead, the ribosome interacts with the anticodon stem and other regions of the tRNA body to optimally orient the acceptor arm for peptide bond formation. It has been proposed that the P site has evolved to tightly grip the tRNA in order to maintain proper mRNA reading frame (32, 33, 46, 47). For example, initiator $tRNA^{fMet}$ is 'gripped' by 16S rRNA residues G1338 and A1339 through A-minor motif interactions with anticodon stem base pairs (**Fig. 3.10B**) (46, 48). Superpositioning of A-site ASL^{SufJ} into the P site by alignment of the anticodon to $tRNA^{fMet}$ reveals the 5' stem adjacent to the insertion site and the C31.5 phosphate would sterically clash with 16S rRNA residue A1339. However, the twist in the ASL^{SufJ} stem prevents the formation of A-minor interactions with 16S rRNA nucleotide G1338 (**Fig. 3.10C**). This predicted lack of interaction indicates that either the gripping of the anticodon stem of $tRNA^{SufJ}$ is different from wild-type tRNAs or a conformational rearrangement of the stem occurs. The remodeling of the anticodon stem could possibly occur during translocation or after translocation into the P site, which in turn, facilitates the movement of mRNA by one nucleotide into the +1 frame.

DISCUSSION

Extragenic +1 frameshift suppressors were predominately identified as nucleotide insertions in the anticodon loops of tRNAs (reviewed in (33)). Although one interpretation of this phenomenon was that the efficiency of +1 frameshifting was dependent on the Watson-Crick complementarity between the insertions located in both the tRNA and codon, the identification of $tRNA^{SufJ}$ necessitated alternative hypotheses (27, 31). While $tRNA^{SufJ}$ does contain an insertion in its anticodon loop, the extra nucleotide is located adjacent to the anticodon stem, distal from the

anticodon and therefore it was unclear whether this insertion actually expanded the anticodon to more than three nucleotides. The structures here reveal that ASL^{SufJ} binds to three +1 suppressible codons in the zero frame allowing only a three nucleotide codon-anticodon cognate interaction in the A site. The C31.5 insertion does not appear to alter the structural integrity of the ASL in the same manner as other frameshift suppressors where disordering of the conserved U turn, the entire 5' stem or nucleotide 32 occurs (29, 44, 49). Instead, ASL^{SufJ} accommodates the insertion through concerted movements of both the 5' and 3' phosphate backbones of the anticodon stem, causing a reorganization of key nucleotide interactions in the anticodon loop. These results indicate that insertions either 5' or 3' of the anticodon that result in +1 frameshifting may adopt different structural changes with an underlying theme being that tRNA plasticity, rather than the codon-anticodon interaction, drives +1 frameshifting.

Our 70S-A-site ASL^{SufJ} structures reveal that the C31.5 insertion does not widen the anticodon loop but, rather, causes a narrowing of both the major and minor grooves of the ASL. Narrowing of the anticodon loop was also observed in a recent 70S structure containing an A-site +1 frameshift suppressor $tRNA^{SufA6}$ (49). In this case, $tRNA^{SufA6}$ contains an insertion 3' to the anticodon between nucleotides 37 and 38, on the opposite side of the loop to C31.5 in $tRNA^{SufJ}$. In contrast, a previously solved 30S structure bound to a +1 frameshift suppressor ASL shows an insertion at 33.5 causes a widening of the loop (29) . It remains unclear whether a narrowing or a widening of frameshift suppressor tRNA anticodon loops indicates a different mechanism by which a +1 reading of the mRNA occurs. However, a common emerging theme is that insertions in the anticodon stem-loops of tRNAs are accommodated in different ways thus reinforcing their structural plasticity.

Although the reorganization of the anticodon loop interactions allows for maintenance of the base pair registry, the major consequence of this preservation and the C31.5 insertion is that the identity of the 32-38 interaction is altered from U32□A38 to C31.5□A38. Anticodon stem nucleotides 32 and 38 are important for tRNA affinity and selection on the ribosome with the

identity of this pair directly correlated to both the Watson-Crick basepair strength of the codon-anticodon interaction and the aminoacyl group attached to the CCA 3' end (50, 51). A strong C32□A38 interaction is predicted to counteract a weak codon-anticodon interaction such as in the case of $tRNA^{Lys}$ (UUU), whereas a weak U32□A38 interaction is normally paired with a strong codon-anticodon interaction such as in the case of $tRNA^{Pro}$ (GGG) (50). This correlation of the 32-38 identity and the codon-anticodon strength allows for the fine tuning of tRNA selection by the ribosome. Surprisingly, compensatory mutations of the rare A32-U38 pair in $tRNA^{Ala}$ to the more common U32-A38 displayed no effects on tRNA binding or incorporation when decoding cognate codons (52). However, $tRNA^{Ala}$ with the strong U32-A38 pair is more rapidly accommodated when a near-cognate codon is present in the A site, indicating a loss of fidelity. Additional evidence for the importance of the 32-38 pairing comes from tRNA suppressor experiments using an amber stop codon. Here, stop codon readthrough efficiencies were increased when 32-38 was mutated to a strong C32•A38 pair, again strongly suggesting a loss of fidelity (53-57). We predict that, in general, the insertion of a nucleotide within an anticodon loop reduces its binding affinity to the ribosomal A site. However, in the case of ASL^{SufJ} where the insertion results in the formation of a new, strong C31.5•A38 interaction, our interpretation is that the predicted lower affinity resulting from expansion of the ASL to 8 nucleotides is counterbalanced by the increased strength of the 31.5•38 interaction. Indeed, our affinity measurements with ASL/$tRNA^{SufJ}$ indicate that the C31.5 insertion slightly increases A-site affinity as compared to wild-type ASL/$tRNA^{Thr}$. Likewise we would predict that if C31.5 were mutated to an uridine resulting in a U31.5•A38 weaker pairing, the binding affinity for the ribosomal A site would be reduced.

Our results examining ASL^{SufJ} in light of our recent studies of ASL^{SufA6} (49) lead us to propose that +1 frameshifting by these suppressors does not occur by quadruplet decoding in the A site. Although the structures of ASL^{SufJ} and ASL^{SufA6} indicate the insertions alter the anticodon loops in distinct manners, both structures involve either the rearrangement or disruption of the 32-

38 pair. This reorganization of the 32-39 pairing occurs despite ASL^{SufJ} forming a cognate interaction while ASL^{SufA6} forms a near-cognate interaction with their +1 suppressible codons in the A site. What remains unclear is if the frameshift occurs during translocation or after translocation of the mRNA-tRNA pair to the P site. Unlike ASL^{SufA6}, the 5' ASL stem of ASL^{SufJ} is ordered. Disordering may be an important stimulus for the +1 frameshift event because EF-G directly interacts with the 5' stem in the A site before translocation (58). Interestingly, the narrowing of the stem and 11.5° tilting of ASL^{SufJ} (**Fig. 3.4B**) suggests that adjustment of P-site interactions with conserved 16S rRNA nucleotides G1338 and A1339 could occur upon translocation. Another possibility is that ASL^{SufJ} would be required to undergo a conformational rearrangement of its anticodon loop to maintain this important gripping interaction, which could facilitate the shifting into the new +1 reading frame. Taken together, these results help to begin to unravel mechanistic details of +1 frameshifting.

MATERIALS AND METHODS

***E. coli* ribosome purification**. 70S ribosomes were purified as previously described with a few modifications (59). Briefly, *E. coli* MRE600 cells was grown in LB to an OD_{600} of 0.6–0.8 and then cooled on ice for 20 min to increase the concentration of run-off 70S ribosomes. Cultures were then pelleted and resuspended in buffer A (20 mM HEPES pH 7.5, 100 mM NH_4Cl, 10.5 mM MgOAc, 0.5 mM EDTA, 0.1 mM benzamidine, 0.1 mM phenylmethanesulfonylfluoride (PMSF) and 6 mM β-mercaptoethanol (β-Me)) and lysed using a EmulsiFlex cell disruptor. The lysate was clarified by centrifugation (30 min at 30,000 rpms) and pelleted over a sucrose cushion (1.1 M sucrose, 20 mM HEPES pH 7.5, 500 mM NH_4Cl, 10.5 mM MgOAc, 0.5 mM EDTA) for 17 hrs at 45,000 rpm at 4 °C. The ribosome pellet was resuspended in buffer C (20 mM Tris-Cl pH 7.5, 400 mM KCl, 10 mM MgOAc, 1.5 M $(NH_4)_2SO_4$, 0.1 mM benzamidine, 0.1 mM PMSF, and 6 mM β-Me) and purified over a Butyl-650S HIC column (Toyopearl) using a reverse $(NH_4)_2SO_4$ gradient. 70S ribosomes were further separated over a 10%–40% sucrose gradient in

buffer E (10 mM HEPES pH 7.5, 50 mM KCl, 10 mM NH_4Cl, 10.25 mM MgOAc, 0.25 mM EDTA, 0.1 mM benzamidine, 0.1 mM PMSF and 6 mM β-Me). Fractions were pooled and concentrated by pelleting over a sucrose cushion, resuspended and dialyzed overnight in buffer G (5 mM HEPES pH 7.5, 50 mM KCl, 10 mM NH_4Cl, 10 mM MgOAc and 6 mM β-Me). Lastly, purified 70S ribosomes were concentrated using an Amicon 100K molecular weight cut-off concentrator (Millipore) and stored at -80 °C.

***In vitro* transcription.** *Salmonella typhimurium* $tRNA^{SufJ}$, along with a 5' T7 promoter site, were subcloned into a pUC19 vector using overlapping DNA oligos (IDT). Plasmid overexpression, purification and *in vitro* transcription reactions were performed as previously described using BstNI (NEB) to linearize the plasmid (60). The 5' triphosphate was removed by Calf Intestinal Phosphatase (NEB) and purified by phenol-chloroform and chloroform extractions followed by ethanol precipitation and stored in Tris-EDTA buffer (10 mM Tris-HCl pH 8.0, 1 mM EDTA) at -20 °C. For the *Salmonella typhimurium* $tRNA^{Thr}$, we encountered difficulties purifying $tRNA^{Thr}$ away from a contaminating RNA band of a similar size after *in vitro* transcription. Therefore we PCR amplified the $tRNA^{Thr}$ gene and a 5' T7 promoter site from overlapping DNA oligos (IDT) and purified the *in vitro* transcribed RNA product as previously described (60).

RNA sequences. The mRNA sequence used in both the filter binding experiments and crystallization trials was 5'-GGCAAGGAGGUAAAA*AUG***ACCH**AAA-3', where H represents an A, U or C nucleotide (threonine codon is in bold and follows the italicized AUG start site). ASL^{Thr} sequence was 5'-CACCCUUGGUAAGGGUG-3' and for ASL^{SufJ} was 5'-CACCC**C**UUGGUAAGGGUG-3' where the anticodon is underlined and nucleotide insertion in ASL^{SufJ} is indicated in bold (IDT).

5'-labeling of ASLs and tRNAs. tRNAs or ASLs (1 μM) were incubated with [γ-^{32}P]-ATP (1μCi/μL, 3000 Ci/mmol, Perkin Elmer) and T4 polynucleotide kinase (PNK, NEB) for 1 hr at 37 °C. Free nucleotide was removed by purification over a Sephadex G-25 spin column (GE Healthcare) and the labeling efficiency was determined by scintillation counting (Beckman LS-5000TD). A typical filter binding reaction contained 200,000 to 700,000 cpm/μM of tRNA or ASL. Labeled tRNA or ASL were stored at a concentration of 10 μM at -20 °C.

70S binding assays. The affinity of tRNAs or ASLs for the 70S A site was measured using filter binding assays as previously described (61). Briefly, purified *E. coli* 70S ribosomes (500 nM) were incubated with mRNA (1 μM) in buffer G at 37 °C for 5 min, followed by the addition of P-site tRNA^{fMet} (1 μM) at 37 °C for 30 min. For some experiments as indicated, paromomycin (100 μM) was incubated for an additional 25 min at room temperature. Two-fold dilutions were made, resulting in a range of ribosome concentrations from 0.98 nM to 500 nM which was experimentally determined to provide full coverage of the equilibrium dissociation curve; overall the ribosome concentration range were measured from 5 nM to 1 μM. A-site tRNA (2 nM) or ASL (2 nM) was added to each solution and the reaction was allowed to come to equilibrium at room temperature. A 3 hr incubation was required for tRNA binding to reach equilibrium, however with the addition of paromomycin only a 2 hr incubation was necessary. The ribosome reaction (30 μL) was then filtered through a 0.45 μm nitrocellulose membrane and washed with buffer G (1 mL). The nitrocellulose filters were dissolved in Filtron-X (National Diagnostics) and counted using a Beckman LS-5000TD scintillation counter. Dissociation constants (K_D) and B_{max} values were obtained by fitting the data to a one site specific binding nonlinear regression using GraphPad Prism as has been done for previous equilibrium binding experiments (51).

70S complex formation and crystallization. *Thermus thermophilus* ribosomes were purified and crystallization trials were performed as previously described with a few minor modifications (46).

Briefly, 70S ribosomes (4.4 μM) were incubated with CC-puromycin (Dharmacon; 22 μM), an aminoacyl mimic consisting of the RNA dinucleotide CC covalently attached to puromycin-5'-monophosphate, for 30 min at 55 °C. This was followed by incubation with a two molar excess of mRNA (IDT; 8.8 μM) for 5 min. Four molar excess of P-site $tRNA^{fMet}$ (Chemical Block; 17.6 μM) was incubated for 30 min at 55 °C and finally, four molar excess of the appropriate ASL (IDT; 22 μM) was incubated for 30 min at 55 °C. The complexes were cooled to room temperature and then incubated with antibiotic paromomycin (0.1 mM) for an additional 20 min at room temperature. Deoxy BigCHAP (Hampton Research; 2.8 μM) was added just prior to crystallization. Crystals were grown by sitting-drop vapor diffusion in 4-5% polyethylene glycol (PEG) 20K, 4-5% PEG 550 MME, 0.1 M Tris-Acetate pH 7.0, 0.2 M KSCN and 10 mM $MgCl_2$, and cryoprotected by increasing PEG 550 MME in a stepwise manner to a final concentration of 30%. Crystals were flash frozen in liquid nitrogen for data collection.

X-ray data collection and structure determination. X-ray diffraction data were collected at the Southeast Regional Collaborative Access Team (SER-CAT) 22-ID beamline and the Northeastern Collaborative Access Team (NE-CAT) 24-IDC beamline at the Advanced Photon Source, Argonne National Laboratory. Each dataset was integrated and scaled using the XDS software package (62). A search model composed of the *Tth* 70S ribosome (PDB codes 2WDG, 2WDH, 2WDI and 2WDJ) with all mRNA and tRNA ligands removed was used for crystallographic refinement with the PHENIX software suite (63). Additional rounds of coordinate refinement were performed with rigid groups defined by the head, body, platform, and 3'-minor domain of the 30S subunit, along with mobile elements of the 50S subunit: 5S rRNA, L1 arm, protein L9, A-site finger, and the central protuberance. Modeling of mRNA, tRNA, and conformational changes in rRNA and ribosomal proteins along with the placement Mg^{2+} ions were performed using Coot (64). Iterative rounds of model building were followed by positional and group atomic

displacement parameter (ADP) refinement in PHENIX, yielding a final model with the statistics reported in **Table 3.2**. Figures were generated using PyMOL (www.pymol.org) (65).

ACKNOWLEDGEMENTS

Support for this work was provided by the Department of Defense through the National Defense Science and Engineering Graduate Fellowship Program and NIH Training Grant T32 GM8367 (to CEF), and National Institute of General Medical Sciences of the NIH Award R01GM093278 (to CMD). CMD is a Pew Scholar in the Biomedical Sciences. We thank G. L. Conn for helpful discussions throughout the project and critical reading of the manuscript; and staff members at both SER-CAT and NE-CAT beamlines for assistance during data collection. This work is based on research conducted at the Advanced Photon Source on the NE-CAT beamlines (supported by National Center for Research Resources [National Institutes of Health (NIH)] Award RR-15301) and SER-CAT beamline. Use of the Advanced Photon Source, an Office of Science User Facility operated for the US Department of Energy (DOE) Office of Science by Argonne National Laboratory, was supported by US DOE Contract DE-AC02-06CH11357.

FIGURES

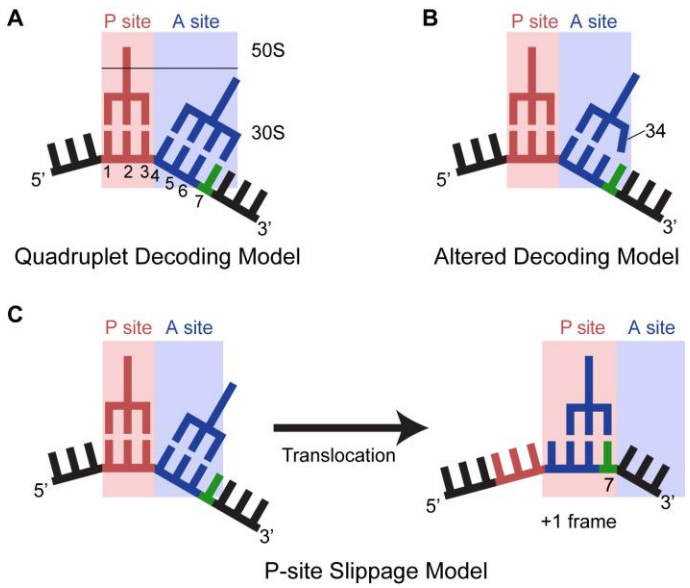

Figure 3.1. Possible model for +1 frameshifting resulting from an eight-nucleotide anticodon stem-loop. (A) The quadruplet decoding model posits that insertions in the anticodon stem-loop of a frameshift suppressor tRNA leads to a four nucleotide anticodon capable of decoding and translocating a four nucleotide mRNA codon (with the extra nucleotide shown in green). The numbering of the mRNA begins with the first position in the P site. **(B)** An alternative model proposed is that the nucleotide insertion in the anticodon stem loop causes a widening of the loop, allowing the anticodon nucleotide 34 to interact with the fourth nucleotide of the A-site codon (green; numbered as 7 in A). **(C)** In the P-site slippage model, normal decoding in the zero frame occurs in the A site, however the transition into the +1 frame occurs after translocation to the P site due to a weakened interaction between the anticodon and codon.

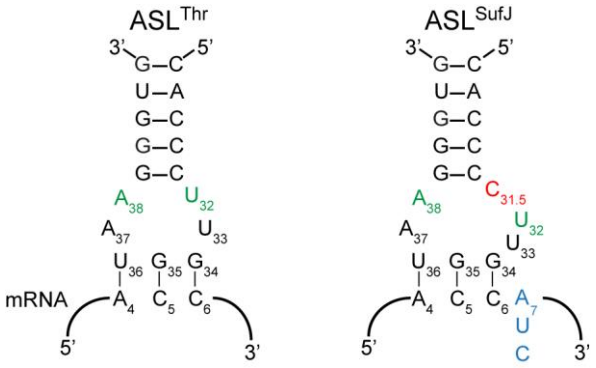

Figure 3.2. Frameshift suppressor tRNA^{SufJ} is a derivative of tRNA^{Thr}. Secondary structure representation of the anticodon stem-loops of tRNAThr and frameshift suppressor tRNASufJ interacting with their respective codons. The C31.5 insertion (red) in ASLSufJ is 5' to the anticodon nucleotides 34, 35 and 36 causing the codon to increase from three to four nucleotides (blue). The conserved U32•A38 interaction (green) in tRNAThr may be altered in tRNASufJ due to the insertion.

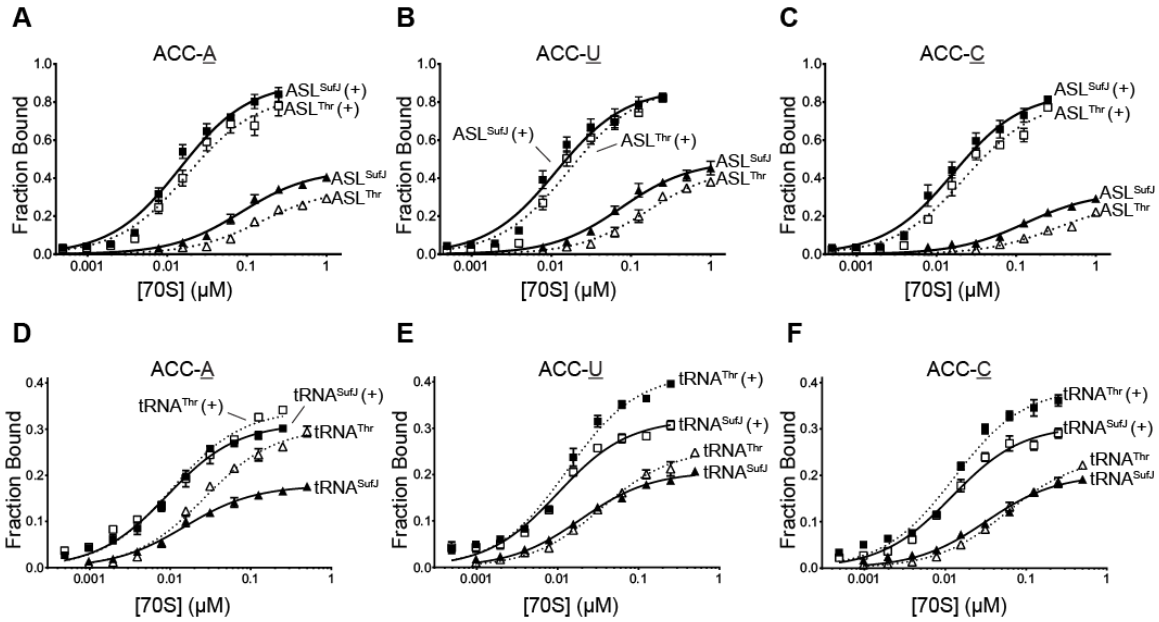

Figure 3.3. A-site binding of ASL^{SufJ}, ASL^{Thr}, $tRNA^{SufJ}$ and $tRNA^{Thr}$. Increasing concentrations of 70S ribosomes were programed with A-site codons **(A)** ACC-A, **(B)** ACC-U or **(C)** ACC-C and mixed with 2 nM [^{32}P] ASL^{Thr} (□/△; dashed lines) or ASL^{SufJ} (■/▲; solid lines). The presence or absence of the antibiotic paromomycin is indicated by '+'. Similar binding experiments were also performed with $tRNA^{Thr}$ ((□/△; dashed lines) or $tRNA^{SufJ}$ (■/▲; solid lines) with A-site codons **(D)** ACC-A, **(E)** ACC-U or **(F)** ACC-C in the presence or absence of paromomycin (indicated by '+').

Table 3.1. Binding affinity of tRNAs or ASLs to the A site of ribosomes programmed with different mRNA codons.

A-site codon	$tRNA^{Thr}$	$tRNA^{SufJ}$	ASL^{Thr}	ASL^{SufJ}
ACC-A	27, 0.30	15, 0.18	150, 0.35	85, 0.44
ACC-A, + paro	10, 0.34	9.2, 0.31	18, 0.84	14, 0.90
ACC-C	58, 0.24	32, 0.20	310, 0.27	130, 0.33
ACC-C, + paro	13, 0.39	12, 0.31	23, 0.81	16, 0.85
ACC-U	35, 0.25	19, 0.21	160, 0.46	76, 0.49
ACC-U, + paro	13, 0.42	10, 0.32	17, 0.89	11, 0.87

Values correspond to K_D (nM) and B_{max}. Binding experiments were also performed in the presence of 100 µM paromomycin and denoted as '+ paro'.

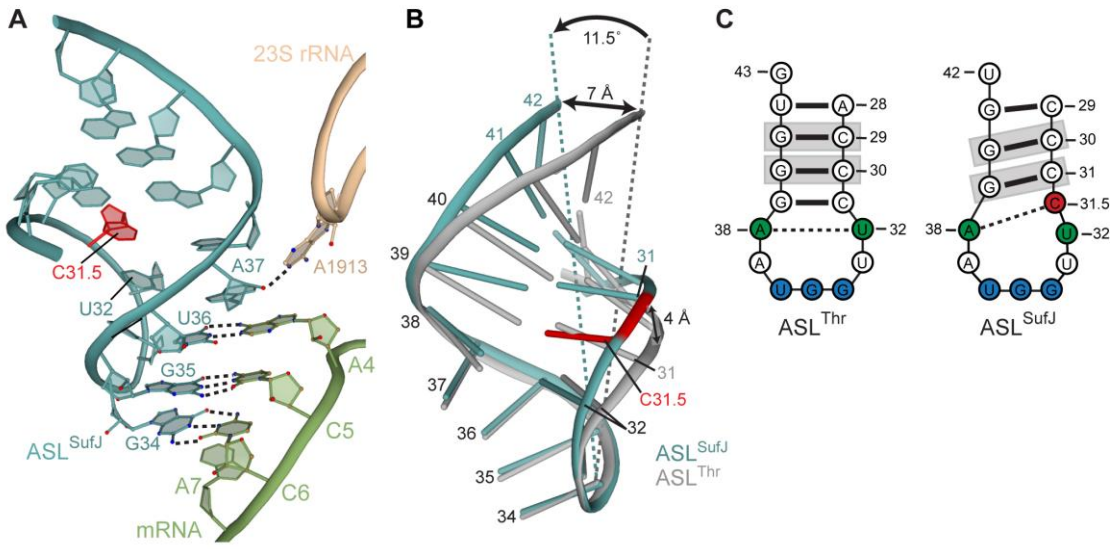

Figure 3.4. Conformation of ASL^{SufJ} in the 70S A site. (A) ASL^{SufJ} (blue) forms three Watson-Crick base pairs with three nucleotides of the ACC-A codon (green) in the zero frame (no paromomycin). Although the C31.5 insertion (red) increases the anticodon loop to eight nucleotides, the ASL is recognized as cognate with 23S rRNA nucleotide A1913 (tan) maintaining a hydrogen bond interaction with the 2'-OH of A37. **(B)** Overlay of ASL^{SufJ} and ASL^{Thr} (gray) bound in the 70S A site shows the C31.5 insertion displaces the 5' and 3' phosphate backbone by 7 Å and 4 Å, respectively. This narrowing of the major and minor grooves of ASL^{SufJ} also results in the entire stem tilting 11.5° towards the back of the A-site decoding center. **(C)** Secondary structure representation of ASL^{Thr} and ASL^{SufJ} shows that the 31.5 insertion changes the conserved interaction between the U32•A38 (green) to C31.5 (red)•A38. The nucleotides that are gripped by 16S rRNA residues G1338 and A1339 upon translocation to the P site are highlighted in gray.

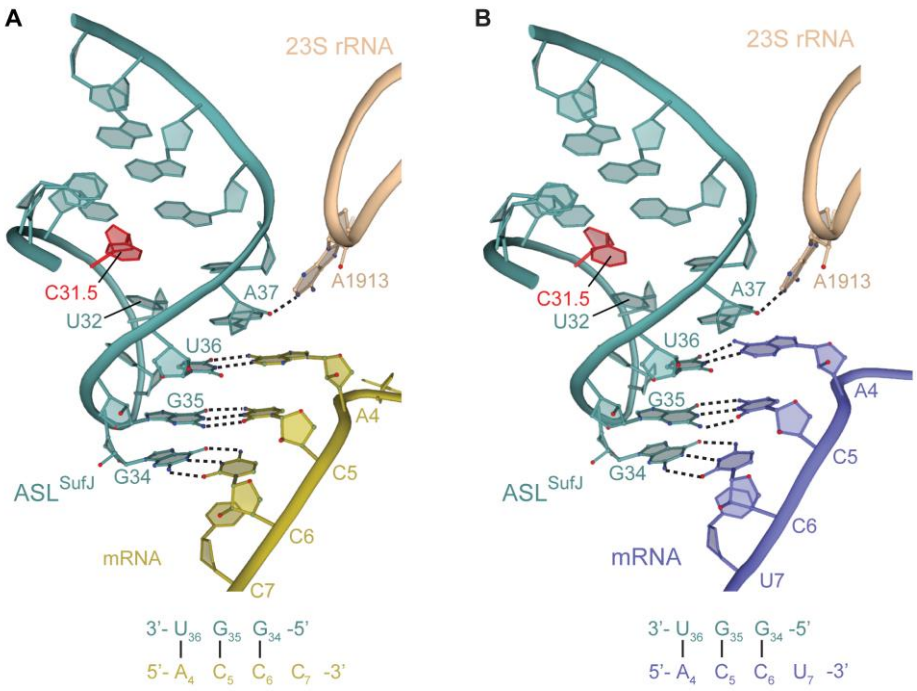

Figure 3.5. ASL^{SufJ} interactions with mRNA in the A site. ASL^{SufJ} (blue) forms three Watson-Crick base pairs with the first three nucleotides of the +1 suppressible codons **(A)** ACC-C (gold) and **(B)** ACC-U (dark blue) in the zero frame. These structures were solved with the antibiotic paromomycin. The C31.5 insertion (red) expands the anticodon loop to eight nucleotides. The ASL is stabilized by hydrogen bonding with 23S rRNA nucleotide A1913 (tan).

Table 3.2. Data collection and refinement statistics

tRNA:	**ASL^{SufJ}**			**ASL^{Thr}**	
mRNA:	**ACC-A***	**ACC-U**	**ACC-C**	**ACC-A**	**ACC-C**
Data collection					
Space group	$P2_12_12_1$	$P2_12_12_1$	$P2_12_12_1$	$P2_12_12_1$	$P2_12_12_1$
Cell dimensions					
a, b, c (Å)	209.4 450.7 622.3	210.8 448.9 621.6	210.5 450.7 621.1	209.0 448.7 621.0	209.0 444.6 616.4
α, β, γ (°)	90.0 90.0 90.0	90.0 90.0 90.0	90.0 90.0 90.0	90.0 90.0 90.0	90.0 90.0 90.0
Resolution (Å)	50.0-3.6 (3.7-3.6)	50.0-3.5 (3.6-3.5)	50.0-3.6 (3.7-3.6)	70.0-3.6 (3.7-3.6)	70.0-3.6 (3.7-3.6)
R_{merge} (%)	28.7 (125.1)	23.1 (114.7)	18.7 (90.8)	21.5 (89.9)	18.7 (90.5)
I/σI	7.3 (1.6)	5.7 (1.2)	7.8 (1.9)	6.8 (1.8)	7.3 (1.7)
Completeness (%)	99.2 (99.6)	99.7 (98.6)	99.9 (99.8)	98.0 (99.3)	96.8 (97.7)
Redundancy	6.6 (6.4)	5.8 (4.8)	5.3 (5.1)	4.1 (4.1)	3.4 (3.4)
Refinement					
Resolution (Å)	50.0-3.6 (3.7-3.6)	50.0-3.5 (3.6-3.5)	50.0-3.6 (3.7-3.6)	70.0-3.6 (3.7-3.6)	70.0-3.6 (3.7-3.6)
No. reflections	668,466	725,686	674,544	656,584	636,863
R_{work} / R_{free} (%)	21.4/25.3	21.4/25.0	20.5/24.4	20.8/25.2	21.7/25.9
No. atoms	292,042	292,242	292,106	292,311	292,320
B-factors (Å^2)					
RNA	104	99.6	103	79.7	96.0
Protein	126	113	120	93.4	112.4
Ligand/ion	66.4/62.6	71.4/48.3	71.5/49.2	45.7/27.2	51.8/40.7
RMS deviations					
Bond lengths (Å)	0.006	0.006	0.006	0.006	0.006
Bond angles (°)	0.959	0.923	0.983	1.007	1.002

Values in parentheses are for highest-resolution shell.

*This structure was solved without paromomycin whereas all other structures contain paromomycin.

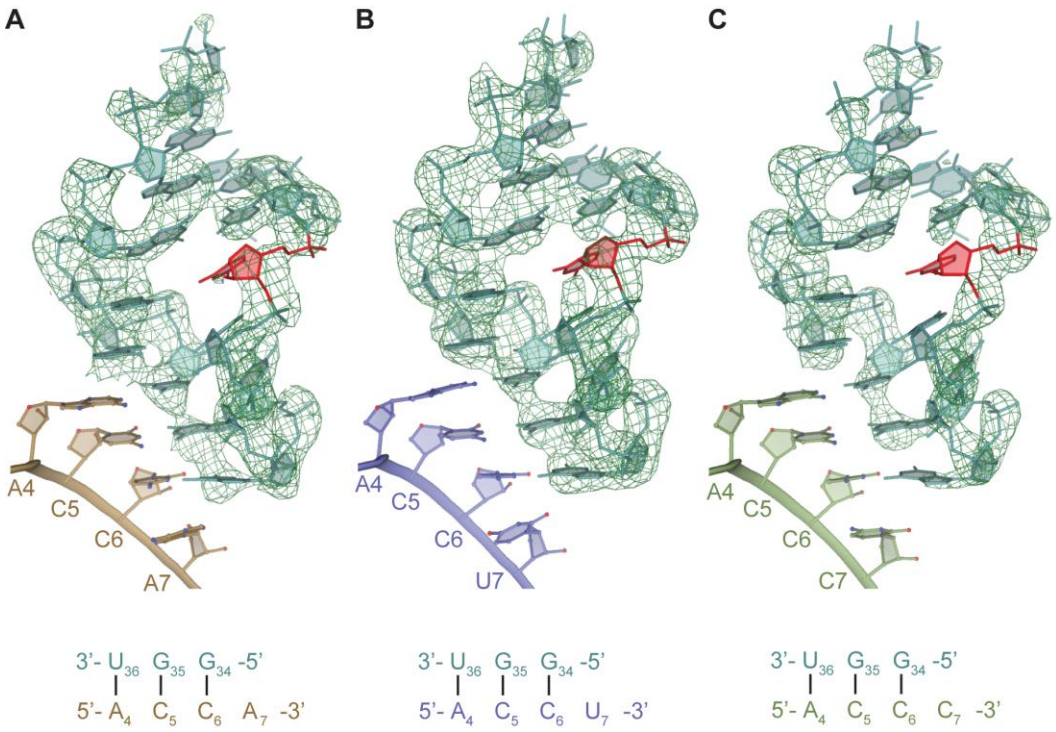

Figure 3.6. Electron density maps for ASL^{SufJ} bound to the A site. Unbiased F_o-F_c electron density map for ASL^{SufJ} (blue) bound to the +1 suppressible codons **(A)** ACC-A **(B)** ACC-U and **(C)** ACC-C shows strong density for nucleotides 29-42 (contoured at 3 σ). The 70S structures containing the **(B)** ACC-U and **(C)** ACC-C codons contain the antibiotic paromomycin while the 70S structure containing the **(A)** ACC-A codon is without.

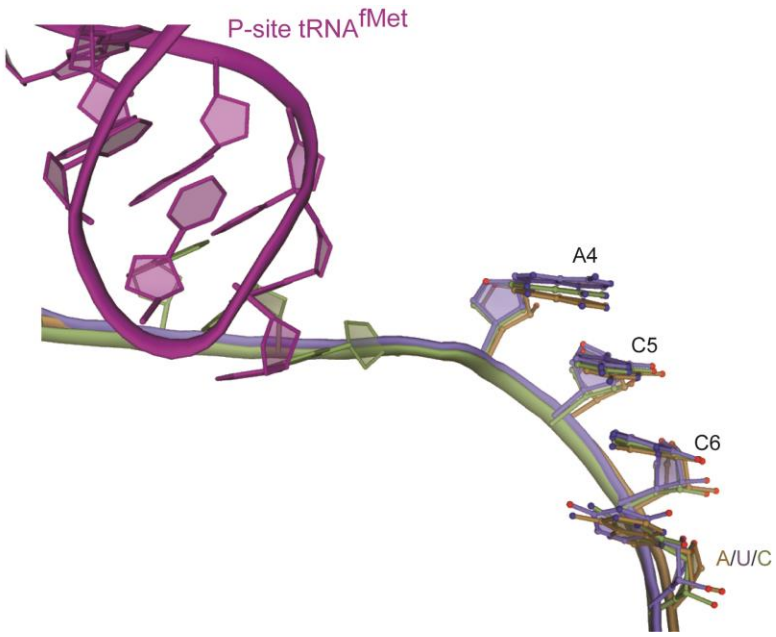

Figure 3.7. The mRNA path of each +1 suppressible codon is similar. The mRNA path is unaffected by the fourth nucleotide in the ACC-A (brown), ACC-U (dark blue) and ACC-C (green) codons. The P-site tRNA^{fMet} is in magenta.

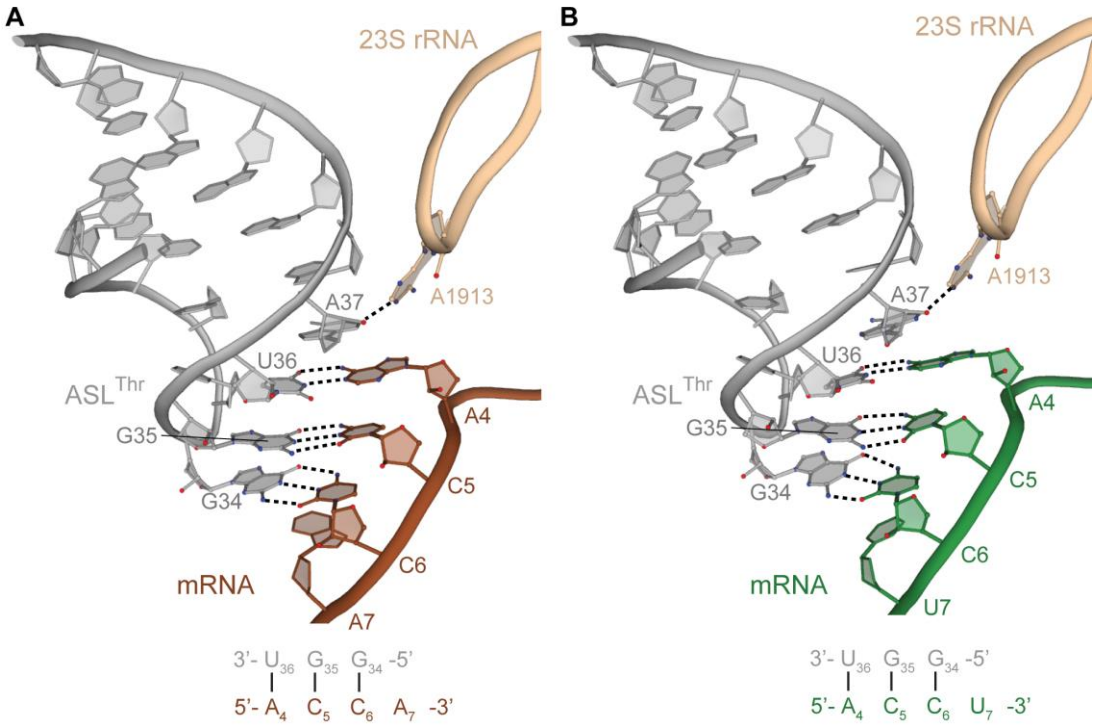

Figure 3.8. ASL^{Thr} interactions with mRNA in the A site. ASL^{Thr} (gray) forms three Watson-Crick base pairs with the first three nucleotides of the +1 suppressible codons **(A)** ACC-A (brown) and **(B)** ACC-C (green) in the zero frame. These structures were solved with the antibiotic paromomycin. The ASL is stabilized by a hydrogen bonding with 23S rRNA nucleotide A1913 (tan).

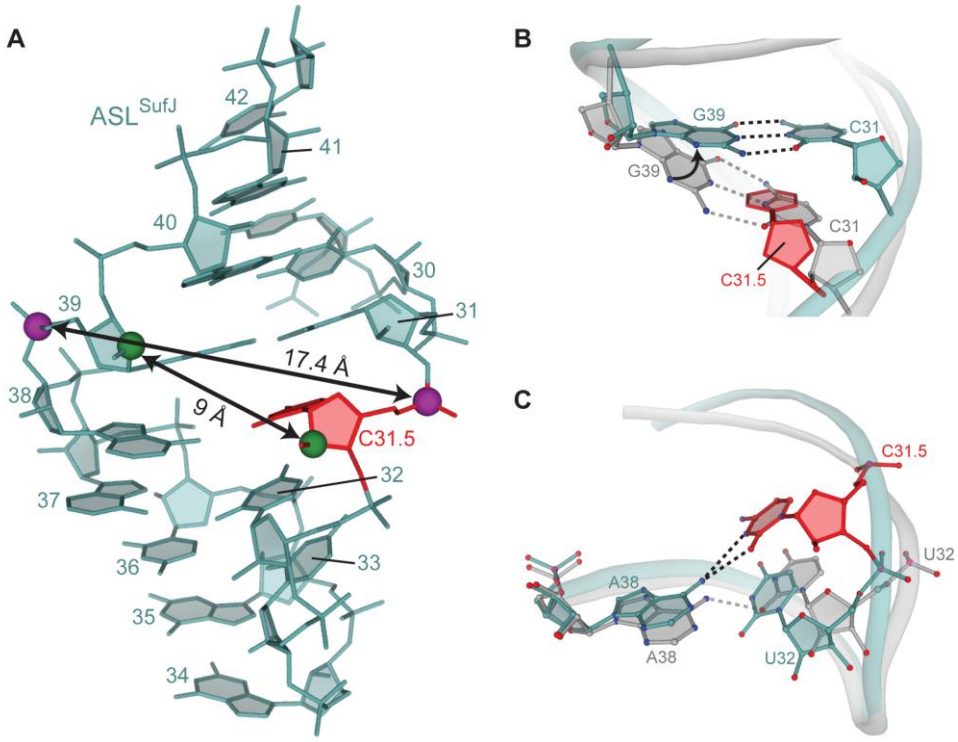

Figure 3.9. Narrowing of ASL^{SufJ} alters anticodon stem base pair interactions. **(A)** Both the major (as measured by C31.5•G39 phosphate-phosphate distances; purple spheres) and minor grooves (as measured by C31.5•G39 C2'-C2' distances; green spheres) are narrowed in ASL^{SufJ} as compared to canonical major and minor groove distances of 18.4 and 14.2 Å, respectively (*e.g.* ASL^{Thr}). The C31.5 insertion is shown as red. **(B)** The C31.5 insertion (red) causes C31 in ASL^{SufJ} (blue) to shift in the 5' direction, however the interaction with G39 (blue) is maintained via a 25° rotation of its base around the glycosidic bond. The canonical C31-G39 interaction of a canonical seven nucleotide ASL^{Thr} is shown for comparison (gray). **(C)** The 5' phosphate backbone movement shifts U32 (blue) closer to the opposite RNA stem while A38 rotates 8° to form a bifurcated hydrogen bond with the inserted C31.5 (red). This new interaction prevents the formation of the conserved U32•A38 base pair of ASL^{Thr} (gray).

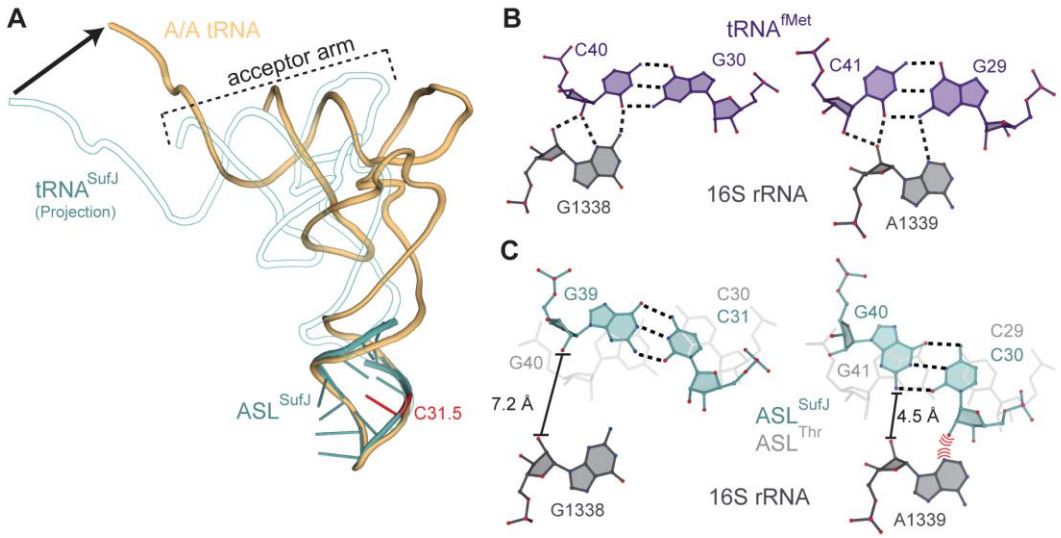

Figure 3.10. Modeling tRNA^{SufJ} in the A and P sites. (A) Modeling studies extending our structure of ASL^{SufJ} (blue) to a full-length tRNA^{SufJ} (white outlined with blue) reveal that the tilting position of the stem region would result in the CCA end of tRNA^{SufJ} >20 Å distant from the position of an accommodated A-site tRNA (gold) (arrow at the CCA end indicates the difference). We predict that conformational rearrangements of tRNA^{SufJ} are required to prevent this interaction with the ribosome. **(B)** The P-site tRNA^{fMet} (purple) is gripped by 16S rRNA G1338 and A1339 (gray) by the formation of A-minor interactions with both C40-G30 and C41-G29 (PDB code 2J02). **(C)** Superpositioning of ASL^{SufJ} on the anticodon of tRNA^{fMet} in the P site suggests that the deformation of the stem domain would prevent the formation of canonical G1338 and A1339 interactions. A semi-transparent overlay of the superpositioning of ASL^{Thr} is shown for comparison (light gray).

REFERENCES

1. Nangle LA, De Crecy Lagard V, Doring V, & Schimmel P (2002) Genetic code ambiguity. Cell viability related to the severity of editing defects in mutant tRNA synthetases. *J Biol Chem* 277(48):45729-45733.
2. Manley JL & Gesteland RF (1978) Suppression of amber mutants in vitro induced by low temperature. *Journal of molecular biology* 125(4):433-447.
3. Lee JW, *et al.* (2006) Editing-defective tRNA synthetase causes protein misfolding and neurodegeneration. *Nature* 443(7107):50-55.
4. Bouadloun F, Donner D, & Kurland CG (1983) Codon-specific missense errors in vivo. *Embo J* 2(8):1351-1356.
5. Edelmann P & Gallant J (1977) Mistranslation in E. coli. *Cell* 10(1):131-137.
6. Kramer EB & Farabaugh PJ (2007) The frequency of translational misreading errors in E. coli is largely determined by tRNA competition. *Rna* 13(1):87-96.
7. Kurland CG (1992) Translational accuracy and the fitness of bacteria. *Annu Rev Genet* 26:29-50.
8. Jorgensen F & Kurland CG (1990) Processivity errors of gene expression in Escherichia coli. *Journal of molecular biology* 215(4):511-521.
9. Rodnina MV (2012) Quality control of mRNA decoding on the bacterial ribosome. *Advances in protein chemistry and structural biology* 86:95-128.
10. Zaher HS & Green R (2009) Fidelity at the molecular level: lessons from protein synthesis. *Cell* 136(4):746-762.
11. Riyasaty S & Atkins JF (1968) External suppression of a frameshift mutant in salmonella. *Journal of molecular biology* 34(3):541-557.
12. Yourno J (1970) Nature of the compensating frameshift in the double frameshift mutant hisD3018 R5 of Salmonella typhimurium. *Journal of molecular biology* 48(3):437-442.
13. Yourno J (1972) Externally suppressible +1 "glycine" frameshift: possible quadruplet isomers for glycine and proline. *Nat New Biol* 239(94):219-221.
14. Riddle DL & Roth JR (1970) Suppressors of frameshift mutations in Salmonella typhimurium. *Journal of molecular biology* 54(1):131-144.
15. Sherman F, Stewart JW, Jackson M, Gilmore RA, & Parker JH (1974) Mutants of yeast defective in iso-1-cytochrome c. *Genetics* 77(2):255-284.
16. Roth JR (1974) Frameshift mutations. *Annu Rev Genet* 8:319-346.
17. Riddle DL & Carbon J (1973) Frameshift suppression: a nucleotide addition in the anticodon of a glycine transfer RNA. *Nat New Biol* 242(121):230-234.
18. Bossi L & Roth JR (1981) Four-base codons ACCA, ACCU and ACCC are recognized by frameshift suppressor sufJ. *Cell* 25(2):489-496.
19. Riddle DL & Roth JR (1972) Frameshift suppressors. 3. Effects of suppressor mutations on transfer RNA. *Journal of molecular biology* 66(3):495-506.
20. Prather NE, Murgola EJ, & Mims BH (1981) Nucleotide insertion in the anticodon loop of a glycine transfer RNA causes missense suppression. *Proceedings of the National Academy of Sciences of the United States of America* 78(12):7408-7411.
21. Cummins CM, Donahue TF, & Culbertson MR (1982) Nucleotide sequence of the SUF2 frameshift suppressor gene of Saccharomyces cerevisiae. *Proceedings of the National Academy of Sciences of the United States of America* 79(11):3565-3569.
22. Yarus M (1982) Translational efficiency of transfer RNA's: uses of an extended anticodon. *Science* 218(4573):646-652.
23. Gaber RF & Culbertson MR (1984) Codon recognition during frameshift suppression in Saccharomyces cerevisiae. *Mol Cell Biol* 4(10):2052-2061.
24. Curran JF & Yarus M (1987) Reading frame selection and transfer RNA anticodon loop stacking. *Science* 238(4833):1545-1550.

25. Moore B, Persson BC, Nelson CC, Gesteland RF, & Atkins JF (2000) Quadruplet codons: implications for code expansion and the specification of translation step size. *Journal of molecular biology* 298(2):195-209.
26. Anderson JC, Magliery TJ, & Schultz PG (2002) Exploring the limits of codon and anticodon size. *Chem Biol* 9(2):237-244.
27. Bossi L & Smith DM (1984) Suppressor sufJ: a novel type of tRNA mutant that induces translational frameshifting. *Proceedings of the National Academy of Sciences of the United States of America* 81(19):6105-6109.
28. Hohsaka T, Ashizuka Y, Taira H, Murakami H, & Sisido M (2001) Incorporation of nonnatural amino acids into proteins by using various four-base codons in an Escherichia coli in vitro translation system. *Biochemistry* 40(37):11060-11064.
29. Dunham CM, *et al.* (2007) Structures of tRNAs with an expanded anticodon loop in the decoding center of the 30S ribosomal subunit. *RNA* 13(6):817-823.
30. Qian Q, *et al.* (1998) A new model for phenotypic suppression of frameshift mutations by mutant tRNAs. *Mol Cell* 1(4):471-482.
31. Farabaugh PJ (2000) Translational frameshifting: implications for the mechanism of translational frame maintenance. *Prog Nucleic Acid Res Mol Biol* 64:131-170.
32. Nasvall SJ, Nilsson K, & Bjork GR (2009) The ribosomal grip of the peptidyl-tRNA is critical for reading frame maintenance. *Journal of molecular biology* 385(2):350-367.
33. Atkins JF & Bjork GR (2009) A gripping tale of ribosomal frameshifting: extragenic suppressors of frameshift mutations spotlight P-site realignment. *Microbiol Mol Biol Rev* 73(1):178-210.
34. Walker SE & Fredrick K (2006) Recognition and positioning of mRNA in the ribosome by tRNAs with expanded anticodons. *Journal of molecular biology* 360(3):599-609.
35. von Ahsen U, Green R, Schroeder R, & Noller HF (1997) Identification of 2'-hydroxyl groups required for interaction of a tRNA anticodon stem-loop region with the ribosome. *Rna* 3(1):49-56.
36. Phelps SS, Jerinic O, & Joseph S (2002) Universally conserved interactions between the ribosome and the anticodon stem-loop of A site tRNA important for translocation. *Mol Cell* 10(4):799-807.
37. Ogle JM, Murphy FV, Tarry MJ, & Ramakrishnan V (2002) Selection of tRNA by the ribosome requires a transition from an open to a closed form. *Cell* 111(5):721-732.
38. Jorgensen T, Siboska GE, Wikman FP, & Clark BF (1985) Different conformations of tRNA in the ribosomal P-site and A-site. *Eur J Biochem* 153(1):203-209.
39. Khade P & Joseph S (2010) Functional interactions by transfer RNAs in the ribosome. *FEBS letters* 584(2):420-426.
40. Ogle JM, *et al.* (2001) Recognition of cognate transfer RNA by the 30S ribosomal subunit. *Science* 292(5518):897-902.
41. Demeshkina N, Jenner L, Westhof E, Yusupov M, & Yusupova G (2013) New structural insights into the decoding mechanism: translation infidelity via a G.U pair with Watson-Crick geometry. *FEBS letters* 587(13):1848-1857.
42. Voorhees RM, Weixlbaumer A, Loakes D, Kelley AC, & Ramakrishnan V (2009) Insights into substrate stabilization from snapshots of the peptidyl transferase center of the intact 70S ribosome. *Nat Struct Mol Biol* 16(5):528-533.
43. Murphy FVt, Ramakrishnan V, Malkiewicz A, & Agris PF (2004) The role of modifications in codon discrimination by tRNA(Lys)UUU. *Nat Struct Mol Biol* 11(12):1186-1191.
44. Phelps SS, *et al.* (2006) Translocation of a tRNA with an extended anticodon through the ribosome. *Journal of molecular biology* 360(3):610-622.

45. Cantara WA, Murphy FVt, Demirci H, & Agris PF (2013) Expanded use of sense codons is regulated by modified cytidines in tRNA. *Proc Natl Acad Sci U S A* 110(27):10964-10969.
46. Selmer M, *et al.* (2006) Structure of the 70S ribosome complexed with mRNA and tRNA. *Science* 313(5795):1935-1942.
47. Jager G, Nilsson K, & Bjork GR (2013) The phenotype of many independently isolated +1 frameshift suppressor mutants supports a pivotal role of the P-site in reading frame maintenance. *PloS one* 8(4):e60246.
48. Lancaster L & Noller HF (2005) Involvement of 16S rRNA nucleotides G1338 and A1339 in discrimination of initiator tRNA. *Mol Cell* 20(4):623-632.
49. Maehigashi T, Dunkle JA, Miles SJ, & Dunham CM (in press) Structural insights into +1 frameshifting promoted by expanded or modification-deficient anticodon stem-loops. *Proc Natl Acad of Sci U S A.*
50. Olejniczak M & Uhlenbeck OC (2006) tRNA residues that have coevolved with their anticodon to ensure uniform and accurate codon recognition. *Biochimie* 88(8):943-950.
51. Ledoux S & Uhlenbeck OC (2008) Different aa-tRNAs are selected uniformly on the ribosome. *Mol Cell* 31(1):114-123.
52. Ledoux S, Olejniczak M, & Uhlenbeck OC (2009) A sequence element that tunes Escherichia coli tRNA(Ala)(GGC) to ensure accurate decoding. *Nat Struct Mol Biol* 16(4):359-364.
53. Yarus M, Cline S, Raftery L, Wier P, & Bradley D (1986) The translational efficiency of tRNA is a property of the anticodon arm. *The Journal of biological chemistry* 261(23):10496-10505.
54. Yarus M, Cline SW, Wier P, Breeden L, & Thompson RC (1986) Actions of the anticodon arm in translation on the phenotypes of RNA mutants. *Journal of molecular biology* 192(2):235-255.
55. Kleina LG, Masson JM, Normanly J, Abelson J, & Miller JH (1990) Construction of Escherichia coli amber suppressor tRNA genes. II. Synthesis of additional tRNA genes and improvement of suppressor efficiency. *Journal of molecular biology* 213(4):705-717.
56. McClain WH, Schneider J, Bhattacharya S, & Gabriel K (1998) The importance of tRNA backbone-mediated interactions with synthetase for aminoacylation. *Proceedings of the National Academy of Sciences of the United States of America* 95(2):460-465.
57. Tsai F & Curran JF (1998) tRNA(2Gln) mutants that translate the CGA arginine codon as glutamine in Escherichia coli. *Rna* 4(12):1514-1522.
58. Brilot AF, Korostelev AA, Ermolenko DN, & Grigorieff N (2013) Structure of the ribosome with elongation factor G trapped in the pretranslocation state. *Proceedings of the National Academy of Sciences of the United States of America* 110(52):20994-20999.
59. Powers T & Noller HF (1991) A functional pseudoknot in 16S ribosomal RNA. *Embo J* 10(8):2203-2214.
60. Linpinsel JL & Conn GL (2012) General protocols for preparation of plasmid DNA template, RNA in vitro transcription, and RNA purification by denaturing PAGE. *Methods Mol Biol* 941:43-58.
61. Olejniczak M, Dale T, Fahlman RP, & Uhlenbeck OC (2005) Idiosyncratic tuning of tRNAs to achieve uniform ribosome binding. *Nat Struct Mol Biol* 12(9):788-793.
62. Kabsch W (2010) Xds. *Acta crystallographica* 66(Pt 2):125-132.
63. Adams PD, *et al.* (2010) PHENIX: a comprehensive Python-based system for macromolecular structure solution. *Acta crystallographica* 66(Pt 2):213-221.
64. Emsley P, Lohkamp B, Scott WG, & Cowtan K (2010) Features and development of Coot. *Acta Crystallogr D Biol Crystallogr* 66(Pt 4):486-501.
65. Ermolenko DN, Cornish PV, Ha T, & Noller HF (2013) Antibiotics that bind to the A site of the large ribosomal subunit can induce mRNA translocation. *RNA* 19(2):158-166.

CHAPTER 4: MOLECULAR BASIS OF RIBOSOMAL P-SITE QUALITY CONTROL MECHANISM

Crystal E. Fagan, Tatsuya Maehigashi, Stacey J. Miles, and Christine M. Dunham

After errors are made in translation, the incorrect tRNA-mRNA pair causes a loss of translational fidelity resulting in the rapid termination of protein synthesis by RFs recognizing a sense codon. Here, I structurally characterized the conformational rearrangements resulting from a P-site near-cognate tRNA-mRNA interaction. My results show the formation of a U•U mismatch base pair at any position in the P-site codon-anticodon helix results in a displacement of the 5' position of the A-site mRNA. These structures in this chapter are still being analyzed and the results have not yet been published.

Author contributions: C.M.D and C.E.F. designed research; S.M. purified the ribosomes; C.E.F. and T.M. crystallized the ribosomal complexes and collected X-ray crystallography data.

INTRODUCTION

Despite proofreading mechanisms in place during tRNA selection, missense errors occur *in vivo* at a rate of one in ~3000 amino acid incorporated (1). After the incorrect tRNA is accommodated into the peptidyl transferase center, the α-amino group of the aa-tRNA is optimally positioned for spontaneous peptide bond formation through the nucleophilic attack of the carbonyl carbon of P-site tRNA (2-4). Until recently, it was believed that once missense errors are incorporated into the nascent peptide chain, it was impossible to identify or even correct the erroneously incorporated amino acids. However, the observed *in vitro* tRNA selection error rate (1 in 500 codons (5)) is significantly higher than the *in vivo* error rates (1 in 3000 (1)), indicating an additional proofreading mechanism exists within the cell (6). Recently, a novel post peptidyl transfer quality control (post PT QC) mechanism was uncovered that identifies the incorrect mRNA-tRNA pair in the P site after incorporation into the nascent peptide chain (7).

Characterization of this post PT QC mechanism using the well-established near-cognate decoding of an asparagine codon (AAU) by $tRNA^{Lys}$ established that when a near-cognate peptidyl-tRNA error is moved to the P site, a loss of translational fidelity occurs in the A site (7-9). In the presence of near-cognate peptidyl-tRNA, cognate and near-cognate ternary complexes are equally stabilized in the A site (8). Additionally, the forward rates of GTPase activation and accommodation are accelerated for the near-cognate ternary complexes (8). After a single missense error, release factors (RFs) can compete with the incoming ternary complex for a sense codon but typically only after incorporation of at least two incorrect residues do high rates of translation termination occur (9).

The same rules regarding the type of allowed mRNA-tRNA base pair interactions during the selection of a cognate aa-tRNA in the A site also apply to this post PT QC mechanism (7). Specifically, the formation of a U•G wobble in the first or second position activates this quality control mechanism, while the U•G wobble in the third position does not. Intriguingly, even

though formation of U•U mismatched in any position of the codon-anticodon helix activates the post PT QC mechanism, mismatches at the second position have the greatest effect on the rate of RF-mediated termination of translation (7). The specificity of this post PT QC mechanism suggests the ribosome can monitor the codon-anticodon helix in the P site.

While the A- and P-sites mRNA-tRNA interactions appear to follow the same rules for allowed base pairs, these interactions are monitored by two very different mechanisms. In the A site, the codon-anticodon base pairs are checked by 16S rRNA residues A1492, A1493, and G530 (10). The only direct interaction between the ribosome and the codon-anticodon helix in the P site is through stacking interactions formed between the wobble pair of the codon-anticodon helix and 16S rRNA nucleotides C1400 and G966 (10). At present, it is unclear how a near-cognate tRNA-mRNA interaction is identified in the P site or how this error is communicated to the A site resulting in a loss of ribosomal fidelity.

Here, we investigate the molecular mechanism used to identify near-cognate tRNA in the P site of the ribosome. Utilizing $tRNA^{Lys}$(anticodon 5'-AAA-3'; all codons and anticodons are shown in the 5'-3' direction) because of its well characterized ability to miscode an Asn codon (11), we analyzed the conformational changes resulting from a near-cognate tRNA in the P site forming a mismatch U•U base pair at each position in the codon-anticodon helix (**Fig. 4.**1). In each structure, the mismatched U•U base pair altered the mRNA path 3' of the P-site codon. The movement of the mRNA path would disrupt the Mg^{2+} coordinated kink in the mRNA backbone responsible for delineating the boundary between the P- and A-site codons. Our results provide novel insights into P-site near-cognate tRNA-mRNA interactions and provide a crucial link between mRNA position and translational accuracy whose signal is allosterically transmitted to the A site.

RESULTS

Near-cognate tRNA in the P site causes a change in the mRNA reading frame. In order to identify the molecular mechanism used to signal a near-cognate tRNA in the P site, we solved four crystal structures of a *Thermus thermophilus* 70S ribosome programmed with a P-site $tRNA^{Lys}$ and a 24-nucleotide-long mRNA containing the Shine-Dalgarno (SD) sequence (5'-AGGAGG-3'), a cognate Lys codon (AAA) or a near-cognate stop, Ile, or Asn codon (UAA, AUA, or AAU respectively) in the P site and a Phe codon (UUC) in the A site (**Fig. 4.1** and **Table 4.1**). The four structures were solved by molecular replacement using the 70S ribosome containing an empty A site with the mRNA and tRNA removed (12). After refinement, the mRNA and tRNA ligands could be seen clearly in the difference Fourier maps. All $tRNA^{Lys}$ are post-transcriptional modified to contain a N6-threonylcarbamoyladenosine (t^6A37) and either a 5-methylaminomethyluridine modification or the 2-thiouridine derivative at the wobble position (mnm^5U34 or s^2U34) (**Fig. 4.1 A** and **Fig. 1.2** in Chapter 1). These two modifications are essential for $tRNA^{Lys}$ binding to the ribosome and are visible in the unbiased F_o-F_c electron density.

In the 70S ribosome structure containing a cognate $tRNA^{Lys}$ in the P site, the mRNA-tRNA helix contains three Watson-Crick A-U base pairs. Even though there is no A-site tRNA, the phosphate of the first nucleotide in the A-site codon is well ordered. The sharp kink between the A- and P-site codons is visible and coordinates a Mg^{2+} ion with the 16S rRNA.

In each of the 70S ribosome programmed with single U•U mismatch at any of the three positions in the codon-anticodon helix, we expected the mRNA-tRNA helix to form two Watson-Crick base pairs. Instead of adopting the canonical seven nucleotide spacing between the Shine-Dalgarno (SD) and P-site codon as observed in the cognate P-site tRNA, the path of the mRNA is elongated resulting in a ten nucleotide spacing and positioning a Phe codon (UUC) in the P site

(**Fig. 4.2B**). The SD mRNA sequence interacts with the 16S rRNA anti-Shine-Dalgarno (ASD) sequence forming a SD-ASD helix. The elongation of the mRNA path was caused by a 15Å of a movement of this SD-ASD helix. This elongated mRNA path has also been observed in 70S ribosome complexes with containing a mRNA comprised of a SD sequence followed by a poly(U) sequence (12, 13). As the poly(U) mRNA is a homopolymer, it is possible for the mRNA to adopt any possible distance between the SD sequence and the P-site codon, suggesting a ten nucleotide spacing represents the lowest energy conformation. In the presence of a near-cognate tRNA, instead of adopting the canonical seven nucleotide spacing through the formation of two Watson-Crick base pair interactions as we expected, the single U:U base pair mismatch weakened the mRNA:tRNA interaction so as to completely disrupt the position of the mRNA.

Elongation of the mRNA message allows for the correct positioning of the P-site codon. Biochemical characterization of the post PT QC mechanism has shown that the loss of translational fidelity is not the result of a change in the mRNA reading frame (7). In order to identify the molecular mechanism used to signal a near-cognate tRNA present in the P site, we needed to elongate the mRNA message to include the ten nucleotide spacing between the SD and the P-site codon (**Fig. 4.2D**). To ensure the correct mRNA codon was being placed in the P site, we used three different mRNAs each with a change in the number of nucleotides 3' of the P-site codon to help identify the position of the mRNA (**Fig. 4.3**).

First, we solved a 70S ribosome structure with a $tRNA^{Lys}$ bound to the near-cognate P-site codon without an A-site codon (**Fig. 4.3A**). The difference Fourier map for this 70S ribosome complex with a truncated mRNA showed strong density for the P-site codon only. The lack of any additional density for a phosphate group indicated the $tRNA^{Lys}$ was interacting with the intended P-site codon at the end of the mRNA. Next, we solved a structure of the same 70S ribosome complex but used a mRNA that included an additional uracil at the 3' end of the

message (**Fig. 4.3B**). The difference Fourier map showed strong density for the P-site codon and the additional uracil in the first position of the A-site codon. These two structures demonstrated that we were able to correctly program the ribosome with the near-cognate tRNA in the P-site using the relaxed mRNA path. To understand how a near-cognate tRNA is identified in the P-site, we solved a final 70S ribosome complex with an mRNA containing a full A-site codon (**Fig. 4.3C**). The difference Fourier map was identical to the complex with the mRNA containing only a single nucleotide in the A-site codon verifying the mRNA was in the intended position with the near-cognate codon in the P-site. This series of three 70S ribosome complexes were solved for each of the near-cognate mRNA-tRNA interactions formed between a $tRNA^{Lys}$ anticodon (UUU) and the mRNA stop (UAA, **Table 4.2**), Ile (AUA, **Table 4.3**) and Asn (AAU, **Table 4.4**) codons.

The U•U mismatch in the first position is stabilized by the t6A37 modification and alters the 3' path of the mRNA. All lysine tRNA contain a t^6A37 nucleotide that forms a planar structure that stacks with the first position of the codon-anticodon helix (14). In the presence of a mismatched U•U base pair at the first position of the codon-anticodon helix, the t^6A37 modification forms the similar planar conformation to stabilize the mismatched U•U base pair through base stacking interactions (**Fig. 4.4B**). A Watson-Crick base pair forms between at the second position of the codon-anticodon interface between U35 of $tRNA^{Lys}$ and A+2 of the mRNA. At wobble position of the codon-anticodon A+3 of the codons adopts a *syn* conformation that prevent the formation of a Watson-Crick base pair. The *syn* conformation of A+3 is stabilized through a bifurcated hydrogen bond between the O4 atom of mnm^5U34 of $tRNA^{Lys}$ and both N6 and N7 of A+3 of the codon (**Fig. 4.4 B**).

The boundary between the A-site and P-site codons is defined by a sharp kink in the phosphate backbone that is stabilized by a Mg^{2+} ion proposed to be important for frame maintenance (10). The Mg^{2+} ion is coordinated by the phosphate oxygen of the +4 or first A-site

codon nucleotide and 16S rRNA nucleotides C1401 and C1402. One possible barrier to slippage of the mRNA frame is the high energy required to move the mRNA from one tRNA binding site to the other. While the *syn* conformation of the third position of the anticodon-codon interaction does not change the minor groove or geometry of the codon-anticodon helix, it alters the position of the A-site codon. The first nucleotide in the A-site codon, U+4 shifts (1.3 Å) away from 16S rRNA C1402 disrupting the coordination of the Mg^{2+}. While we cannot see the full A-site codon, it is possible that the movement of the mRNA would result in a loss of sharp kink in the phosphate backbone of the mRNA, not only destroying the boundary between the A- and P-site codons but irrevocably altering the position of the A-site codon.

The U•U mismatch in the second position narrows the codon-anticodon helix. The near-cognate interaction of $tRNA^{Lys}$ with the Ile codon AUA, contains a mismatched U•U base pair at the second position of the codon-anticodon helix (**Fig. 4.5**). In order to accommodate the mismatched U35•U+2 base pair, the tRNA nucleotide U35 moves (1.3 Å) towards the mRNA, narrowing the minor groove of the codon-anticodon helix (~1 Å) (**Fig. 4.5 B**). The distortion in the codon-anticodon helix resulting from the second position U•U mismatch prevents the formation of a canonical Watson-Crick base pair at the wobble position of the codon-anticodon interface. Instead, mnm^5U34 and A+3 form a typical Hoogsteen base pair (**Fig. 4.5B**). The A-site nucleotide U+4 shifts moves ~2 Å away from 16S rRNA C1402, again preventing the coordination of a Mg^{2+} (**Fig. 4.5 C**).

Movement of the third position U•U mismatch destabilizes the mRNA kink. The mismatched U•U base pair in the wobble position of the codon-anticodon helix is accommodated by a twisting of the tRNA nucleotide mnm^5U34 (1.8 Å) towards the mRNA, while the U+3 nucleotide moves closer to form a single hydrogen bond between the N3 atom of U+3 of the mRNA and the O4 of mnm^5U34 (1.8 Å) of $tRNA^{Lys}$. The distortion in the 3' end of the P-site codon-anticodon helix

does not inhibit the formation of A-U Watson-crick base pairs at the first and second positions (**Fig. 4.6**). However, the conformational distortion in the codon-anticodon helix resulting from the mismatched mnm^{5}U34•U34 base pair alter the mRNA path, moving the phosphate of U+4 away from 16S rRNA C1402 by 1.9 Å.

CONCLUSIONS/FUTURE STUDIES

During translation, the mRNA is decoded by the incoming tRNA through the formation of a three base pair codon-anticodon helix (15). Similar to other polymerases in the central dogma, selection of correct incoming substrate depends on the ability to for Watson-Crick base pairing interactions. Once correct Watson-Crick base pair geometry is identified by the polymerase, the incoming substrate is incorporated into the nascent chain. However, in contrast to DNA and RNA polymerase, the ribosome lacks the capability to remove an error after it has been incorporated into the nascent peptide chain. Instead of expending cellular resources in the production of an erroneous protein, translation is terminated by a post PT QC mechanism (5).

Our structural characterization of near-cognate tRNA^{Lys} in the P site shows missense errors alter the position of the A-site codon. Each mismatched U•U base pair changes the wobble position of the P-site codon-anticodon helix moving the mRNA away the 16S rRNA. This change in the mRNA path resulting in the loss of a Mg^{2+} ion believed to responsible for stabilizing the mRNA kink that delineates the boundary between the P-site and A-site codons. I believe it is this movement of the mRNA that is the molecular mechanism used to signal a near-cognate tRNA in the P site.

After a near-cognate tRNA is translocated to the P site, a global loss of ribosomal fidelity occurs. The ribosome is no longer able to stabilize cognate tRNA nor control the acceleration of GTPase activation for cognate tRNA compared to near-cognate tRNA. Even though these structures appear to suggest a role for the P-site tRNA in positioning the A-site codon, our analysis of the post PT QC remains incomplete. In the absence of an A-site tRNA, the A-site

codon and key 16S rRNA nucleotide in the decoding center are disordered. Additional structural characterization of a cognate and near-cognate A-site tRNA is needed to determine if the position of the A-site codon is altered and how this might affect tRNA selection.

MATERIALS AND METHODS

Ribosome complex formation and crystallization. *Thermus thermophilus* 70S purification, complex formation, crystallization and cryoprotection were performed as previously described (10). *E. coli* $tRNA^{Lys}$ was purchased from Chemical Block and mRNAs were purchased from IDT (**Table 4.5**).

Structural data collection and refinement. X-ray diffraction data was collected at Northeastern Collaborative Access Team (NE-CAT) ID24-C or ID24-E at the Advanced Photon Source (Argonne, IL). The XDS software package was used to integrate and scale the data (16). The structures were solved by molecular replacement using the PHENIX software suite using the 70S ribosome structure (PDB ID 3I9B and 3I9C) as a search model (17). Iterative rounds of coordinate refinement using individual sites and rigid group refinement with the PHENIX software suite and manual building in Coot (18). All figures were prepared in PyMOL (19).

FIGURES

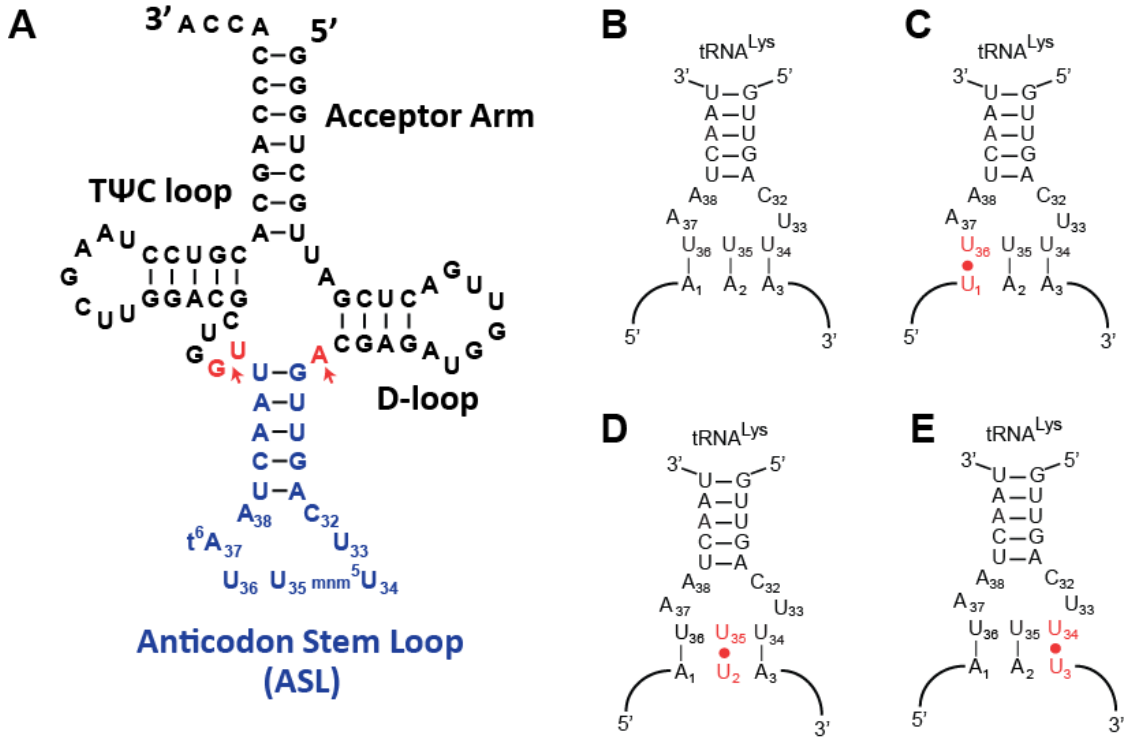

Figure 4.1. Overview of miscoding codon-anticodon interactions. (A) The secondary structure cloverleaf diagram of $tRNA^{Lys}$ showing the hinge region (red) between nucleotides A26, U44, and G45. The anticodon stem loop is shown in blue. Structures of P-site coding complexes were solved with a full length $tRNA^{Lys}$ bound to the P site of the 70S ribosome programmed with the cognate AAA **(B)**, near-cognate UAA **(C)**, near-cognate AUA **(D)**, or near-cognate AAU **(E)** P-site mRNA codons in the absence of an A-site ASL. The mismatched codon-anticodon base pair is shown in red.

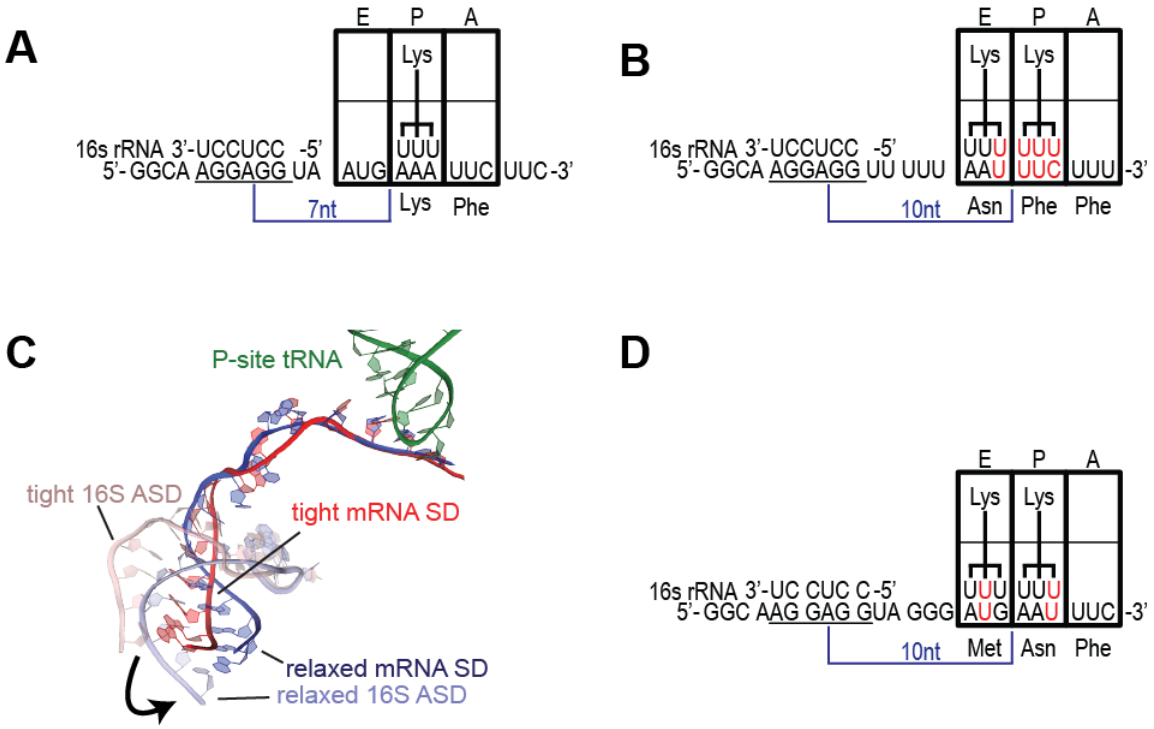

Figure 4.2. The spacing between the Shine-Dalgarno and P-site codon affects the mRNA frame. (A) Cognate mRNA-tRNA interactions results in a 'tight' mRNA conformation characterized by a seven nucleotide spacing between the middle of the SD sequence and the start of the P-site codon. (B) Near-cognate peptidyl-tRNA decoding resulted in a relaxed mRNA conformation characterized by a ten nucleotide spacing between the middle of the SD sequence and the start of the P-site codon. (C) The change in distance between the tight mRNA conformation (red, PDB ID 2HGR) and the relaxed mRNA conformation (blue) is caused by a movement of the SD-ASD helix. P-site tRNA is shown in green. (D) Increasing the spacing between the SD sequence and the start of the P-site codon to ten nucleotides resulted in proper placement of the P-site codon

Table 4.1 Data collection and refinement statistics a seven nucleotide spacing between SD and P site

P-site anticodon	3'-UUU-5'	3'-**U**UU-5'	3'-U**U**U-5'	3'-UU**U**-5'
P-site codon	5'-AAA-3'	5'-**U**AA-3'	5'-A**U**A-3'	5'-AA**U**-3'
Data collection				
Space group	$P2_12_12_1$	$P2_12_12_1$	$P2_12_12_1$	$P2_12_12_1$
Cell dimensions				
a, b, c (Å)	211.2 453.6 617.4	212.0 451.2 605.2	214.1 449.0 604.4	211.8 449.5 607.2
α, β, γ (°)	90.0 90.0 90.0	90.0 90.0 90.0	90.0 90.0 90.0	90.0 90.0 90.0
Resolution (Å)	50.0-3.9 (4.0-3.9)	50.0-3.8 (3.9-3.8)	50.0-3.9 (4.0-3.8)	50.0-3.9 (4.0-3.9)
R_{merge} (%)	16.7 (127.5)	46.9 (146.5)	39.5 (142.1)	20.1 (83.1)
I/σI	6.6 (1.1)	4.61 (1.6)	5.62 (1.3)	6.5 (1.7)
Completeness (%)	96.5 (97.3)	97.9 (99.5)	93.4 (82.8)	96.4 (98.8)
Redundancy	3.2 (3.1)	3.2 (3.3)	12.2 (8.2)	3.3 (3.3)
Refinement				
Resolution (Å)	50.0-3.9 (4.0-3.9)	50.0-3.8 (3.9-3.8)	50.0-3.8 (3.9-3.8)	50.0-3.7 (3.8-3.7)
No. reflections	516,451	601,873	529,513	601,861
R_{work} / R_{free} (%)	26.1/27.9	24.3/28.1	25.5/29.2	24.8/28.2
No. atoms	291,285	295,630	295,630	295,630
RMSD				
Bond lengths (Å)	0.008	0.015	0.017	0.015
Bond angles (°)	1.030	1.119	1.128	1.079

Values in parentheses are for highest-resolution shell.

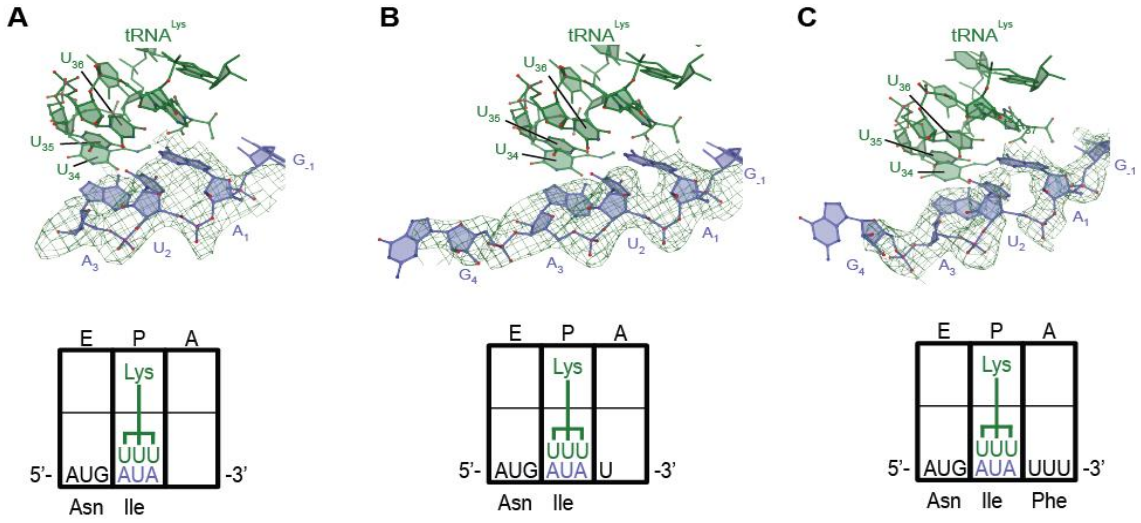

Figure 4.3. Electron density maps for the position of the P-site codon using the relaxed mRNA ten nucleotide SD spacing. (A) The unbiased F_o-F_c electron density map (3 σ) for a truncated mRNA only shows strong density for a P-site codon. **(B)** Strong electron density can be observed with the addition of a single nucleotide in the A-site codon. **(C)** The addition of a full A-site codon does not alter the electron density.

Table 4.2 Data collection and refinement statistics of near-cognate decoding of UAA codon with a ten nucleotide spacing between SD and P site

P-site anticodon	3'-**U**UU-5'		
P-site codon	5'-**U**AA-3'		
A-site codon	None	5'-U-3'	5'-UUC-3'
Data collection			
Space group	$P2_12_12_1$	$P2_12_12_1$	$P2_12_12_1$
Cell dimensions			
a, b, c (Å)	212.1 455.1 616.8	211.5 452.1 614.3	213.6 451.6 611.2
α, β, γ (°)	90.0 90.0 90.0	90.0 90.0 90.0	90.0 90.0 90.0
Resolution (Å)	50.0-3.9 (4.0-3.9)	50.0-3.9 (4.0-3.9)	50.0-3.9 (3.6-3.5)
R_{merge} (%)	12.8 (115.3)	16.2 (144.5)	20.7 (90.1)
I/σI	7.0 (1.1)	9.9 (1.6)	6.7 (1.7)
Completeness (%)	96.9 (97.4)	98.8 (99.6)	97.9 (98.7)
Redundancy	3.3 (3.2)	7.5 (7.2)	3.2 (3.2)
Refinement			
Resolution (Å)	70.0-3.9 (4.0-3.9)	70.0-3.9 (4.0-3.9)	70.0-3.5 (3.6-3.5)
No. reflections	521,351	525,053	771,833
R_{work} / R_{free} (%)	28.3/30.1	28.7/30.4	23.9/26.2
No. atoms	286,930	286,930	289,353
RMSD			
Bond lengths (Å)	0.007	0.007	0.016
Bond angles (°)	1.070	1.070	0.991

Values in parentheses are for highest-resolution shell.

Table 4.3 Data collection and refinement statistics of near-cognate decoding of AUA codon with a ten nucleotide spacing between SD and P site

P-site anticodon	3'-U**U**U-5'		
P-site codon	5'-A**U**A-3'		
A-site codon	None	5'-U-3'	5'-UUC-3'
Data collection			
Space group	$P2_12_12_1$	$P2_12_12_1$	$P2_12_12_1$
Cell dimensions			
a, b, c (Å)	211.2 452.3 612.9	213.6 454.0 607.6	211.2 452.1 615.7
α, β, γ (°)	90.0 90.0 90.0	90.0 90.0 90.0	90.0 90.0 90.0
Resolution (Å)	70.0-3.9 (40.-3.9)	70.0-3.6 (3.7-3.6)	70.0-3.7 (3.8-3.7)
R_{merge} (%)	14.1 (100.3)	19.0 (108.9)	12.0 (82.1)
I/σI	5.8 (1.1)	8.1 (1.6)	9.3 (1.7)
Completeness (%)	96.9 (96.7)	91.0 (93.4)	97.7 (98.9)
Redundancy	3.1 (2.9)	5.5 (5.4)	3.6 (3.5)
Refinement			
Resolution (Å)	70.0-3.9 (4.0-3.9)	70.0-3.6 (3.7-3.6)	70.0-3.7 (3.8-3.7)
No. reflections	512,902	615,320	660,039
R_{work} / R_{free} (%)	29.9/31.4	25.2/27.7	24.4/28.7
No. atoms	286,930	289,682	291,392
RMSD			
Bond lengths (Å)	0.007	0.007	0.010
Bond angles (°)	1.080	1.020	1.012

Values in parentheses are for highest-resolution shell.

Table 4.4 Data collection and refinement statistics of near-cognate decoding of AAU codon with a ten nucleotide spacing between SD and P site

P-site anticodon	3'-UU**U**-5'		
P-site codon	5'-AA**U**-3'		
A-site codon	None	5'-U-3'	5'-UUC-3'
Data collection			
Space group	$P2_12_12_1$	$P2_12_12_1$	$P2_12_12_1$
Cell dimensions			
a, b, c (Å)	213.3 450.0 605.9	210.8 453.2 618.3	211.0 449.2 618.1
α, β, γ (°)	90.0 90.0 90.0	90.0 90.0 90.0	90.0 90.0 90.0
Resolution (Å)	50.0-4.7 (4.8-4.7)	50.0-3.9 (4.0-3.9)	50.0-3.9 (40.-3.9)
R_{merge} (%)	42.3 (113.9)	15.8 (87.8)	20.7 (100.0)
I/σI	5.3 (1.8)	8.8 (1.5)	6.5 (1.7)
Completeness (%)	99.7 (99.9)	96.0 (96.4)	98.5 (99.4)
Redundancy	5.9 (6.0)	3.5 (3.5)	4.7 (4.5)
Refinement			
Resolution (Å)	50.0-4.7 (4.8-4.7)	50.0-3.9 (4.0-3.9)	50.0-3.9 (40.-3.9)
No. reflections	341,986	512,495	609,414
R_{work} / R_{free} (%)	26.5/28.9	27.2/29.6	27.2/.529
No. atoms	290,252	290,248	288,967
RMSD			
Bond lengths (Å)	0.009	0.009	0.014
Bond angles (°)	1.048	1.040	1.058

Values in parentheses are for highest-resolution shell.

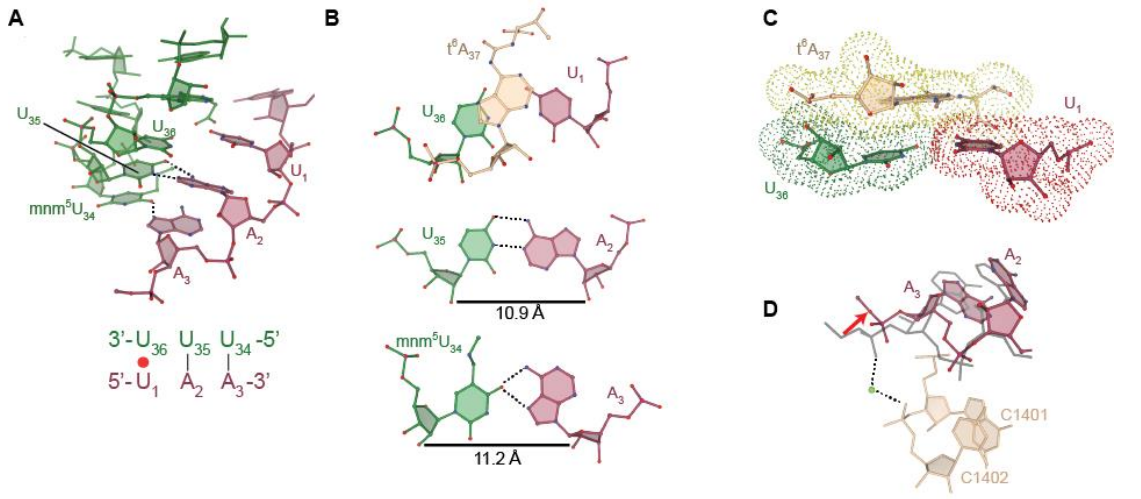

Figure 4.4. The near-cognate decoding of the stop codon UAA. (A) Near-cognate $tRNA^{Lys}$ (green) forms interactions with the second and third nucleotides of the UAA stop codon (red). (B) A detailed view of the base pair interactions between $tRNA^{Lys}$ and the UAA codon show the modified t^6A37 (tan) stacks with the U•U mismatch. While normal Watson-Crick base pairing occurs at the second position of the codon-anticodon helix, the *syn* conformation of A3 prevents this in the third position. (C) The t^6A37 (tan) nucleotide stacks with the mismatch U36•U1 pair (van der Waals surfaces represented as dots). (D) The near-cognate decoding causes the mRNA to shift away from 16S rRNA nucleotides C1402 and C1401 (tan) preventing the formation of the Mg^{2+}-mediated kink (green sphere) that is present with cognate complexes (gray).

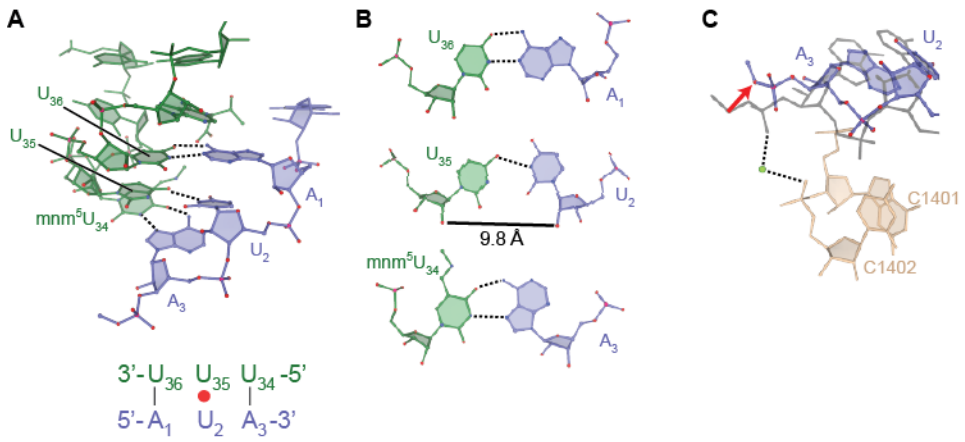

Figure 4.5. The near-cognate decoding of the Ile codon AUA. **(A)** Near-cognate tRNA^{Lys} (green) interacts with all three Ile codon nucleotides AUA (blue). **(B)** A detailed view of the interactions between the anticodon of tRNA^{Lys} and the AUA codon show Watson-Crick base pairing only occurs at the first position. The second position of the codon-anticodon helix forms a U35•U2 mismatched base pairing interaction and a Hoogsteen mnm^{5}U34•A3 base pair is formed in the third position. **(C)** The mRNA away from 16S rRNA nucleotides C1402 and C1401 (tan) preventing the formation of the Mg^{2+} (green) mediated kink that is still observed during cognate P site decoding. The canonical interactions formed by tRNA^{Lys} decoding the cognate lysine codon are shown in gray for comparison.

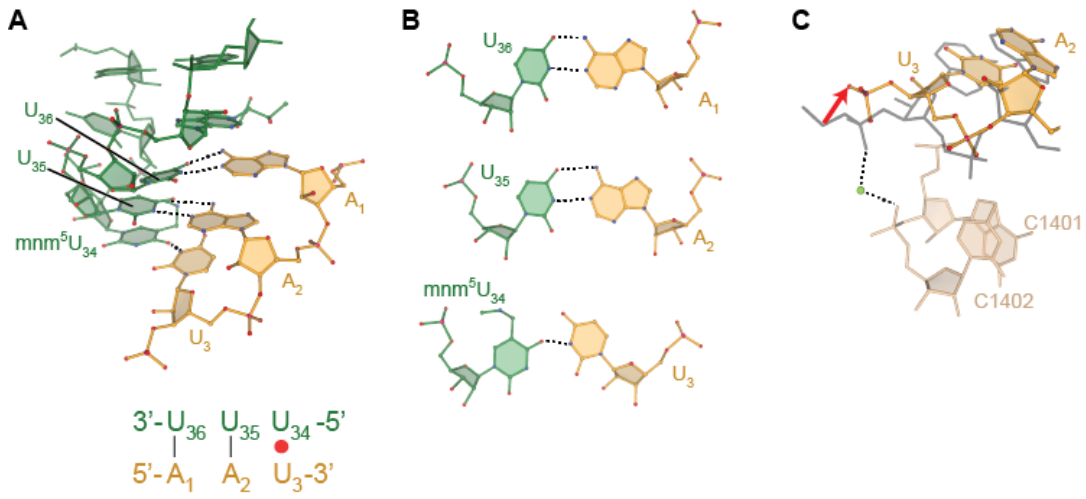

Figure 4.6. Near-cognate interaction of tRNALys with the Asn codon AAU. (A) Near-cognate $tRNA^{Lys}$ (green) forms interactions with all three nucleotides in the Asn codon AAU (orange).**(B)** A detailed view of the base pair decoding between $tRNA^{Lys}$ and the AAU codon show Watson-Crick base pairing in the first and second positions. The tRNA nucleotide mnm^5U34 forms a U•U base pair with U3 of the mRNA. The canonical interactions formed by $tRNA^{Lys}$ decoding the cognate lysine codon are shown in gray for comparison. **(C)** Near-cognate decoding moves the mRNA away from 16S rRNA nucleotides C1402 and C1401 (tan) preventing the formation of the Mg^{2+} (green) mediated kink that is still observed during cognate P site decoding.

Table 4.5 mRNA sequences used in this study

LysP_PheA_ctrl	GGCAAGGAGGUAAUG**AAA***UUC*UUC
TermP_PheA	GGCAAGGAGGUUUUU**UAA***UCU*UUU
IleP_PheA	GGCAAGGAGGUUUUU**AUA***UUC*UUU
AsnP_PheA	GGCAAGGAGGUUUUU**AAU**UUCUUU
fMetE_TermP_noA	GGCAAGGAGGUAAAAAUG**UAA**
GfMetE_TermP_UA	GGC AAGGAGGUAGGGAUG**UAA***U*
GfMetE_TermP_PheA	GGCAAGGAGGUAGGGAUG**UAA***UUC*
fMetE_IleP_noA	GGCAAGGAGGUAAAAAUG**AUA**
GfMetE_IleP_UA	GGCAAGGAGGUAGGGAUG**AUA***U*
GfMetE_IleP_PheA	GGCAAGGAGGUAGGGAUG**AUA***UUC*
fMetE_Lys-p_noA	GGCAAGGAGGUAAAAAUG**AAU**
fMetE_AsnP_UA	GGCAAGGAGGUAAAAAUG**AAU***U*
fMetE_AsnP_PheA	GGCAAGGAGGUAAAAAUG**AAU***UUC*

Shine-Dalgarno sequence is underlined
P-site codon is bold
A-site codon is italicized

REFERENCES

1. Bouadloun F, Donner D, & Kurland CG (1983) Codon-specific missense errors in vivo. *EMBO J* 2:1351-1356.
2. Voorhees RM, Weixlbaumer A, Loakes D, Kelley AC, & Ramakrishnan V (2009) Insights into substrate stabilization from snapshots of the peptidyl transferase center of the intact 70S ribosome. *Nat Struct Mol Biol* 16(5):528-533.
3. Hiller DA, Singh V, Zhong M, & Strobel SA (2011) A two-step chemical mechanism for ribosome-catalysed peptide bond formation. *Nature* 476(7359):236-239.
4. Nissen P, Hansen J, Ban N, Moore PB, & Steitz TA (2000) The structural basis of ribosome activity in peptide bond synthesis. *Science* 289(5481):920-930.
5. Zaher HS & Green R (2009) Fidelity at the molecular level: lessons from protein synthesis. *Cell* 136:746-762.
6. Kurland CG (1992) Translational accuracy and the fitness of bacteria. *Annu Rev Genet* 26:29-50.
7. Zaher HS & Green R (2009) Quality control by the ribosome following peptide bond formation. *Nature* 457:161-166.
8. Zaher HS & Green R (2010) Kinetic basis for global loss of fidelity arising from mismatches in the P-site codon:anticodon helix. *Rna* 16:1980-1989.
9. Zaher HS & Green R (2011) A primary role for release factor 3 in quality control during translation elongation in Escherichia coli. *Cell* 147(2):396-408.
10. Selmer M, *et al.* (2006) Structure of the 70S ribosome complexed with mRNA and tRNA. *Science* 313(5795):1935-1942.
11. Precup J & Parker J (1987) Missense misreading of asparagine codons as a function of codon identity and context. *The Journal of biological chemistry* 262:11351-11355.
12. Jenner LB, Demeshkina N, Yusupova G, & Yusupov M (2010) Structural aspects of messenger RNA reading frame maintenance by the ribosome. *Nature Structural & Molecular Biology* 17:555-560.
13. Yusupova G, Jenner L, Rees B, Moras D, & Yusupov M (2006) Structural basis for messenger RNA movement on the ribosome. *Nature* 444(7117):391-394.
14. Murphy FVt, Ramakrishnan V, Malkiewicz A, & Agris PF (2004) The role of modifications in codon discrimination by tRNA(Lys)UUU. *Nat Struct Mol Biol* 11(12):1186-1191.
15. Crick FH, Griffith JS, & Orgel LE (1957) Codes without Commas. *Proceedings of the National Academy of Sciences of the United States of America* 43(5):416-421.
16. Kabsch W (2010) Xds. *Acta crystallographica. Section D, Biological crystallography* 66:125-132.
17. Adams PD, *et al.* (2010) PHENIX: a comprehensive Python-based system for macromolecular structure solution. *Acta crystallographica. Section D, Biological crystallography* 66:213-221.
18. Emsley P & Cowtan K (2004) Coot: model-building tools for molecular graphics. *Acta Crystallogr D Biol Crystallogr* 60:2126-2132.
19. DeLano WL (2002) The PyMOL Molecular Graphics System. (DeLano Scientific, Palo Alto).

CHAPTER 5. GENERAL DISCUSSION

In order for the ribosome to accurately decode mRNA, both selection of the correct tRNA and the preservation of the mRNA frame need to be maintained. If errors occur, a quality control mechanism can be activated to terminate synthesis of that protein. The work presented here builds upon previous genetic and biochemical research using x-ray crystallography to determine the structural basis for both missense and frameshift errors as well as the quality control mechanism these errors could activate.

How is selection of the correct tRNA signaled?

Almost half a century of genetic, biochemical, and structural characterization of the ribosome have provided significant insights into the molecular mechanisms controlling tRNA selection (1-7). The correct selection of tRNA is controlled by a kinetic proofreading mechanism where cognate tRNAs utilize an induced fit mechanism to accelerate the rates of both EF-Tu-mediated-GTP hydrolysis and accommodation of the aa-tRNA (3, 8, 9). This kinetic proofreading mechanism requires the signaling of cognate tRNA decoding from the A-site decoding center in the 30S subunit to the GTPase activating center of the 50S subunit ~80 Å away (see **Fig. 1.9** in Chapter 1) (10). Moreover, cognate decoding results in a global conformational change of the 30S subunit termed "domain closure" where the inward rotation of the shoulder domain helps stabilize the position of EF-Tu on the ribosome (10, 11).

Domain closure is proposed to be the primary signal used to indicate the correct decoding of the mRNA message triggering the activation of EF-Tu-mediated GTP hydrolysis required for tRNA selection (5, 12). Error-inducing antibiotics, such as paromomycin, help stabilize the closed conformation of the ribosome accelerating the rate of GTPase activation for near-cognate tRNA (4, 9). Mutations that localize along the interface of ribosomal proteins S4 and S5 that cause a miscoding or *ribosomal ambiguity* (*ram*) phenotype are believed to alter tRNA selection by destabilizing this protein-protein interface reducing the energetic barrier for domain closure (4,

5). Mutations that are expected to increase the energetic barrier for domain closure, such as those found in ribosomal protein S12, result in a hyperaccurate or restrictive phenotype (13, 14).

A growing body of experimental evidence indicates additional conformational changes not explained by the domain closure are required for the GTPase activation step of tRNA selection. High resolution structure of the 70S ribosome shows streptomycin induces a conformational distortion in the decoding center altering the tRNA selection in a way that cannot be explained by the domain closure model (15). A mutation in the ribosomal protein S12 that produces a streptomycin-dependent (SmD) phenotype causes a distortion of the decoding center that stalls tRNA selection at a step in between codon recognition, represented by domain closure, and GTPase activation (16). Some mutations that can disrupt the S4-S5 interface actually reduce tRNA selection errors (17, 18) suggesting that mutations in the S4 and S5 proteins alter tRNA selection through conformational change in the surrounding 16S rRNA that are not directly associated with domain closure. Each of these studies suggest a conformational rearrangement of 16S rRNA not currently explained by the two state domain closure model is necessary for the GTPase activation step of tRNA selection.

The identification of rRNA mutations affecting the GTPase activation step of tRNA selection has been hindered by the multiple copies of the rRNA genes present in most model system. Alteration of the anti-Shine-Dalgarno (ASD) sequence of the 16S rRNA generates a specialized ribosome only capable of translating mRNA with the corresponding Shine-Dalgarno (SD) sequence. Using this specialized ribosome system, the 16S rRNA was screened for mutation that altered ribosomal fidelity (19). A number of 16S rRNA *ram* mutations were identified in either the decoding center where the codon-anticodon helix is monitored or near regions of the 30S shoulder domain that were expected to alter the energetic barrier for domain closure. A third class of 16S rRNA *ram* mutations were identified, clustering around the intersubunit bridge B8 near the point of interaction between EF-Tu and h5 of 16S rRNA (see **Fig. 2.1** in Chapter 2) (19-21). These mutations showed intersubunit bridge B8 was a negative regulator of GTPase activation.

GTPase activation occurs through the precise positioning of EF-Tu, such that the catalytic residue in EF-Tu can be activated by interacting with the sarcin-ricin loop (SRL) of 23S rRNA in the GTPase activating center (**Fig. 5.1**) (10, 11). EF-Tu is stabilized on the 70S ribosome through interactions formed by the β-hairpin of EF-Tu and h5 of the 16S rRNA shoulder domain. My work presented in Chapter 2 shows intersubunit bridge B8 acts as a 'turnstile'-like barrier to the GTPase activating center regulating the GTPase activation step of tRNA selection (22). Disruption of bridge B8, and not domain closure, results in the necessary conformational rearrangement of h5 and h14 for productive interactions with the β-hairpin of EF-Tu (**Fig. 5.1B** and **Fig. 2.9** in Chapter 2). Under normal conditions, cognate ternary complexes are unimpeded by bridge B8, having paid the energetic toll for accessing the GTPase activating center by the correct decoding of the mRNA and are able to access the pocket formed by 16S rRNA residues h5 and h14. However, near-cognate ternary complexes are unable to disrupt this intersubunit bridge and as a result cannot adopt the precise conformation necessary for GTPase activation. In the presence of 16S rRNA *ram* mutants G299A or G347U, h5 and h14 adopt the GTPase-activated conformation in the absence of EF-Tu circumventing this key checkpoint in the tRNA selection process. Additional crystallographic analysis of 16S rRNA *ram* mutations containing an empty A site, or a near-cognate tRNA bound to the A-site decoding center could lead to a greater understanding of the role bridge B8 plays in regulating tRNA selection.

My work with the 16S rRNA *ram* mutations also provides insight into the mechanisms used to coordinate interactions between distant sites on the ribosome required for tRNA selection. Characterization of the 16S rRNA *ram* mutation G299A illustrates that the domains of the small subunit are quite dynamic with each small movement facilitating conformational rearrangements in disparate regions of the ribosome as it traverses the free-energy landscape. The small movement of h12 due to the G299A mutation (see **Fig. 2.4** in Chapter 2) presumably alters the

conformational equilibrium of the ribosome making the GTPase activated state more accessible even in the absence of cognate decoding. The fact that the G299A mutation increases the rate of EF-Tu dependent GTP hydrolysis, particularly in the presence of a near-cognate ternary complex, supports this allosteric link between h12 and bridge B8. The proximal location of S4 and S5 *ram* mutations to h12 suggest these *ram* mutations also alter tRNA selection by changing the conformational dynamics of the ribosome explaining how mutations could disrupt the S4/S5 interface and still reduce tRNA selection errors (19).

Is the intersubunit bridge B8 a global regulator of the GTPase activation?

My results, in collaboration with the Fredrick lab, indicate the intersubunit bridge B8 functions as a regulator for the GTPase activation of EF-Tu during tRNA selection. Additional analyses by the Fredrick lab reveal that disruption of bridge B8 through the deletion of two base pairs in h14, also shows increased rates of GTP hydrolysis for both EF-Tu and EF-G (23). These initial observations with EF-G indicate that perhaps B8 plays a global regulatory role. Indeed, structural studies of RF3 and RelA bound to the 70S reveal that intersubunit bridge B8 is also disrupted (24-26). While these structural interactions suggest the intersubunit bridge B8 could be a universal regulator of GTP hydrolysis, the effect of bridge B8 disruption has not yet been analyzed.

How is the three-nucleotide mRNA reading frame maintained?

The accuracy of protein synthesis also depends on maintaining the three-nucleotide mRNA reading frame. A change in the triplet mRNA reading frame resulting from a shift in the 5' or 3' direction leads to the synthesis of nonsense polypeptides after the shift. The importance of maintaining a non-overlapping three nucleotide reading frame was established by Crick in 1957 quickly giving rise to the idea that the triplet decoding process was immutable (27). We now know that all three domains of life use changes in the mRNA reading frame or 'programmed'

frameshifts to regulate gene expression (28). Despite the fundamental importance of regulating the mRNA reading frame, the molecular mechanisms responsible for maintaining the mRNA reading frame are still poorly understood.

The first study demonstrating that the mRNA reading frame could be altered came from genetic suppressor screens in *Saccharomyces cerevisiae* and *Salmonella typhimurium* (29-35) where several mutant tRNAs capable of reading a four nucleotide codon were identified. Many of these altered tRNA contained an insertion in the anticodon-stem loop (ASL) either within or near the anticodon resulting in a model for +1 frameshifting where the insertion was proposed to cause a conformational rearrangement of the tRNA resulting in a four nucleotide anticodon (see **Fig. 3.1A** in Chapter 3) (35-39). Subsequent characterization of these identified frameshift suppressor tRNAs suggest +1 frameshifting isn't the result of an enlarged anticodon, but occurs during or immediately after translocation from the A to the P site by a realignment of the codon-anticodon helix (**Fig. 3.1**) (40-43). Each of these models suggests a different role for both the ribosome and the tRNA in maintaining the three-nucleotide mRNA reading frame.

By determining the mechanism used by these frameshift suppressor tRNAs to alter the mRNA reading frame, we can answer fundamental questions regarding the ribosome and reading frame maintenance. If changes in the mRNA reading frame occur by the enlargement of the anticodon to four nucleotides or quadruplet decoding, the movement of the codon-anticodon helix from the A site to the P site would require the translocation of four nucleotides instead of the canonical three. This model suggests the movement of the mRNA reading frame depends primarily on the codon-anticodon helix and the ribosome has only a passive role in maintaining the mRNA reading frame. However, if changes in the mRNA reading frame occur by a realignment of the codon-anticodon helix in the P site as suggested by the P-site slippage model, changes in the mRNA reading frame would require a disruption of the codon-anticodon helix in order for realignment of the mRNA to occur. The efficiency of four-nucleotide decoding would

depend on the ability to disrupt the mRNA-tRNA interaction in the P site possibly due to a change in the interactions between the tRNA and the ribosome.

Currently, three examples types of expanded ASLs, each containing an eight nucleotide anticodon loop, have been structurally characterized during the initial decoding step of translation in the A site. The frameshift suppressor ASL^{SufA6} containing an insertion at position 37.5 that destabilizes the 32•38 base pair (**Fig. 5.2**), interacts with the first three nucleotides of the mRNA codon, in the zero frame (43). My work with ASL^{SufJ} containing a C31.5 insertion that is accommodated through a deformation of the ASL stem domain and changes the 32•38 base pair (see **Fig. 3.4** in Chapter 3), also forms three Watson-Crick base pairs with the mRNA in the zero frame. Finally, structural characterization of engineered ASLs containing an insertion immediately 5' of the anticodon at position 33.5 (**Fig. 5.2**) showed the insertion disrupted the conserved U-turn completely disordering of the 5' side of the ASL (44, 45). Even though the 33.5 insertion allowed the wobble nucleotide of the anticodon to interact with the fourth nucleotide in the codon, these non-natural ASLs bound to the A-site in the zero frame (see **Fig. 3.1** in Chapter 3). While each insertion in the ASL causes a different conformational change, crystal structures of these expanded ASLs bound to the 70S ribosome reveal they do not adopt a four nucleotide anticodon. Structural characterization of ASL^{SufJ} presented here, and the previously analyzed ASL^{SufA6} (43) suggests changes in the tRNA structure drive +1 frameshifting, instead of codon-anticodon interactions.

Structural characterization of frameshift suppressor tRNAs demonstrate the changes in the mRNA reading frame do not occur in the A site. Further characterization of these frameshift suppressors could reconcile whether the changes in the mRNA reading frame occur during translocation, by altered interactions with the translocation factor EF-G, or after moving to the P site. A recent Cryo-EM structure of EF-G bound to the 70S ribosome in the pre-translocated state shows Gln507 of domain four of EF-G interacts with the phosphate backbone of the tRNA in the A-site decoding center near the 32•38 base pair (**Fig. 5.3**) (46). Superpositioning of ASL^{SufJ} onto

the tRNA in this structure indicates that the C31.5 insertion could alter this interaction between EF-G and ASL^{SufJ} during translocation leading to a change in the mRNA reading frame (**Fig. 5.3**). A pre-translocation structure of EF-G bound to the 70S in the presence of $tRNA^{SufJ}$ would show whether the C31.5 insertion changes the way EF-G interacts with the ASL stem, inducing a rearrangement of the codon-anticodon helix.

After translocation to the P site, the anticodon stem is held in place by 16S rRNA nucleotides G1338 and A1339 (see **Fig. 3.10B** in Chapter 3). Superpositioning of ASL^{SufJ} into the P site indicates that the distortion of the stem domain in ASL^{SufJ} would prevent the formation of these 'gripping' interactions by 16S rRNA (see **Fig. 3.10C** in Chapter 3). A structure of the 70S ribosome with $tRNA^{SufJ}$ bound to the P site would show how the gripping of the anticodon stem is affected by the C31.5 insertion in ASL^{SufJ}.

The structural plasticity observed in frameshift suppressor tRNA suggests the mRNA reading frame is preserved through gripping interactions with translational machinery. Frameshift suppressor tRNAs induce a repairing of the codon-anticodon helix either during or immediately after translocation to the P site. Many programmed frameshifts used to regulate gene expression require a similar realignment of the mRNA reading frame (28, 47). Even though programmed frameshifts use 'slippery' sequences of secondary structural elements in the mRNA, these programmed frameshift suppressors would have to overcome the same gripping interactions with translational machinery required to induce a change in the mRNA reading frame.

How is the low efficiency of frameshift suppression by $tRNA^{SufJ}$ maintained?

Most frameshift suppressor tRNAs exhibit a low frameshift suppression efficiency, for $tRNA^{SufJ}$ this efficiency is between 1-3% (38, 39, 48). Expansion of the anticodon loop to eight nucleotides general reduces the binding affinity potentially reducing the efficiency of frameshift suppression (49). However, experiments measuring the affinity of $tRNA^{SufJ}$ for the A site shows that the C31.5 insertion slightly increases the affinity of this tRNA as compared to a canonical

$tRNA^{Thr}$ (**Fig. 3.3**). Perhaps this low frameshift suppression efficiency is due to a reduced concentration of post-transcriptionally modified and aminoacylated $tRNA^{SufJ}$ that can be incorporated into a ternary complex. Nucleotide A37 of the canonical $tRNA^{Thr}$ is post-transcriptionally modified to an N^6-methyl-N^6-threonylcarbamoyladenosine (m^6t^6A37) using a series of enzymes that recognize and interact with the anticodon domain (50). Charging of $tRNA^{Thr}$ is accomplished through a class II aminoacyl synthetase that also requires recognition of the anticodon domain (51, 52). It is possible that the conformational changes observed in ASL^{SufJ} would prevent these post-transcriptional modification or aminoacylation reactions by inhibiting proper recognition of the anticodon. In the absence of an aminoacyl group, $tRNA^{SufJ}$ would not be incorporated into a ternary complex and could not interact with the ribosome to decode the mRNA. While the m^6t^6A37 modification is not required for aminoacylation, it is believed to help stabilize the mRNA-tRNA helix (53). A loss of the similar t^6A37 modification on $tRNA^{Lys}$ is essential for translocation of the tRNA from the A site to the P site (54). With the aforementioned changes in ASL^{SufJ} interactions with EF-G, it is likely that the low levels of +1 frameshift efficiency could be due to an incompatibility with the translational machinery.

Another viable explanation for the low frameshift suppression efficiency of $tRNA^{SufJ}$ is that the mRNA-tRNA interaction in the +1 mRNA reading frame disrupts the position of the mRNA leading to activation of the post peptidyl transfer quality control (post PT QC) mechanism discussed in Chapter 4. In the +1 reading frame, $tRNA^{SufJ}$ would form a near-cognate U•C base pair in the first position of the codon-anticodon helix with all three frameshift suppressible codons. Potentially, $tRNA^{SufJ}$ could stimulate a change in the mRNA reading frame more often than suggested by the low frameshift suppression efficiency; however activation of the post PT QC mechanism would rapidly terminate translation preventing the synthesis of a full length protein.

How does a near-cognate tRNA in the P site alter ribosomal fidelity?

Translocation of a near-cognate tRNA to the P-site, initiates a post peptidyl transfer quality control (post PT QC) mechanism that causes a global loss of translational fidelity resulting in the termination of translation (55-57). After a single misincorporation event, the ribosome loses the ability to discriminate between cognate and near-cognate tRNAs in the A-site decoding center. Multiple misincorporation errors lead to the premature termination of translation by release factors (RFs) in the absence of a stop codon. While a kinetic characterization of this post PT QC mechanism suggests that the integrity of the P-site codon-anticodon helix influences both the tRNA and RF selection processes (56), we know very little about the structural basis for this phenomenon.

Structural characterization of near-cognate $tRNA^{Lys}$ in the P site demonstrates that a mismatched U•U base pair at any position in the P-site codon-anticodon helix can change the mRNA path. By moving the first nucleotide in the A-site codon, the near-cognate tRNA disrupts the sharp 45° kink in the mRNA phosphate backbone which is responsible for delineating the boundary between the P- and A-site codons. This movement of the mRNA backbone prevents the coordination of a Mg^{2+} ion that forms a bridging interaction between the mRNA and 16S rRNA. I believe it is this movement of the mRNA and the subsequent loss of the Mg^{2+} ion that signals a near-cognate tRNA is present in the P site.

The selection of an aa-tRNA in the decoding center involves an induced fit mechanism where 16S rRNA nucleotides A1492, A1493, and G530 interrogate the codon-anticodon helix (4). While a near-cognate peptidyl-tRNA disrupts the selection of the cognate aa-tRNA, the structures presented in Chapter 4 are unable to demonstrate how this loss of fidelity occurs. In the absence of an A-site tRNA, the A-site codon and 16S rRNA nucleotides A1492 and A1493 become disordered. Structural characterization of a near-cognate tRNA in the P site and cognate or near-cognate tRNA in the A site would provide additional insights into the molecular basis for this post PT QC mechanism.

The biochemical characterization of this same post PT QC mechanism shows RFs can bind to the A-site decoding center in the presence of a non-stop codon (58). Perhaps the change in the position of the mRNA, in response to near-cognate peptidyl-tRNA, allows RFs to bind to the decoding center in the presence of a non-stop codon. The structural characterization of RF2 bound to a non-stop codon in the A site, in the presence a near-cognate tRNA in the P site, would further our understanding of this post PT QC mechanism and provide insights into the fidelity of translational termination.

CONCLUSION

The work presented here expands our understanding of bacterial translation and the molecular mechanisms employed to maintain ribosomal fidelity. The ribosome has evolved the ability to monitor the accuracy of protein synthesis through the precise positioning of several key components. The ribosomal intersubunit bridge B8 act as a 'turnstyle-type' barrier for tRNA selection by negatively regulating the rate of GTPase activation to ensure only cognate tRNAs are selected. The mRNA reading frame is maintained by 'gripping' interactions with the peptidyl-tRNA. Finally, the ribosome has evolved a unique post PT QC mechanism that presumably is responsive to changes in the mRNA path due to near-cognate peptidyl-tRNA, resulting in the rapid termination of translation.

Perhaps one of the most important lessons derived from this work is the importance of using multiple experimental approaches to understand complex cellular systems through key collaborations. The ribosome has been studied for over fifty years, however we are just beginning to be able to answer many questions regarding the regulation the movement of the mRNA-tRNA interface during translocation and the specificity of tRNA selection. Genetic experiments identified key components important for fidelity, whereas biochemistry provided a detailed mechanistic understanding. My work with ribosomal and tRNA mutations provides the necessary structural basis required to understand their effects on the regulation of translation. For example,

the identification of allosteric link between distal components of the ribosome not only reconcile the location of restrictive and *ram* mutation found in ribosomal proteins S12 and S4 and their effects on tRNA selection, but also demonstrates the ribosome in a dynamic molecule that uses both local conformational changes and long-range interactions to regulate the translation of the mRNA. While my work with frameshift suppressor $tRNA^{SufJ}$ and the post PT QC mechanism raises many questions regarding the structural basis for translocation and proofreading mechanisms, these studies demonstrate how structural biology can be used to enhance our understanding the selectivity and regulation of ribosomal accuracy.

FIGURES

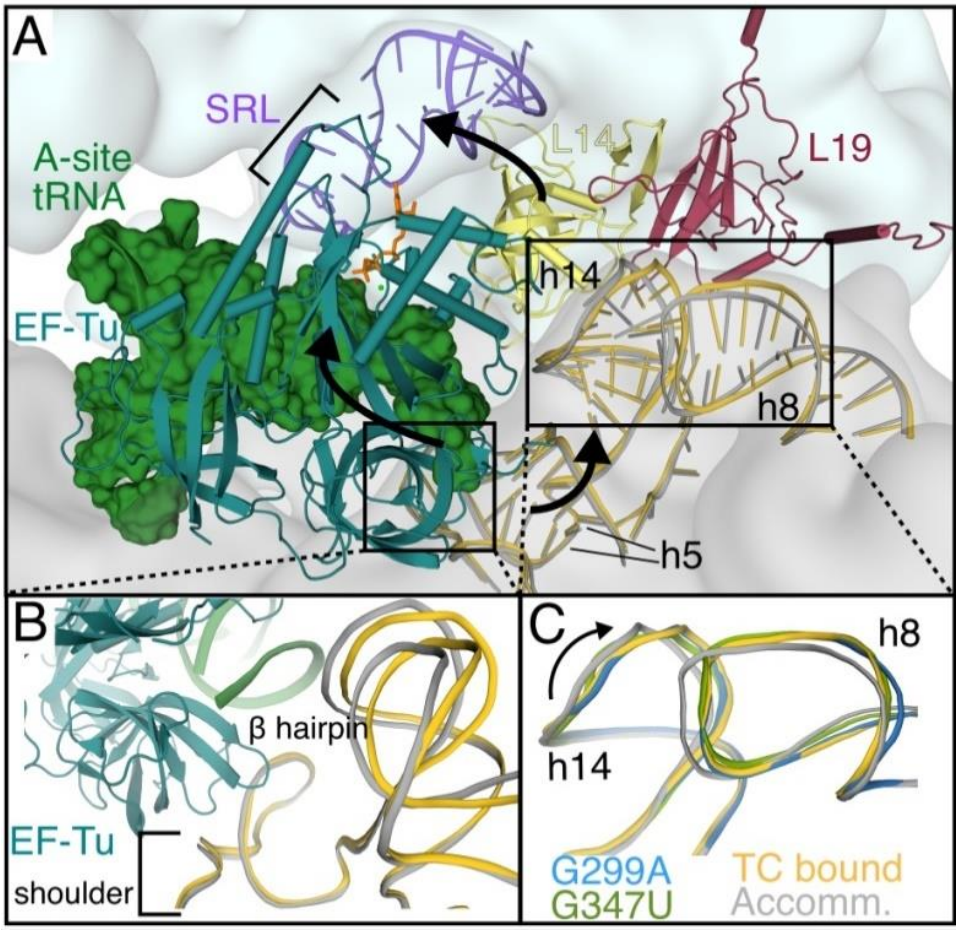

Fig. 5.1. Structural rearrangements of h8 and h14 resemble the conformational changes that result upon ternary complex (TC) binding to the ribosome. (A) Structure of 70S with EF-Tu (teal) bound to an incoming bent tRNA (green surface rendering). L14 (yellow) and L19 (maroon) are shown as cartoons while 23S rRNA (light blue) and 16S rRNA (gold) are shown in space filling representation. Overlaid of 16S rRNA h5, h8 and h14 from the A-site tRNA accommodated 70S structure shown as sticks (PDB ID 2WDG; gray (59)). **(B)** Previous structural basis for GTPase activation is that the shoulder domain (h5) moves closer to domain 1 of EF-Tu, resulting in a movement of the beta hairpin to promote GTP hydrolysis. Overlaid is the A-site tRNA accommodated 70S structure (gray) with the 70S TC-bound structure (gold). **(C)** Zoomed in view of how both 16S rRNA mutations, G299A (blue) and G347U (green) result in the

movement of h8 and h14, disrupting the intersubunit B8 interaction in a similar manner as observed when TC binds to the ribosome (PDB ID 2WRN, gold (10)).

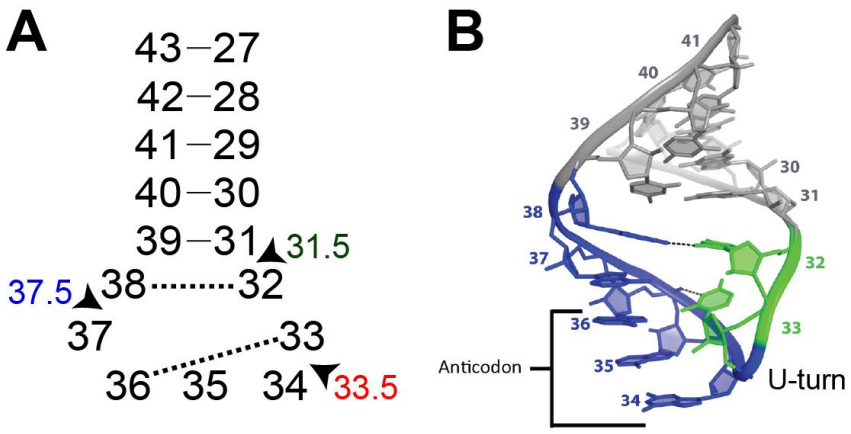

Figure 5.2. The anticodon stem domain. (A) The anticodon stem loop (ASL) is composed of a five base pair stem domain and a seven nucleotide unpaired loop. The location engineered insertions at 33.5 are labeled in red. The location of frameshift suppressor tRNA insertions are labeled for $tRNA^{SufA6}$ (blue) and $tRNA^{SufJ}$ (green). **(B)** The canonical seven nucleotide anticodon loop is arranged into two separate stacking domains separated by a sharp bend in the phosphate backbone caused by an invariant uracil at position 33. This characteristic "V" shape of the unpaired anticodon loop is stabilized through two important cross-strand interactions, the U-turn between U33 and the phosphate oxygen at position 36, and a 32•38 non Watson-Crick base pair interaction that brings together the ends of unpaired loop.

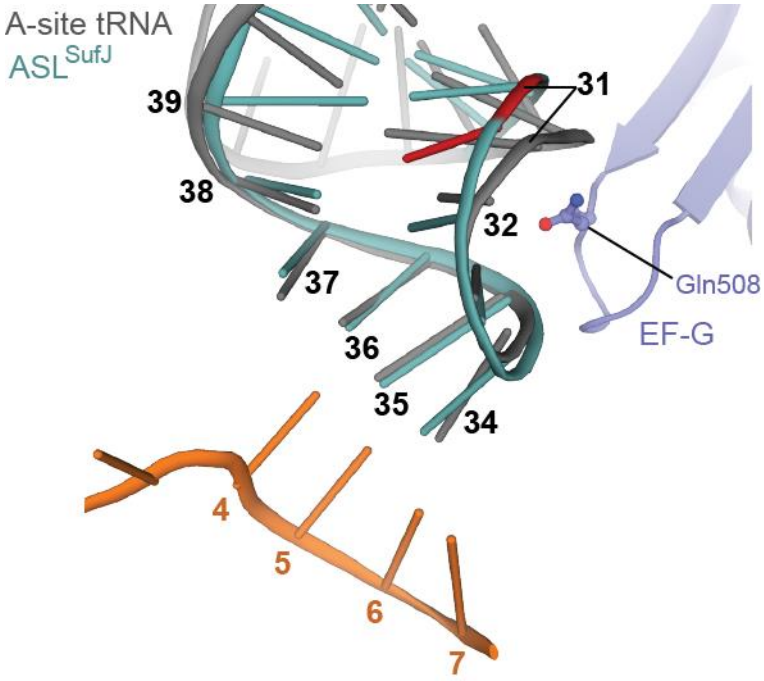

Figure 5.3. Superpositioning of ASLSufJ onto pre-translocated tRNA in the A site. EF-G (blue) contacts the phosphate backbone of the pre-translocated tRNA (gray) in the A site. The superpositioning of ASL^{SufJ} (light blue) indicates the C31.5 insertion (red) could alter this interaction. The mRNA codon is shown in orange.

REFERENCES

1. Davies J, Gilbert W, & Gorini L (1964) Streptomycin, Suppression, and the Code. *Proceedings of the National Academy of Sciences of the United States of America* 51:883-890.
2. Gorini L & Kataja E (1964) Phenotypic Repair by Streptomycin of Defective Genotypes in E. Coli. *Proceedings of the National Academy of Sciences of the United States of America* 51:487-493.
3. Pape T, Wintermeyer W, & Rodnina MV (1998) Complete kinetic mechanism of elongation factor Tu-dependent binding of aminoacyl-tRNA to the A site of the E. coli ribosome. *Embo J* 17(24):7490-7497.
4. Ogle JM, *et al.* (2001) Recognition of cognate transfer RNA by the 30S ribosomal subunit. *Science* 292:897-902.
5. Ogle JM, Murphy FV, Tarry MJ, & Ramakrishnan V (2002) Selection of tRNA by the ribosome requires a transition from an open to a closed form. *Cell* 111:721-732.
6. Gromadski KB & Rodnina MV (2004) Kinetic determinants of high-fidelity tRNA discrimination on the ribosome. *Molecular cell* 13:191-200.
7. Selmer M, *et al.* (2006) Structure of the 70S ribosome complexed with mRNA and tRNA. *Science* 313(5795):1935-1942.
8. Pape T, Wintermeyer W, & Rodnina M (1999) Induced fit in initial selection and proofreading of aminoacyl-tRNA on the ribosome. *EMBO J* 18(13):3800-3807.
9. Pape T, Wintermeyer W, & Rodnina MV (2000) Conformational switch in the decoding region of 16S rRNA during aminoacyl-tRNA selection on the ribosome. *Nat Struct Biol* 7(2):104-107.
10. Schmeing TM, *et al.* (2009) The crystal structure of the ribosome bound to EF-Tu and aminoacyl-tRNA. *Science* 326:688-694.
11. Voorhees RM, Schmeing TM, Kelley AC, & Ramakrishnan V (2010) The mechanism for activation of GTP hydrolysis on the ribosome. *Science (New York, N.Y.)* 330:835-838.
12. Ogle JM, Carter AP, & Ramakrishnan V (2003) Insights into the decoding mechanism from recent ribosome structures. *Trends Biochem Sci* 28(5):259-266.
13. Birge EA & Kurland CG (1969) Altered ribosomal protein in streptomycin-dependent Escherichia coli. *Science* 166(3910):1282-1284.
14. Ozaki M, Mizushima S, & Nomura M (1969) Identification and functional characterization of the protein controlled by the streptomycin-resistant locus in E. coli. *Nature* 222(5191):333-339.
15. Demirci H, *et al.* (2013) A structural basis for streptomycin-induced misreading of the genetic code. *Nature communications* 4:1355.
16. Demirci H, *et al.* (2013) The central role of protein S12 in organizing the structure of the decoding site of the ribosome. *Rna* 19(12):1791-1801.
17. Bjorkman J, Samuelsson P, Andersson DI, & Hughes D (1999) Novel ribosomal mutations affecting translational accuracy, antibiotic resistance and virulence of Salmonella typhimurium. *Mol Microbiol* 31(1):53-58.
18. Vallabhaneni H & Farabaugh PJ (2009) Accuracy modulating mutations of the ribosomal protein S4-S5 interface do not necessarily destabilize the rps4-rps5 protein-protein interaction. *Rna* 15(6):1100-1109.
19. McClory SP, Leisring JM, Qin D, & Fredrick K (2010) Missense suppressor mutations in 16S rRNA reveal the importance of helices h8 and h14 in aminoacyl-tRNA selection. *Rna* 16(10):1925-1934.
20. Maisnier-Patin S, Paulander W, Pennhag A, & Andersson DI (2007) Compensatory evolution reveals functional interactions between ribosomal proteins S12, L14 and L19. *Journal of molecular biology* 366:207-215.

21. Sun Q, Vila-Sanjurjo A, & O'Connor M (2011) Mutations in the intersubunit bridge regions of 16S rRNA affect decoding and subunit-subunit interactions on the 70S ribosome. *Nucleic acids research* 39:3321-3330.
22. Fagan CE, *et al.* (2013) Reorganization of an intersubunit bridge induced by disparate 16S ribosomal ambiguity mutations mimics an EF-Tu-bound state. *Proceedings of the National Academy of Sciences of the United States of America* 110(24):9716-9721.
23. Liu Q & Fredrick K (2013) Contribution of intersubunit bridges to the energy barrier of ribosomal translocation. *Nucleic acids research* 41(1):565-574.
24. Jin H, Kelley aC, & Ramakrishnan V (2011) Crystal structure of the hybrid state of ribosome in complex with the guanosine triphosphatase release factor 3. *Proceedings of the National Academy of Sciences*:1-6.
25. Preis A, *et al.* (2014) Cryoelectron Microscopic Structures of Eukaryotic Translation Termination Complexes Containing eRF1-eRF3 or eRF1-ABCE1. *Cell reports* 8(1):59-65.
26. Agirrezabala X, *et al.* (2013) The ribosome triggers the stringent response by RelA via a highly distorted tRNA. *EMBO Rep* 14(9):811-816.
27. Crick FH, Griffith JS, & Orgel LE (1957) Codes without Commas. *Proceedings of the National Academy of Sciences of the United States of America* 43(5):416-421.
28. Dinman JD (2012) Mechanisms and implications of programmed translational frameshifting. *Wiley interdisciplinary reviews. RNA* 3(5):661-673.
29. Riyasaty S & Atkins JF (1968) External suppression of a frameshift mutant in salmonella. *Journal of molecular biology* 34(3):541-557.
30. Riddle DL & Roth JR (1970) Suppressors of frameshift mutations in Salmonella typhimurium. *Journal of molecular biology* 54(1):131-144.
31. Yourno J (1970) Nature of the compensating frameshift in the double frameshift mutant hisD3018 R5 of Salmonella typhimurium. *Journal of molecular biology* 48(3):437-442.
32. Yourno J & Tanemura S (1970) Restoration of in-phase translation by an unlinked suppressor of a frameshift mutation in Salmonella typhimurium. *Nature* 225(5231):422-426.
33. Yourno J (1972) Externally suppressible +1 "glycine" frameshift: possible quadruplet isomers for glycine and proline. *Nat New Biol* 239(94):219-221.
34. Kohno T, Bossi L, & Roth JR (1983) New suppressors of frameshift mutations in Salmonella typhimurium. *Genetics* 103(1):23-29.
35. Bossi L & Smith DM (1984) Suppressor sufJ: a novel type of tRNA mutant that induces translational frameshifting. *Proceedings of the National Academy of Sciences of the United States of America* 81(19):6105-6109.
36. Yarus M (1982) Translational efficiency of transfer RNA's: uses of an extended anticodon. *Science* 218(4573):646-652.
37. Gaber RF & Culbertson MR (1984) Codon recognition during frameshift suppression in Saccharomyces cerevisiae. *Mol Cell Biol* 4(10):2052-2061.
38. Curran JF & Yarus M (1987) Reading frame selection and transfer RNA anticodon loop stacking. *Science* 238(4833):1545-1550.
39. Moore B, Persson BC, Nelson CC, Gesteland RF, & Atkins JF (2000) Quadruplet codons: implications for code expansion and the specification of translation step size. *Journal of molecular biology* 298(2):195-209.
40. Atkins JF & Bjork GR (2009) A Gripping Tale of Ribosomal Frameshifting: Extragenic Suppressors of Frameshift Mutations Spotlight P-Site Realignment. *Microbiology and Molecular Biology Reviews* 73:178-210.
41. Nasvall SJ, Nilsson K, & Bjork GR (2009) The ribosomal grip of the peptidyl-tRNA is critical for reading frame maintenance. *Journal of molecular biology* 385(2):350-367.

42. Jager G, Nilsson K, & Bjork GR (2013) The phenotype of many independently isolated +1 frameshift suppressor mutants supports a pivotal role of the P-site in reading frame maintenance. *PloS one* 8(4):e60246.
43. Maehigashi T, Dunkle JA, Miles SJ, & Dunham CM (2014) Structural basis for +1 frameshifting promoted by expanded or modification-deficient anticodon stem-loops. *Proceedings of the National Academy of Sciences of the United States of America*.
44. Phelps SS, *et al.* (2006) Translocation of a tRNA with an extended anticodon through the ribosome. *Journal of molecular biology* 360(3):610-622.
45. Dunham CM, *et al.* (2007) Structures of tRNAs with an expanded anticodon loop in the decoding center of the 30S ribosomal subunit. *Rna* 13:817-823.
46. Brilot AF, Korostelev AA, Ermolenko DN, & Grigorieff N (2013) Structure of the ribosome with elongation factor G trapped in the pretranslocation state. *Proceedings of the National Academy of Sciences of the United States of America* 110(52):20994-20999.
47. Dinman JD (2006) Programmed Ribosomal Frameshifting Goes Beyond Viruses: Organisms from all three kingdoms use frameshifting to regulate gene expression, perhaps signaling a paradigm shift. *Microbe* 1(11):521-527.
48. Bossi L & Roth JR (1981) Four-base codons ACCA, ACCU and ACCC are recognized by frameshift suppressor sufJ. *Cell* 25(2):489-496.
49. Walker SE & Fredrick K (2006) Recognition and positioning of mRNA in the ribosome by tRNAs with expanded anticodons. *Journal of molecular biology* 360(3):599-609.
50. Elkins BN & Keller EB (1974) The enzymatic synthesis of N-(purin-6-ylcarbamoyl)threonine, an anticodon-adjacent base in transfer ribonucleic acid. *Biochemistry* 13(22):4622-4628.
51. Brunel C, *et al.* (1993) Translational regulation of the Escherichia coli threonyl-tRNA synthetase gene: structural and functional importance of the thrS operator domains. *Biochimie* 75(12):1167-1179.
52. Sankaranarayanan R, *et al.* (1999) The structure of threonyl-tRNA synthetase-tRNA(Thr) complex enlightens its repressor activity and reveals an essential zinc ion in the active site. *Cell* 97(3):371-381.
53. Agris PF, Vendeix FA, & Graham WD (2007) tRNA's wobble decoding of the genome: 40 years of modification. *Journal of molecular biology* 366(1):1-13.
54. Durant PC, Bajji AC, Sundaram M, Kumar RK, & Davis DR (2005) Structural effects of hypermodified nucleosides in the Escherichia coli and human tRNALys anticodon loop: the effect of nucleosides s2U, mcm5U, mcm5s2U, mnm5s2U, t6A, and ms2t6A. *Biochemistry* 44(22):8078-8089.
55. Zaher HS & Green R (2009) Quality control by the ribosome following peptide bond formation. *Nature* 457:161-166.
56. Zaher HS & Green R (2010) Kinetic basis for global loss of fidelity arising from mismatches in the P-site codon:anticodon helix. *Rna* 16:1980-1989.
57. Zaher HS & Green R (2011) A primary role for release factor 3 in quality control during translation elongation in Escherichia coli. *Cell* 147(2):396-408.
58. Petropoulos AD, McDonald ME, Green R, & Zaher HS (2014) Distinct roles for release factor 1 and release factor 2 in translational quality control. *The Journal of biological chemistry* 289(25):17589-17596.
59. Voorhees RM, Weixlbaumer A, Loakes D, Kelley AC, & Ramakrishnan V (2009) Insights into substrate stabilization from snapshots of the peptidyl transferase center of the intact 70S ribosome. *Nat Struct Mol Biol* 16(5):528-533.

APPENDIX 1: MACROLIDE-PEPTIDE CONJUGATES AS PROBES OF THE PATH OF TRAVEL OF THE NASCENT PEPTIDES THROUGH THE RIBOSOME

Arren Z. Washington, Derek B.Benicewicz, Joshua C. Canzoneri, Crystal E. Fagan, Sandra C. Mwakwari, Tatsuya Maehigashi, Christine M. Dunham and Adegboyega K. Oyelere

Specific nascent peptide chains interact with the ribosomal exit tunnel to alter translation. Here, a novel class of peptide probes were synthesized and characterized for their ability to selectively target the bacterial ribosome and present the peptide sequence to the exit tunnel. These probes formed by the covalent linkage of an oligopeptide to a ketolide analog bound to the 50S macrolide binding site of the ribosome near the exit tunnel. Instead of inserting into the exit tunnel, the peptide tail extended in the opposite direction towards the peptidyl transferase center. For this work, I structurally characterized one of these probes bound to the 70S ribosomal exit tunnel. This work has been submitted for publication.

Author contributions: A.K.O. and C.M.D. designed research, A.Z.W., D.B.B., J.C.C., S.C.M., synthesized and biochemically characterized the compounds C.E.F. crystallized the ribosomal complex; refined and analyzed the structure; and A.Z.W., C.E.F., C.M.D, and A.K.O wrote the paper.

ABSTRACT

The identity, location and complex interworking of many components of the ribosome have been extensively analyzed over recent decades. Despite careful analysis of the bacterial ribosome, the ribosomal exit tunnel is still poorly understood. It has been suggested that the exit tunnel is simply an empty space serving solely as a convenient route of egress for the nascent polypeptide chain. In contrast, certain protein sequences serve to slow the rate of translation, suggesting some degree of interaction between the nascent peptide chain and the exit tunnel. To understand how the ribosome interacts with nascent peptide sequences, we synthesized and characterized a novel class of probe molecules. These peptide-macrolide (or "peptolide") conjugate probes were designed to present unique peptide sequences to the exit tunnel. Biochemical and X-ray structural analyses of the interactions between these probes and the ribosome demonstrate interesting insights about the exit tunnel. Using translation inhibition and RNA structure probing assays we find the exit tunnel has a relaxed preference for the directionality (N → C or C → N orientation) of the nascent peptides. Moreover, the X-ray crystal structure of one peptolide derived from a positively charged reverse Nuclear Localization Sequence (NLS) peptide, bound to the 70S bacterial ribosome, reveals that the macrolide ring of the peptolide binds in the same position as other macrolides. However, the peptide tail folds back over the macrolide ring, oriented toward the base of the peptidyl transferase center. Additionally, the peptide tail interacts specifically with 23S rRNA C2442 and His69 of ribosomal protein L4, two components of the exit tunnel previously unappreciated as nascent peptide binding partners. The availability of such molecular probes that allow for precise placement of any peptide sequence within a defined region of the peptide exit tunnel could enrich our knowledge of the roles of this crucial ribosome structure in translation.

INTRODUCTION

The ribosome, through well-choreographed processes, translates genetically encoded messages on mRNAs to polypeptides. While structural and biochemical studies of 70S prokaryotic ribosome have enhanced our understanding of the role many of these components play during translation (1-6), little is understood about the ribosomal peptide exit tunnel. During elongation of the nascent peptide, the growing peptide chain extends from the peptidyl transferase center (PTC) to the backside of the ribosome through the peptide exit tunnel, an 80Å long, 20 Å wide exit tunnel that extends across the large subunit of the ribosome from the base of the PTC and opens at the back of the subunit (4, 7, 8). The role of the peptide exit tunnel is primarily to act as a route of egress for the nascent peptide (4, 9, 10), however in some cases, specific interactions between the nascent peptide and the exit tunnel walls have been shown to alter translational regulation (9, 11-13). Currently, it is not well understood how the ribosome could distinguish and respond to specific peptide sequences while facilitating an unhindered passage of the vast majority of peptides through the peptide exit tunnel.

Efforts aimed at mapping the paths of the nascent peptide through the ribosome have focused mainly on trapping sequence-specific peptides known to interact directly with the exit tunnel (11, 14). Specifically, fluorescence resonance energy transfer (FRET)**,** molecular-dynamics simulation, and crosslinking experiments have furnished biochemical insights into the interactions between a 17 amino acid motif near the C terminus of SecM and the components of the *Escherichia coli* (*E. coli*) ribosome exit tunnel which results in translation arrest (11, 15, 16). Cryo–EM and single-particle reconstructions have revealed the presence of a relay mechanism involving direct interactions between the nascent peptide and ribosomal exit tunnel resulting in the ribosome stalling during translation of both the ErmBL leader peptide in the presence of erythromycin and the *tnaC* leader gene (14, 17). Moreover, analysis of primer extension inhibition has led to the postulation of similar peptide-dependent ribosome stalling relay mechanisms at the regulatory cistron of the antibiotic resistance gene *ermA* (18). While each of

these experiments analyze the exit tunnel interactions with distinct peptide sequences, these experiments illustrate the importance of designing molecular probes which can precisely position any peptide sequence within a defined region of the peptide exit tunnel.

Recently, analogs of 16-membered macrolides tylosin, desmycosin, and 5-O-mycominosyltylonolide incorporating esters of amino acids, di- and tri-peptides have been shown to engage the exit tunnel through distinct interactions with ribosomal components, presumably using their amino acid and peptide moieties (19, 20). Specifically, molecular dynamics simulations suggest that the N-acylglycyl moiety of the aminoacylated 5-O-mycominosyl-tylonolide derivative could be positioned to form hydrogen bonds with 23S rRNA A752 and Lys 90 of ribosomal protein L22. These hydrogen bonds could potentially disrupt the essential A752-U2609 base pair which has previously been shown to play a role in both peptide stalling and macrolide antibiotic interactions (20-22). However, the peptide moieties of these conjugates are short and are expected to interrogate only a short segment of the exit tunnel, particularly the tunnel entrance.

In an effort to understand how nascent peptide could interact with the exit tunnel, our collaborators designed a novel set of peptide-ketolide (peptolide) compounds formed by the covalent attachment of a oligopeptide to a ketolide analog (**Fig. A1.1**). These probes were designed using the structural analysis of telithromyocin (TEL) bound to the 50S as a model for the placement of the flexible alkyl arm connecting the ketolide macrocyclic ring to the oligopeptide (**Fig. A1.1A**).

X-ray crystallographic studies have shown that the alkyl-aryl arm of TEL can adopt three distinct conformations: extending towards the A752-U2609 base pair (*E. coli* and *T. thermophilus*), down the peptide exit tunnel in the same direction as a nascent chain (*D. radiodurans*), or folded back over the macrolide ring in the direction of the PTC (*H. marismortui*) (**Fig. A1.1B**) (21, 22, 24, 25).

In each of the structures, the alkyl-aryl arm is engaged in different stabilizing interactions. In *E. coli* and *T. thermophilus*, the arm is stabilized by stacking against the rRNA A752-U2609 base pair. In *H. marismortui*, which lacks the A752-U2609 base pair, the arm is stabilized by a hydrogen bond with the O2' of U2609 while in *D. radiodurans*, the arm extends down the exit tunnel and is potentially engaged in van der Waals interactions with the rRNA (6). As long as these crucial energy-minimizing interactions remain intact, it is feasible that the arm could be modified beyond the aryl group and allow new ligands to be added while preserving the ketolide binding mode. The path of travel through the ribosome by the modified TEL flexible arm could be influenced by the identity of the substituents on its aryl moiety. For the proposed peptolides, it is conceivable that the identity (and/or sequence) of the peptide attached to the modified alkyl-aryl arm could dictate the placement of the peptides within the ribosome through preferential adoption of one of the three distinct alkyl-aryl arm positions (**Fig. A1.1B**) (21, 22, 24, 25).

Our collaborators demonstrated these peptolides were capable of inhibiting protein synthesis using *in vitro* translation assays. Their results also showed the peptolides bound to the macrolide binding site of the *E. coli* ribosome in a charge specific manner using RNA structure footprinting experiments. In order to visualize the placement of the peptide tail within the exit tunnel, I solved the X-ray crystal structure of one peptolide bound to the 70S. My structure shows that the peptolide adopts a conformation with its peptide tail oriented back towards the PTC and the subunit interface close to 23S rRNA residue U1963 located between the A and P sites. Taken together, our results indicate these distinct peptolides could be useful probes for interrogating nascent peptide-exit tunnel interaction between the PTC to the L4/L22 constriction site. This approach could provide a general means for a precise placement of peptides into both the exit tunnel and path from the PTC to the tunnel entrance.

RESULTS AND DISCUSSION

Structural studies of peptolide 12c bound to the 70S ribosome. Previous X-ray crystallographic studies of similar ketolides, TEL and CEM101, show these macrolides bind to the macrolide binding pocket in the upper portion of the ribosomal exit tunnel, adjacent to the L22 and L4 constriction site (21, 22, 24, 25). In order to determine if these peptolides bind in the same macrolide-binding site with a similar orientation for the modified alkyl-aryl tail, we co-crystallized the peptolide **12c**, derived from the propyl-linked (n=1) azido-ketolide **7a** and the positively charged NLS peptide attached in the reverse polarity, with *T. thermophilus* 70S ribosomes programmed with mRNA, P-site $tRNA^{fMet}$, and A-site $tRNA^{Phe}$. The peptolide (1 μM final concentration) was incubated with programmed ribosome complexes just prior to crystallization. X-ray diffraction data was collected, processed, and the structure was solved to 3.6 Å using molecular replacement with a 70S ribosome structure where the tRNA and mRNA ligands removed (40). Unbiased Fo-Fc difference electron density maps show clear and connected density of the ketolide macrocyclic ring and eight of the twelve residues in the peptide tail except for the side chain of Lys5 (**Fig. A1.2** and **Fig. A1.3**).

The 70S-peptolide **12c** structure shows the ketolide macrocyclic ring adopts a similar orientation in the peptidyl transferase center on the 50S subunit as observed in previous structures (21, 22, 24, 25). Specifically, the desosamine sugar at position 5 of the ketolide macrocyclic ring hydrogen bonds with the base of 23S rRNA A2058 and the surface of this ring forms hydrophobic packing interactions with the bases of U2611, A2058, and A2059. These results indicate the addition of the peptide tail does not alter the ketolide macrocyclic ring position as observed in other crystal structures.

Similar to other ketolides, the peptolides described in this study also contain a flexible alkyl-aryl arm. Previous crystal structures have shown three distinct conformations of the alkyl-aryl arm of TEL. When bound to *E. coli* or *T. thermophilus* 70S, the alkyl-aryl arm of TEL packs against the U2609-A752 base pair (21, 22). In *H. marismortui*, the alkyl-aryl arm folds back over

the top of the macrolactone ring (25) while in *D. radiodurans*, the alkyl-aryl arm extends further down the peptide exit towards the L4/L22 constriction site (24). This altered conformation of the alkyl-aryl arm observed in *H. marismortui* and *D. radiodurans* has been hypothesized to be a consequence of the absence of a U2609-A752 base pair (22).

Our 70S-peptolide **12c** structure indicates the alkyl-aryl arm of the peptolide extends further down the peptide exit tunnel in a similar conformation as observed with *D. radiodurans* (**Fig. A1.1B, Fig. A1.2,** and **Fig. A1.4**). However despite the positioning of the alkyl-aryl arm towards the L4/L22 constriction site, the peptide portion of the peptolide turns and folds back over the top of the ketolide macrocyclic ring oriented toward the PTC with its position stabilized through the formation of two new hydrogen bonds (**Fig. A1.2**). The peptolide residue Lys6 hydrogen bonds to the phosphate oxygen of 23S rRNA C2442 while Lys7 hydrogen bonds with the side chain of His69 of ribosomal protein L4 (**Fig. A1.2**). The electron density of the peptolide tail is disordered beyond the eighth amino acid of the attached peptide chain and therefore the last four residues were not built. While the well-ordered portion of the peptide tail does not extend past the exit tunnel L4/L22 constriction site, the entire exit site tunnel is blocked by the peptide tail folding back on top of the ketolide macrocyclic ring (**Fig. A1.2**). While the peptide tail is too short to directly interact with U1963 that is protected in the CMCT footprinting experiments, the peptide tail may cause a rearrangement of the adjacent 23S rRNA residues in the PTC thereby indirectly resulting in U1962 protection.

CONCLUSION

Ribosome structures have given us a molecular understanding of the roles that specific ribosomal components play during translation (1-6, 41). However, the nascent peptide exit tunnel is a ribosome component that has yet to be fully characterized. The rRNA-lined tunnel serves as the route of travel for nascent peptides from the PTC towards the exterior surface of the ribosome (7, 8). Initially, the exit tunnel was proposed to have little impact on specific nascent chain

sequences and exist solely to facilitate an unhindered passage of peptides to the exterior of the ribosome. A growing body of research has shown specific amino acid sequences interact with the components of the exit tunnel, concomitantly influencing many aspects of translation such as the translation rate, ribosome stalling and even changes in mRNA frame maintenance (9, 13, 42-44). Despite these new insights, the molecular mechanisms used by the ribosome to identify and interact with specific nascent peptide sequences are not well understood.

In an effort to understand how nascent peptide chains interactions with the exit tunnel of the ribosome, our collaborators generated and biochemically characterized of novel molecular probes capable of presenting unique peptides to the ribosome exit tunnel. The location of the peptolide **12c** in the exit tunnel in the context of a programmed 70S was determined by X-ray crystallography to 3.6 Å. My structural data places the ketolide macrocyclic ring in the same place as previous structures (21, 22, 24, 25). While the position of the alkyl-aryl arm extends further down the exit tunnel similar to position observed in the *D. radiodurans* structure, the peptide tail however folds back over the ketolide macrocyclic ring, extending in the opposite direction back towards the PTC.

In summary, these data suggest that the peptolides disclosed therein are viable probes for interrogating nascent peptide-exit tunnel interaction from the PTC to the exit tunnel entrance. Ongoing effort is focused on designing a new generation of peptolides which would be able to insert their peptide tails into the exit tunnel from the PTC entrance to obtain a complete set of probes for the full length of the tunnel.

METHODS

X-ray crystallographic studies of the *Thermus thermophilus* 70S ribosome bound to the peptolide 12c. *T. thermophilus* ribosomes were purified, crystallized, cryoprotected and crystallographically solved as previously described (3). *Escherichia coli* $tRNA^{fMet}$ and $tRNA^{Phe}$ were purchased from Chemical Block. The mRNA oligonucleotide was chemically synthesized

by Integrated DNA Technology with a sequence of 5′-GGCAAGGAGGUAAAAAUGUUCAAAA-3′, where the underlined AUG and UUC represent the P- and A-site codons, respectively. Briefly, the programmed 70S complexes were formed using previously established conditions with the additional step being the incubation at 37° C for 30 min of peptolide **12c** prior to crystallization. X-ray diffraction data were collected from four crystals for the 70S-**12c** complex at the Northeastern Collaborative Access Team (NE-CAT) beamline at the Advanced Proton Source, Argonne National Laboratory. Each diffraction dataset was integrated and scaled using the XDS software package (47). The structures were solved by molecular replacement with the PHENIX software suite (48) using an initial search model composed of the *Tth* 70S ribosome (PDB ID codes 2WDG, 2WDH, 2WDI, and 2WDJ) with all ligands and ions removed. An initial round of coordinate refinement was performed using each of the ribosomal subunits as a single rigid group. Additional rounds of rigid and Translation, Liberation, Screw-movement (TLS) refinements were performed using defined rigid and TLS groups comprised of the head, body, platform, and 3' minor domains for the 30S subunit and the 5S rRNA, L1 arm, A-site finger, central protuberance, and protein L9 domains for the 50S subunit. Modeling of the 12C peptolide, tRNA, mRNA, and placement of the Mg^{2+} ions was performed using Coot (49). Iterative rounds of model building and positional and atomic displacement parameter (ADP) refinements were performed in PHENIX to yield a final model with the statistics reported in Table 2. Figures were generated using PyMol (50).

FIGURES

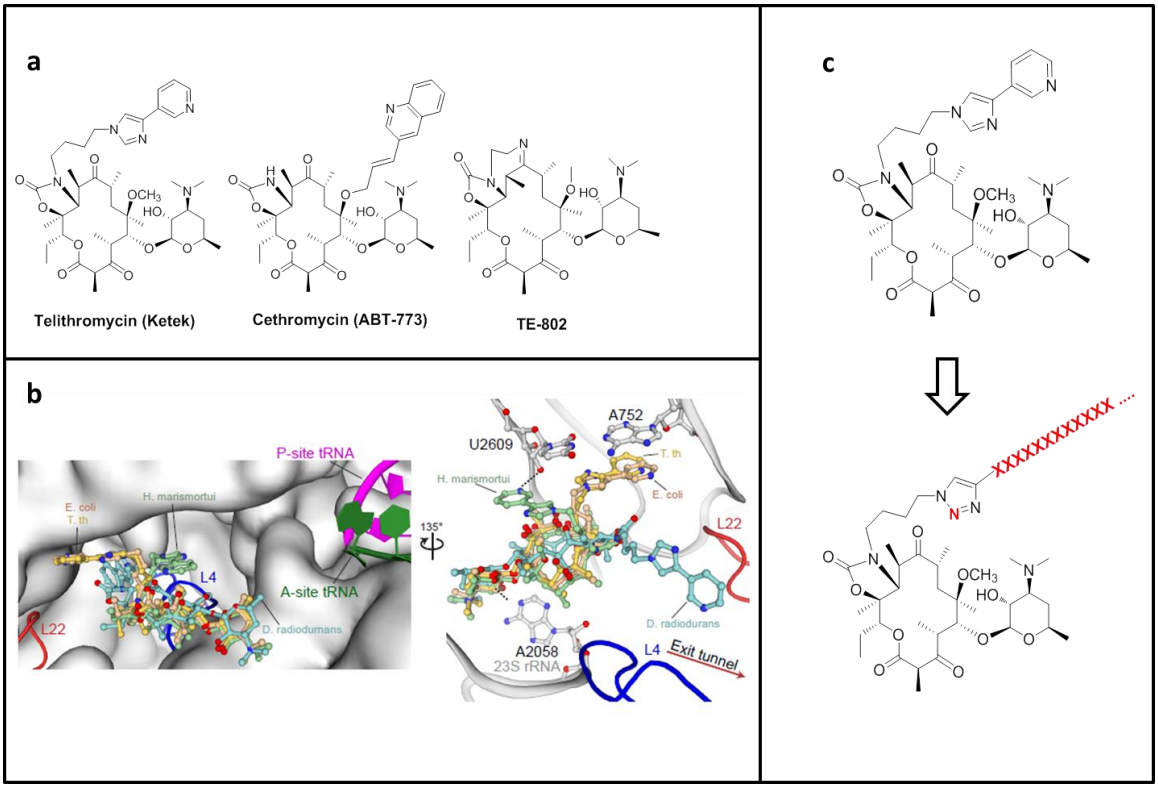

Figure A1.1. Design of peptide-ketolide (peptolide) compounds. (a) Structures of representative ketolides – Telithromycin (TEL), Cethromycin and TE-802. **(b)** Binding of TEL to the 50S subunit of the ribosome. (Left) An overlay of TEL shows alternate positioning of the alkyl-aryl arm when bound to *T. thermophilus* (yellow, PDB ID 3OI3), *E. coli* (beige, PDB ID 3OAT), *H. marismortui* (green, PDB ID 1YIJ), and *D. radiodurans* (cyan, PDB ID 1P9X) . TEL binds to the 50S exit tunnel in between the PTC represented by the P-site and A site-tRNA, and the constriction site in the exit tunnel near 50S r-protein L4 (blue) and L22 (red). (Right) In each of the macrolide structure, the desosamine sugar hydrogen bonds with A2058 stabilizing the macrolactone ring. The alkyl-aryl arm stacks against the A752-U2609 base pair in *T. thermophilus.* (yellow) and *E. coli* (beige). In the absence of the A752-U2609, the alkyl-aryl arm hydrogen bonds to U2609 in *H. marismortui* (green) or extends towards down the exit tunnel in *D. radiodurans* (cyan). **(c)** General structure of peptolide derived from TEL. Changes to the TEL

template to yield the target peptolide probes are highlighted in red with –XXXX- indicating polypeptide containing any combination of amino acids of interest.

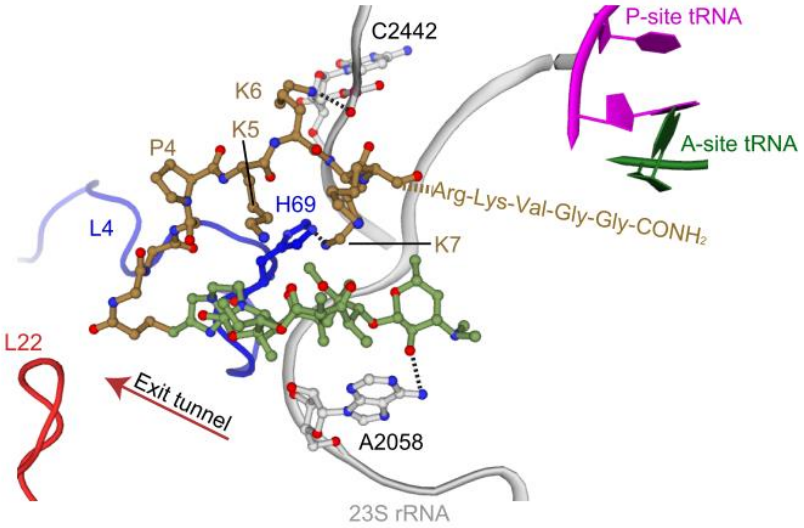

Figure A1.2. Binding site of peptolide 12c in the 50S subunit of the ribosome. Similar to TEL, peptolide 12c binds to the 50S exit tunnel just before the L4 (blue) constriction site. The peptide tail folds back over the macrolactone ring, extending towards the P-site and A-site tRNA in the PTC. The macrolactone ring (green) is stabilized through a hydrogen bond between A2058 and the desosamine sugar. The peptide tail (gold) is stabilized through hydrogen bonds with 23S rRNA C2442 and His69 of ribosomal protein L4 (blue). The last four amino acids of the peptide tail, represented by a dashed line, extend towards the PTC.

Table A1.1. Summary of crystallographic data and refinement

Data collection	
Space group	$P2_12_12_1$
Cell dimensions	
a, b, c (Å)	209.2 443.5 618.6
α, β, γ (°)	90.0 90.0 90.0
Resolution (Å)	50.0-3.6 (3.7-3.6)
R_{merge} (%)	27.7 (116.9)
$R_{p.i.m}$[1] (%)	10.2 (47.2)
I/σI	7.6 (1.8)
Completeness (%)	98.0 (95.8)
Redundancy	7.4 (6.1)
Refinement	
Resolution (Å)	50.0-3.6 (3.7-3.6)
No. reflection	646,099
R_{work}/R_{free} (%)	22.1/25.5
No. atoms	295,491
RMSD	
Bond lengths (Å)	0.006
Bond angles (°)	0.887

Values in parentheses are for the highest-resolution shell.

[1] $R_{p.i.m.} = \frac{\sum_{hkl}\sqrt{\frac{1}{n-1}\sum_{i=1}^{n}|I_i(hkl)-\langle I(hkl)\rangle|}}{\sum_{hkl}\sum_i I_i(hjk)}$

.

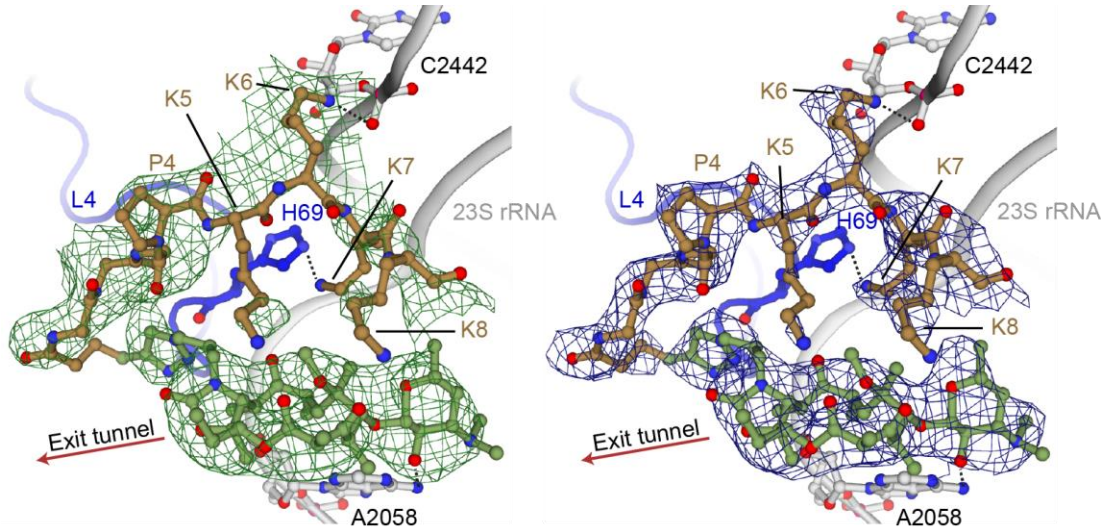

Figure A1.3. Electron density maps for peptolide 12c bound to the 70S ribosome. (Left) Unbiased F_o-F_c electron density map (contoured at 3 σ) for peptolide 12c bound to the macrolide binding pocket shows strong peaks for the macrolactone ring (green) and portions of the peptide tail (gold). All side chains of the peptolides are visible except for Lys5. The peptolide is stabilized through the formation of hydrogen bonds with 23S rRNA nucleotide C2442 (gray) and His69 of ribosomal protein L4 (blue). (Right) The $2F_o$-F_c electron density map after refinement for peptolide 12C (contoured at 1.5 σ).

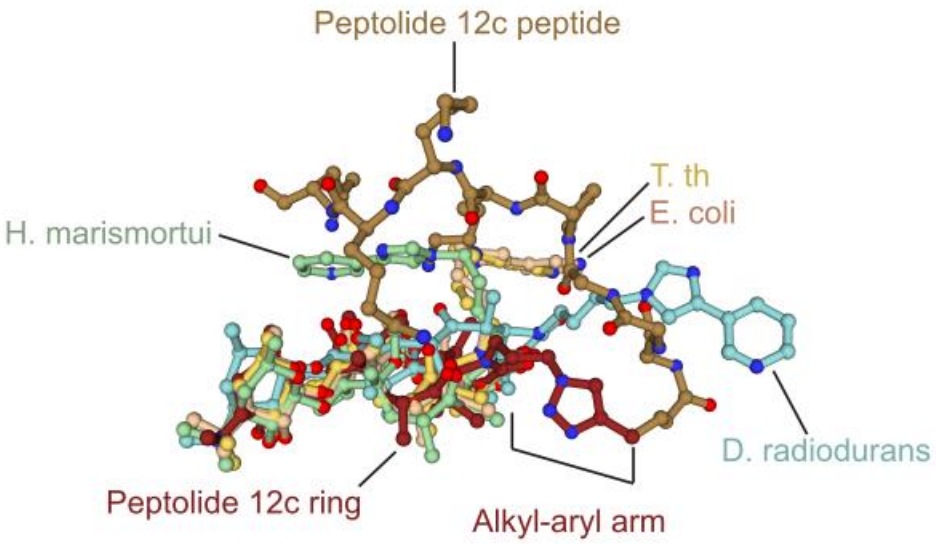

Figure A1.4. Superposition of peptolide 12c and TEL bound to the macrolide binding pocket of the 50S subunit. The ketolide macrocyclic ring of peptolide 12c (brown) binds in the same orientation as TEL when bound to *T. thermophilus* (yellow, PDB ID 3OI3), *E. coli* (beige, PDB ID 3OAT), *H. marismortui* (green, PDB ID 1YIJ) and *D. radiodurnans* (cyan, PDB ID 1P9X). The flexible alkyl-aryl arm of peptolide 12c adopts a similar conformation as observed when TEL is bound to D. radiodurans, however the peptide tail folds back over the top of the ketolide macrocyclic ring.

REFERENCES

1. Wimberly BT, *et al.* (2000) Structure of the 30S ribosomal subunit. *Nature* 407:327-339.
2. Schuwirth BS, *et al.* (2005) Structures of the bacterial ribosome at 3.5 A resolution. *Science* 310(5749):827-834.
3. Selmer M, *et al.* (2006) Structure of the 70S ribosome complexed with mRNA and tRNA. *Science* 313(5795):1935-1942.
4. Ban N, Nissen P, Hansen J, Moore PB, & Steitz TA (2000) The complete atomic structure of the large ribosomal subunit at 2.4 A resolution. *Science* 289:905-920.
5. Nissen P, Hansen J, Ban N, Moore PB, & Steitz TA (2000) The structural basis of ribosome activity in peptide bond synthesis. *Science* 289(5481):920-930.
6. Schluenzen F, *et al.* (2000) Structure of functionally activated small ribosomal subunit at 3.3 angstroms resolution. *Cell* 102(5):615-623.
7. Voss NR, Gerstein M, Steitz TA, & Moore PB (2006) The geometry of the ribosomal polypeptide exit tunnel. *Journal of molecular biology* 360(4):893-906.
8. Jenni S & Ban N (2003) The chemistry of protein synthesis and voyage through the ribosomal tunnel. *Curr Opin Struct Biol* 13(2):212-219.
9. Mankin AS (2006) Nascent peptide in the "birth canal" of the ribosome. *Trends Biochem Sci* 31(1):11-13.
10. Cruz-Vera LR, Sachs MS, Squires CL, & Yanofsky C (2011) Nascent polypeptide sequences that influence ribosome function. *Curr Opin Microbiol* 14(2):160-166.
11. Gumbart J, Schreiner E, Wilson DN, Beckmann R, & Schulten K (2012) Mechanisms of SecM-mediated stalling in the ribosome. *Biophysical journal* 103(2):331-341.
12. Vazquez-Laslop N, Thum C, & Mankin AS (2008) Molecular mechanism of drug-dependent ribosome stalling. *Mol Cell* 30(2):190-202.
13. Gupta P, Sothiselvam S, Vazquez-Laslop N, & Mankin AS (2013) Deregulation of translation due to post-transcriptional modification of rRNA explains why erm genes are inducible. *Nature communications* 4:1984.
14. Seidelt B, *et al.* (2009) Structural insight into nascent polypeptide chain-mediated translational stalling. *Science* 326(5958):1412-1415.
15. Woolhead CA, Johnson AE, & Bernstein HD (2006) Translation arrest requires two-way communication between a nascent polypeptide and the ribosome. *Mol Cell* 22(5):587-598.
16. Yap MN & Bernstein HD (2009) The plasticity of a translation arrest motif yields insights into nascent polypeptide recognition inside the ribosome tunnel. *Mol Cell* 34(2):201-211.
17. Arenz S, *et al.* (2014) Molecular basis for erythromycin-dependent ribosome stalling during translation of the ErmBL leader peptide. *Nature communications* 5:3501.
18. Ramu H, *et al.* (2011) Nascent peptide in the ribosome exit tunnel affects functional properties of the A-site of the peptidyl transferase center. *Mol Cell* 41(3):321-330.
19. Starosta AL, *et al.* (2010) Interplay between the ribosomal tunnel, nascent chain, and macrolides influences drug inhibition. *Chem Biol* 17(5):504-514.
20. Shishkina A, *et al.* (2013) Conjugates of amino acids and peptides with 5-o-mycaminosyltylonolide and their interaction with the ribosomal exit tunnel. *Bioconjugate chemistry* 24(11):1861-1869.
21. Bulkley D, Innis CA, Blaha G, & Steitz TA (2010) Revisiting the structures of several antibiotics bound to the bacterial ribosome. *Proceedings of the National Academy of Sciences of the United States of America* 107(40):17158-17163.
22. Dunkle JA, Xiong L, Mankin AS, & Cate JH (2010) Structures of the Escherichia coli ribosome with antibiotics bound near the peptidyl transferase center explain spectra of

drug action. *Proceedings of the National Academy of Sciences of the United States of America* 107(40):17152-17157.
23. Kannan K & Mankin AS (2011) Macrolide antibiotics in the ribosome exit tunnel: species-specific binding and action. *Annals of the New York Academy of Sciences* 1241:33-47.
24. Berisio R, *et al.* (2003) Structural insight into the antibiotic action of telithromycin against resistant mutants. *J Bacteriol* 185(14):4276-4279.
25. Tu D, Blaha G, Moore PB, & Steitz TA (2005) Structures of MLSBK antibiotics bound to mutated large ribosomal subunits provide a structural explanation for resistance. *Cell* 121(2):257-270.
26. Mwakwari SC, *et al.* (2010) Non-peptide macrocyclic histone deacetylase inhibitors derived from tricyclic ketolide skeleton. *Journal of medicinal chemistry* 53(16):6100-6111.
27. Oyelere AK, *et al.* (2009) Non-peptide macrocyclic histone deacetylase inhibitors. *Journal of medicinal chemistry* 52(2):456-468.
28. Kashimura M, Asaka T, Misawa Y, Matsumoto K, & Morimoto S (2001) Synthesis and antibacterial activity of the tricyclic ketolides TE-802 and its analogs. *The Journal of antibiotics* 54(8):664-678.
29. Agouridas C, *et al.* (1998) Synthesis and antibacterial activity of ketolides (6-O-methyl-3-oxoerythromycin derivatives): a new class of antibacterials highly potent against macrolide-resistant and -susceptible respiratory pathogens. *Journal of medicinal chemistry* 41(21):4080-4100.
30. Kolb HC, Finn MG, & Sharpless KB (2001) Click Chemistry: Diverse Chemical Function from a Few Good Reactions. *Angew Chem Int Ed Engl* 40(11):2004-2021.
31. Rostovtsev VV, Green LG, Fokin VV, & Sharpless KB (2002) A stepwise huisgen cycloaddition process: copper(I)-catalyzed regioselective "ligation" of azides and terminal alkynes. *Angew Chem Int Ed Engl* 41(14):2596-2599.
32. Tornoe CW, Christensen C, & Meldal M (2002) Peptidotriazoles on solid phase: [1,2,3]-triazoles by regiospecific copper(i)-catalyzed 1,3-dipolar cycloadditions of terminal alkynes to azides. *The Journal of organic chemistry* 67(9):3057-3064.
33. Pearson DA, Blanchette M, Baker ML, & Guindon CA (1989) Trialkylsilanes as Scavengers for the Trifluoroacetic-Acid Deblocking of Protecting Groups in Peptide-Synthesis. *Tetrahedron Lett* 30(21):2739-2742.
34. Pratt SD, *et al.* (2004) A strategy for discovery of novel broad-spectrum antibacterials using a high-throughput Streptococcus pneumoniae transcription/translation screen. *Journal of biomolecular screening* 9(1):3-11.
35. Thorne CA, *et al.* (2011) A biochemical screen for identification of small-molecule regulators of the Wnt pathway using Xenopus egg extracts. *Journal of biomolecular screening* 16(9):995-1006.
36. Tijerina P, Mohr S, & Russell R (2007) DMS footprinting of structured RNAs and RNA-protein complexes. *Nature protocols* 2(10):2608-2623.
37. Shaw LC & Lewin AS (1995) Protein-induced folding of a group I intron in cytochrome b pre-mRNA. *The Journal of biological chemistry* 270(37):21552-21562.
38. Xiong L, Korkhin Y, & Mankin AS (2005) Binding site of the bridged macrolides in the Escherichia coli ribosome. *Antimicrob Agents Chemother* 49(1):281-288.
39. Agrawal RK, *et al.* (2004) Visualization of ribosome-recycling factor on the Escherichia coli 70S ribosome: functional implications. *Proceedings of the National Academy of Sciences of the United States of America* 101(24):8900-8905.
40. Voorhees RM, Weixlbaumer A, Loakes D, Kelley AC, & Ramakrishnan V (2009) Insights into substrate stabilization from snapshots of the peptidyl transferase center of the intact 70S ribosome. *Nat Struct Mol Biol* 16(5):528-533.

41. Ben-Shem A, Jenner L, Yusupova G, & Yusupov M (2010) Crystal structure of the eukaryotic ribosome. *Science* 330(6008):1203-1209.
42. Voss C, Eyol E, Frank M, von der Lieth CW, & Berger MR (2006) Identification and characterization of riproximin, a new type II ribosome-inactivating protein with antineoplastic activity from Ximenia americana. *FASEB J* 20(8):1194-1196.
43. Wilson DN & Beckmann R (2011) The ribosomal tunnel as a functional environment for nascent polypeptide folding and translational stalling. *Curr Opin Struct Biol* 21(2):274-282.
44. Ito K, Chiba S, & Pogliano K (2010) Divergent stalling sequences sense and control cellular physiology. *Biochem Biophys Res Commun* 393(1):1-5.
45. Merryman C & Noller HF (1998) Footprinting and modification-interference analysis of binding sites on RNA. *RNA: protein interactions, a practical approach. Oxford University Press, Oxford, United Kingdom*:237-253.
46. Amit M, *et al.* (2005) A crevice adjoining the ribosome tunnel: hints for cotranslational folding. *FEBS letters* 579(15):3207-3213.
47. Kabsch W (2010) Xds. *Acta crystallographica. Section D, Biological crystallography* 66:125-132.
48. Adams PD, *et al.* (2010) PHENIX: a comprehensive Python-based system for macromolecular structure solution. *Acta crystallographica. Section D, Biological crystallography* 66:213-221.
49. Emsley P, Lohkamp B, Scott WG, & Cowtan K (2010) Features and development of Coot. *Acta Crystallogr D Biol Crystallogr* 66(Pt 4):486-501.
50. The PyMOL Molecular Graphics System, Version 1.5.0.4 Schrödinger, LLC